

NASA TN D-7917

NASA TECHNICAL NOTE



NASA TN D-7917 C. /

2. u/u

LOAN COPY: RI  
AFWL TECHNICA D  
KIRTLAND AFB



4.  
★ MOMENTUM ANALYSIS OF HELICOPTERS  
AND AUTOGYROS IN INCLINED DESCENT,  
WITH COMMENTS ON OPERATIONAL RESTRICTIONS

Harry H. Heyson

Langley Research Center  
Hampton, Va. 23665

3. 5.  
NATIONAL AERONAUTICS AND SPACE ADMINISTRATION • WASHINGTON, D. C. • OCTOBER 1975





0133612

1. Report No. NASA TN D-7917	2. Government Accession No.	3. Recipient's Catalog No.	
4. Title and Subtitle <b>A MOMENTUM ANALYSIS OF HELICOPTERS AND AUTOGYROS IN INCLINED DESCENT, WITH COMMENTS ON OPERATIONAL RESTRICTIONS</b>		5. Report Date October 1975	
7. Author(s) Harry H. Heyson		6. Performing Organization Code	
9. Performing Organization Name and Address NASA Langley Research Center Hampton, Va. 23665		8. Performing Organization Report No. L-10045	
12. Sponsoring Agency Name and Address National Aeronautics and Space Administration Washington, D.C. 20546		10. Work Unit No. 505-10-21-04	
15. Supplementary Notes		11. Contract or Grant No.	
		13. Type of Report and Period Covered Technical Note	
		14. Sponsoring Agency Code	
16. Abstract  A momentum theory is developed for rotors in descending flight. Comparison with available experimental data indicates that the theory, when properly interpreted, yields the optimum performance of the rotor. Power settling can be explained on the basis of the theory. The reasons and the need for operational restrictions on descending flight are discussed. The maximum autorotative performance of a rotor is determined. The theory shows good agreement with flight measurements in autorotation. An appendix develops similar equations for a wing, shows that the ideal performance of an autorotating rotor is identical to that of a wing of equal aspect ratio, and obtains a limiting maximum wing lift coefficient which is confirmed by existing experimental data.			
17. Key Words (Suggested by Author(s)) Helicopters Autogyros Maximum lift	18. Distribution Statement Unclassified - Unlimited		
Subject Category 02			
19. Security Classif. (of this report) Unclassified	20. Security Classif. (of this page) Unclassified	21. No. of Pages 82	22. Price* \$4.75



## CONTENTS

	Page
SUMMARY . . . . .	1
INTRODUCTION . . . . .	1
SYMBOLS . . . . .	3
DERIVATION OF MOMENTUM EQUATIONS . . . . .	5
Assumptions . . . . .	5
Induced Velocities . . . . .	5
The Wake Skew Angle . . . . .	8
Shaft Power . . . . .	9
VERTICAL FLIGHT . . . . .	10
Flow Patterns Near the Rotor . . . . .	10
The Induced Velocity . . . . .	11
Shaft Power . . . . .	13
Power to Climb . . . . .	14
Control of Descent Rate . . . . .	16
Reversed Response to Power and Collective Pitch . . . . .	16
Multiengine Helicopters . . . . .	17
Ideal Autorotation . . . . .	17
Vertical-Drag Coefficient . . . . .	18
DESCENT IN FORWARD FLIGHT . . . . .	19
Shaft Power Required . . . . .	19
Power Settling . . . . .	20
Recovery From Power Settling . . . . .	21
Avoidance of Power Settling . . . . .	22
AUTOROTATION IN FORWARD FLIGHT . . . . .	22
Ideal Autorotation . . . . .	22
Conditions for Ideal Autorotation . . . . .	23
Minimum Speed for Autorotation . . . . .	24
Maximum Vertical-Force Coefficient . . . . .	24
Maximum Lift Coefficient . . . . .	25
Performance in Autorotation . . . . .	27

	Page
Comparison With Flight Measurements . . . . .	27
Autorotative conditions . . . . .	27
Additional comments . . . . .	28
CONCLUDING REMARKS . . . . .	28
APPENDIX – COMPARISON OF THE MAXIMUM PERFORMANCE OBTAINABLE FROM AUTOROTATING ROTORS AND FINITE WINGS . . . . .	30
REFERENCES . . . . .	35
FIGURES . . . . .	37

# A MOMENTUM ANALYSIS OF HELICOPTERS AND AUTOGYROS IN INCLINED DESCENT, WITH COMMENTS ON OPERATIONAL RESTRICTIONS

Harry H. Heyson  
Langley Research Center

## SUMMARY

A momentum theory is developed for rotors in descending flight. Comparison with available experimental data indicates that the theory, when properly interpreted, yields the optimum performance of the rotor. Power settling can be explained on the basis of the theory. The reasons and the need for operational restrictions on descending flight are discussed. The maximum autorotative performance of a rotor is determined. The theory shows good agreement with flight measurements in autorotation. An appendix develops similar equations for a wing, shows that the ideal performance of an autorotating rotor is identical to that of a wing of equal aspect ratio, and obtains a limiting maximum wing lift coefficient which is confirmed by existing experimental data.

## INTRODUCTION

Some specific problems which have no counterpart in level flight are encountered by rotorcraft in descending flight. One aspect of descent is autorotation, where the unusual aerodynamic characteristics of the rotor are a contributing factor to a relatively high accident rate. For example, reference 1 indicates that over a recent 3-year period more than 40 percent of all United States Army noncombat helicopter accidents involved autorotation. The problems of descending flight are not limited to full autorotation. Additional problems appear when descent is attempted under partial-power conditions. One of these phenomena is power settling, where the helicopter continues to descend at an increasing rate despite the application of additional power. An associated problem is an initially reversed response to an increase in power or collective pitch, where an increased, rather than a decreased, rate of descent may be obtained under certain conditions.

Because of the high accident rate incurred in descent, the present study was conducted in order to provide some basic understanding of the aerodynamic phenomena which determine the descent capabilities of rotorcraft. The particular emphasis in this paper is the development and application of generalized momentum theory to inclined descent. The results illustrate the flow and power characteristics of the descending rotor.

The problem areas of descending flight are generally encountered within or near a rotor flow regime termed the "vortex-ring state." This flow condition was described first by De Bothezat (ref. 2) in 1918; however, the current concept of the vortex-ring state is based largely on the work of Lock, Bateman, and Townend (ref. 3) in 1925. The flow in the vortex-ring state is circulatory and unsteady on a large scale. There is no semblance of a smooth slipstream such as that postulated by momentum theory; thus, the theory is generally considered to be invalid. On the other hand, the existence of the rotor thrust in this condition argues that there must be a transfer of momentum to the surrounding air, even if this transfer occurs under less than ideal conditions. Therefore, there remains the possibility that momentum theory, when properly interpreted, may still be useful in defining the minimum power requirements of ideal rotors in descent despite the inconsistencies in the theoretical formulation. Such a usage of the momentum theory is validated in the present study by comparing the theoretical results with experimental data (refs. 4 and 5) for rotors operating over a range of descent conditions including the vortex-ring state.

The generalized momentum theory of reference 6 is extended herein to steady descending flight along an arbitrary glide slope. A single set of equations is developed which may be used throughout the entire flight range including vertical descent. The analysis of reference 6 is also extended to the calculation of the shaft power required in descent.

The calculated shaft power is the key to an understanding of several rotary-wing descent problems. The results indicate conditions which cause and aggravate power settling in inclined flight. Furthermore, the results illustrate reasons for the initially reversed responses to power applications that occur in certain regions of flight. The reasons for severe operational restrictions on the descending flight of a rotor are apparent in calculations based on the theory. These restrictions are discussed in the text. Conditions which should avoid problems in descending flight are also noted. The shaft-power requirements in vertical flight have severe implications on the design of multiengine helicopters and these implications are also discussed.

Furthermore, the theory is used to define those conditions which allow an ideal rotor to fly in autorotational flight and to determine the minimum flight speeds and maximum lift and vertical-force coefficients of the autorotating rotor. An appendix elaborates this latter analysis and extends it to finite wings; thus a direct comparison of the performance of wings and rotors in autorotation is allowed.

The present analysis is presented in several major divisions. The first of these divisions presents a derivation of the generalized momentum equations. Next, the special case of vertical flight is treated independently including a comparison of the theory with experimental data. The third division discusses the application of the theory to the general case of inclined descent with particular emphasis on those conditions conducive to power

settling. The final division is concerned with full autorotation including the conditions which permit autorotation and the performance obtainable in autorotation.

### SYMBOLS

A	aspect ratio, $\frac{b^2}{S}$
$A_m$	momentum area
b	wing span
$C_{D,V}$	equivalent vertical-drag coefficient of a rotor in vertical descent, $\frac{F_Z}{qS}$
$C_L$	lift coefficient, $\frac{L}{qS}$
$C_Z$	vertical-force coefficient, $\frac{F_Z}{qS}$
$C_\mu$	jet momentum coefficient, $\frac{\text{Thrust}}{qS}$
D	drag
$\dot{E}_P$	rate of gain of potential energy, $-F_Z V_G \sin \gamma$
$\bar{F}$	induced-force vector produced by rotor (perpendicular to tip-path plane)
$F_X$	horizontal component of force produced by rotor, positive rearward
$F_Z$	vertical component of force produced by rotor, positive upward
L	component of $\bar{F}$ normal to glide slope, positive above glide slope
$P_c$	additional power required to climb
$P_h$	power required to hover with $F_X = 0$
$P_s$	shaft power
q	dynamic pressure

R	rotor radius
S	wing area (or swept area of a rotor, $\pi R^2$ )
$u_0$	mean, or momentum theory, value of horizontal component of induced velocity, positive rearward
$\bar{V}$	resultant velocity vector at rotor or wing
$V_G$	velocity along glide slope, generally positive
$V_R$	absolute value of $\bar{V}$
$w_0$	mean, or momentum theory, value of vertical component of induced velocity, positive upward
$w_h$	a reference velocity, value of $w_0$ when hovering with vertical force = $F_Z$ and $F_X = 0$ , negative for positive lift
$\alpha$	rotor angle of attack, angle measured from glide slope to leading edge of rotor tip-path plane, positive with leading edge up
$\gamma$	glide-slope angle, angle between horizontal and flightpath, positive for descending flight
$\theta$	rotor inclination, angle measured from horizontal to leading edge of tip-path plane, positive with leading edge up
$\rho$	mass density of air
$\dot{x}$	wake skew angle, angle measured positive rearward from vertical to center of wake as defined by $\bar{V}$
$x_G$	wake skew angle measured from normal to glide slope, $x - \gamma$

Subscripts:

max maximum value

min minimum value

## DERIVATION OF MOMENTUM EQUATIONS

### Assumptions

It is assumed that the flow influenced by the rotor is equal to the quantity of flow passing through an area equal to the swept area of the rotor with a velocity equal to the vectorial sum of the free-stream and induced velocities. This flow is assumed to be affected uniformly and the remainder of the flow is assumed to be unperturbed by the rotor. These assumptions can be recognized as the basis of the treatments of Glauert (ref. 7) and Wald (ref. 8). It can be observed further that, in level flight, the analysis of reference 9 has shown that these assumptions lead to results identical to those obtained by simple vortex theory.

### Induced Velocities

The rotor is presumed to be descending at a uniform speed  $V_G$  along a path defined by a glide-slope angle  $\gamma$ . The force and velocity diagrams at the rotor for this condition are shown in figure 1. The vertical and horizontal forces of the rotor are equal to the time rate of change of momentum in the vertical and horizontal directions. Note that the mass-flow rate is  $\rho\pi R^2 V_R$  and that the total velocity imparted to this flow rate is twice the induced velocity; thus,

$$F_Z = \rho\pi R^2 V_R (-2w_0) \quad (1)$$

$$F_X = \rho\pi R^2 V_R (-2u_0) \quad (2)$$

The ratio of horizontal force to vertical force in terms of the induced velocities is obtained by dividing equation (2) by equation (1) to yield

$$\frac{F_X}{F_Z} = \frac{u_0}{w_0} \quad (3)$$

The resultant velocity at the rotor is obtained from the vector diagram of figure 1 as

$$V_R = \sqrt{(-w_0 - V_G \sin \gamma)^2 + (V_G \cos \gamma + u_0)^2} \quad (4)$$

Equation (4) may be nondimensionalized by dividing both sides by  $-w_0$ , and then using equation (3), to yield

$$\frac{V_R}{w_0} = \sqrt{\left(\frac{V_G}{w_0} \cos \gamma + \frac{F_X}{F_Z}\right)^2 + \left(1 + \frac{V_G}{w_0} \sin \gamma\right)^2} \quad (5)$$

At this point, it is desirable to define a convenient reference velocity  $w_h$  which can be chosen as the vertical component of induced velocity in hovering flight; that is,  $w_h$  is the value of  $w_0$  when  $V_G$  and  $F_X$  are both zero. Under these specified conditions,  $w_h = w_0$  and, from equation (5),  $V_R = -w_h$ . Now, substitute these values into equation (1) and solve for  $w_h$  to obtain

$$w_h = -\sqrt{\frac{F_Z}{2\rho\pi R^2}} \quad (6)$$

Observe that the negative sign of the square root in equation (6) is chosen because, in the present notation, a positive force is produced by a negative induced velocity. Next, solve equation (1) for  $w_0$  and divide the resulting equation by equation (6) squared to yield

$$\frac{w_0}{w_h^2} = \frac{\frac{-F_Z}{2\rho\pi R^2} V_R}{\frac{F_Z}{2\rho\pi R^2}} = \frac{-1}{V_R} \quad (7)$$

Multiplication of both sides of equation (7) by  $w_0$  leads to the general result that

$$\left(\frac{w_0}{w_h}\right)^2 = \frac{-w_0}{V_R} \quad (8)$$

For the present problem of the descending flight of a rotor, substitute equation (5) into equation (8) and square both sides of the resulting equation to eliminate the radical in order to obtain the momentum quartic as

$$\left(\frac{w_0}{w_h}\right)^4 = \frac{1}{\left(1 + \frac{V_G}{w_0} \sin \gamma\right)^2 + \left(\frac{V_G}{w_0} \cos \gamma + \frac{F_X}{F_Z}\right)^2} \quad (9)$$

It is known that at the low and moderate speeds of primary concern herein, the induced force of a rotor is essentially normal to the tip-path plane; that is,

$$\frac{F_X}{F_Z} = \tan \theta \quad (10)$$

Substitute equation (10) into equation (9) to obtain

$$\left(\frac{w_0}{w_h}\right)^4 = \frac{1}{\left(1 + \frac{V_G}{w_0} \sin \gamma\right)^2 + \left(\frac{V_G}{w_0} \cos \gamma + \tan \theta\right)^2} \quad (11)$$

The simplest way to solve equation (11) when  $\theta$  and  $\gamma$  are given is to choose values of  $V_G/w_0$ , solve for  $w_0/w_h$ , and then note the identity

$$\frac{V_G}{w_h} = \frac{V_G}{w_0} \frac{w_0}{w_h} \quad (12)$$

Unfortunately, this technique may require considerable iteration in order to find the induced velocity ratio at a specified value of  $V_G/w_h$ . An alternate procedure is to multiply both sides of equation (11) by the denominator of the right-hand side and then to simplify the result in order to obtain

$$(1 + \tan^2 \theta) \left(\frac{w_0}{w_h}\right)^4 + 2 \frac{V_G}{w_h} (\sin \gamma + \cos \gamma \tan \theta) \left(\frac{w_0}{w_h}\right)^3 + \left(\frac{V_G}{w_h}\right)^2 \left(\frac{w_0}{w_h}\right)^2 - 1 = 0 \quad (13)$$

Equation (13) is solved easily on a computer and, in general, either one or three positive real roots can be obtained at a given  $V_G/w_h$ . The multiple roots occur at larger velocities ( $|V_G/w_h|$  greater than about 2) and more frequently for positive tip-path plane inclination. In contrast, solution of equation (11) at a given  $V_G/w_0$  yields only one positive real root. The difference is in the reference velocities of the two velocity ratios which are related in a highly nonlinear manner through equation (12).

### The Wake Skew Angle

A parameter of interest in the subsequent analysis is the wake skew angle  $\chi$ , the angle between the vertical and the center line of the wake. An expression for the tangent of this angle may be written by inspection of the flow vectors in figure 1 (and by using eqs. (3) and (10)) as

$$\tan \chi = \frac{\frac{V_G}{w_0} \cos \gamma + u_0}{-\frac{V_G}{w_0} \sin \gamma} = -\frac{\frac{V_G}{w_0} \cos \gamma + \tan \theta}{1 + \frac{V_G}{w_0} \sin \gamma} \quad (14)$$

Multiply both sides of equation (14) by  $\left(1 + \frac{V_G}{w_0} \sin \gamma\right)$  to obtain

$$\frac{V_G}{w_0} \cos \gamma + \tan \theta = -\tan \chi \left(1 + \frac{V_G}{w_0} \sin \gamma\right) \quad (15)$$

Now substitute equation (15) into equation (11) to yield

$$\left(\frac{w_0}{w_h}\right)^4 = \frac{1}{\left(1 + \frac{V_G}{w_0} \sin \gamma\right)^2 \left(1 + \tan^2 \chi\right)} = \frac{\cos^2 \chi}{\left(1 + \frac{V_G}{w_0} \sin \gamma\right)^2} \quad (16)$$

Finally, solve equation (16) for  $\cos \chi$  to obtain

$$\cos \chi = \left(\frac{w_0}{w_h}\right)^2 \left(1 + \frac{V_G}{w_0} \sin \gamma\right) = \frac{w_0}{w_h} \left(\frac{w_0}{w_h} + \frac{V_G}{w_h} \sin \gamma\right) \quad (17)$$

### Shaft Power

The shaft power is merely the scalar (or dot) product of the force and velocity vectors or, using the present sign convention,

$$P_s = -\vec{F} \cdot \vec{V} \quad (18)$$

Substitute the force and velocity vectors from figure 1 into equation (18) to obtain

$$P_s = -F_X(V_G \cos \gamma + u_0) - F_Z(w_0 + V_G \sin \gamma) \quad (19)$$

The power in hovering is obtained by setting  $u_0$  and  $V_G$  to zero in equation (19) and then noting that in hover  $w_0 = w_h$ ; thus,

$$P_h = -F_Z w_h \quad (20)$$

The nondimensionalized power is obtained by dividing equation (19) by equation (20) and then substituting equation (3) into the result in order to obtain, after some simplification,

$$\frac{P_s}{P_h} = \frac{F_X}{F_Z} \left( \frac{V_G}{w_h} \cos \gamma \right) + \left[ 1 + \left( \frac{F_X}{F_Z} \right)^2 \right] \frac{w_0}{w_h} + \frac{V_G}{w_h} \sin \gamma \quad (21)$$

or using, in addition, equation (10) to give

$$\frac{P_s}{P_h} = \frac{V_G}{w_h} \tan \theta \cos \gamma + \frac{w_0/w_h}{\cos^2 \theta} + \frac{V_G}{w_h} \sin \gamma \quad (22)$$

The physical significance of the three terms on the right-hand side of equation (21) is noteworthy. The central term represents the induced power required to produce the vertical and horizontal rotor forces;  $w_0/w_h$  by itself is the power required to produce the vertical force, and  $\left[ 1 + (F_X/F_Z)^2 \right]$  is an expansion factor signifying that the resultant force at the rotor is the vectorial sum of the horizontal and vertical forces. Note that  $V_G/w_h$  is intrinsically negative. Thus, the final term represents a reduction in power caused by the rate at which potential energy is lost as the rotor descends.

The first term on the right-hand side of equation (21) is of particular interest since its effect differs according to the sign of  $F_X/F_Z$ . If  $F_X/F_Z$  is negative, this entire term is positive and represents the power required to maintain a horizontal propulsive thrust so as to overcome, for example, fuselage parasite drag. On the other hand, if

$F_X/F_Z$  is positive, this entire term is negative and the rotor must be extracting power from the air in order to reduce the shaft power. The reduction in shaft power is not free, because some external application of power (such as separate propulsion engines) is required to overcome  $F_X$  so as to maintain balanced flight.

The preceding discussion indicates that equations (21) and (22) contain all the terms normally considered in rotor performance analyses with the exception of the blade-profile power. The various power demands are not as independent as might be suggested by the foregoing term-by-term examination, since  $w_0/w_h$  is an implicit function of  $V_G/w_h$ ,  $F_X/F_Z$ , and  $\gamma$ . (See eqs. (9) and (12).) Thus, the terms of equations (21) and (22) are interdependent and, particularly at low speeds, a change in one term affects the remaining terms. The interplay of the three terms allows the shaft power to vary over a wide range. Indeed, the shaft power may be zero, or negative, even when the rotor is in level flight. In subsequent sections of the present paper, this aspect of the problem is examined in greater detail.

## VERTICAL FLIGHT

The present understanding of the character of the flow near a descending rotor is largely based on consideration (ref. 3, for example) of the simple case of vertical flight. In order to provide a basis for some of the later sections, in this portion of the paper some of the major features of earlier studies are reviewed, the application of the generalized theory to this case is shown, and the theoretical results are compared with available experimental data (refs. 4 and 5).

### Flow Patterns Near the Rotor

In vertical climb, a well-defined slipstream exists. This slipstream contracts continuously as the flow passes from far above the rotor, through the rotor, and then far below the rotor (fig. 2(a)). The limit of this regime is hovering where a definitive slipstream exists only below the rotor. Because of the similarity of this condition to the normal mode of operation of a propeller, this regime is designated as the "normal working state." Although the generalized theory developed in the preceding sections of this paper applies equally as well to the normal working state, such operation receives only minor attention herein.

As the rotor begins to descend, the smooth continuous slipstream disappears. The external flow is from below to above the rotor; yet, within the rotor and perhaps for some distance below it, the net flow is downward (fig. 2(b)). Within the constraint of steady-flow concepts, this flow might be considered as containing one or more major vortex

rings of varying location with respect to the rotor. Because of this steady-flow concept, this regime is generally termed the "vortex-ring state."

When the descent rate continues to increase, the maximum induced velocities of the rotor eventually are exceeded by the descent rate. Under such conditions, the entire flow, both within and outside the rotor, must be directed upward (fig. 2(c)). Once more a definite slipstream is observed, expanding continuously as it passes upward, through, and beyond the rotor. This type of flow is similar to that of a windmill extracting energy from the wind; thus, it is classified as the "windmill-brake state."

Figure 3 presents a series of smoke-flow photographs (from ref. 10) of the various working states of a rotor in vertical descent. The continuous slipstreams of the normal working state and of the windmill-brake state are evident. The flow of the intermediate descent rates is usually that termed the vortex-ring state. This flow is obviously not as simple as the flow postulated from steady-state concepts. Great "chunks" of rolled-up vorticity, rather than vortex rings, are shed sporadically from the rotor. (Even the appendix of ref. 3 notes that the name "vortex-ring state" may be a misnomer.) The vortex shedding is erratic and often aperiodic. No semblance of a steady wake exists.

The formulation of the momentum theory implicitly assumes a continuous, steady slipstream which obviously does not exist in the vortex-ring state. On the other hand, the fact that the rotor thrust exists on a time-averaged basis implies that the rotor must transfer momentum to the flow on a time-averaged basis.

Momentum theory presents a highly idealized picture of rotor performance. Since momentum theory omits all viscous losses and all losses caused by nonuniformity of momentum transfer, its real function is only to obtain the maximum possible efficiency of the system. Thus, the major concern in applying momentum theory to the vortex-ring state is not whether a well defined slipstream exists; the real concern is whether the theory still obtains the maximum possible efficiency of the rotor. This question can be answered only by recourse to experiment and, if the answer is affirmative, the theory is still usable on a qualitative basis.

#### The Induced Velocity

Prior to a comparison of the theoretical results with the experimental data, it is useful to apply the previously developed general equations to the special case of vertical descent. In vertical descent the glide-slope angle  $\gamma$  is  $90^\circ$  and the tip-path plane inclination  $\theta$  must be  $0^\circ$  to maintain the vertical path. Under these conditions, equation (11) reduces to

$$\left(\frac{w_0}{w_h}\right)^4 = \frac{1}{\left(1 + \frac{V_G}{w_0}\right)^2} \quad (23a)$$

or

$$\left(\frac{w_0}{w_h}\right)^4 \left(1 + \frac{V_G}{w_0}\right)^2 - 1 = 0 \quad (23b)$$

Equation (23b) factors immediately to yield the following pair of quadratic equations:

$$\left(\frac{w_0}{w_h}\right)^2 \left(1 + \frac{V_G}{w_0}\right) - 1 = 0 \quad (24a)$$

$$\left(\frac{w_0}{w_h}\right)^2 \left(1 + \frac{V_G}{w_0}\right) + 1 = 0 \quad (24b)$$

Equations (24) are easily shown to be identical (except for notation) with the expressions derived in a more restrictive manner in reference 11 (pp. 128-129). The solutions to equations (24) are

$$\frac{w_0}{w_h} = -\frac{1}{2} \frac{V_G}{w_h} + \frac{1}{2} \sqrt{\left(\frac{V_G}{w_h}\right)^2 + 4} \quad (25a)$$

and

$$\frac{w_0}{w_h} = -\frac{1}{2} \frac{V_G}{w_h} \pm \frac{1}{2} \sqrt{\left(\frac{V_G}{w_h}\right)^2 - 4} \quad (25b)$$

The physically impossible negative square root has been eliminated from equation (25a). Observe that this equation then yields a single-valued, continuously increasing induced-velocity ratio as the descent rate  $V_G$  increases. In contrast, equation (25b) is double valued but has no physically possible solutions unless  $V_G > 2|w_h|$ .

Figure 4 shows the solutions of equations (25) and compares them with a wide range of experimental data from references 4 and 5. It may be seen that the experimentally determined induced-velocity ratios of reference 5 are somewhat greater than the theoretical values from equation (25a) until  $V_G > 1.5|w_h|$ . The experimental values then decrease rapidly as  $V_G$  increases, finally meeting and then attaining values somewhat greater than those calculated for the lower branch of equation (25b). In fact, for the highly twisted blades of reference 5, the experimental data indicate an essentially discontinuous jump from equation (25a) to equation (25b) at almost precisely  $V_G/w_h = -2$ .

Time histories of the rotor thrust and torque were obtained during the experiments of reference 4. These quantities were found to be extremely unsteady even during runs at constant conditions. The shaded region indicates the range of induced-velocity ratios obtained from reference 4. This region tends to confirm the average values obtained from reference 5; furthermore, as noted in reference 4, the lower bound of the shaded region tends to conform to the simple momentum theory over a wide range of descent rates.

Except for a small range of descent rates over which the data transfer between the theoretical curves, figure 4 demonstrates that the momentum theory provides a lower bound for the induced-velocity ratio. (It is shown in the next section that this fact represents a maximum bound on efficiency.) Indeed, if a straight-line transfer from equation (25a) at  $V_G/w_h = -1.5$  to equation (25b) at  $V_G/w_h = -2$  was assumed, the theory would represent a minimum induced velocity for all descent rates. Therefore, the theory should be usable in a qualitative manner despite genuine concern over its basic formulation.

#### Shaft Power

For vertical flight ( $\gamma = 90^\circ$ ) at zero inclination ( $\theta = 0^\circ$ ), equation (22) reduces to

$$\frac{P_s}{P_h} = \frac{w_0}{w_h} + \frac{V_G}{w_h} \quad (26)$$

In equation (26), the first term on the right-hand side represents the induced power required to produce the thrust. The final term represents the reduction in shaft power as a result of the loss of potential energy caused by the descent rate. If the induced power were constant with descent rate, the shaft power would be

$$\frac{P_s}{P_h} = 1 + \frac{\dot{E}_P}{P_h} \quad (27)$$

However, in vertical flight, the induced power is not independent of descent rate as has been shown in equations (25). Substitute those equations into equation (26) to yield (corresponding to eqs. (25a) and (25b))

$$\frac{P_s}{P_h} = \frac{1}{2} \frac{V_G}{w_h} + \frac{1}{2} \sqrt{\left(\frac{V_G}{w_h}\right)^2 + 4} \quad (28a)$$

$$\frac{P_s}{P_h} = \frac{1}{2} \frac{V_G}{w_h} \pm \frac{1}{2} \sqrt{\left(\frac{V_G}{w_h}\right)^2 - 4} \quad (28b)$$

Even though  $V_G/w_h$  is negative, it is evident that equation (28a) always yields a positive shaft power. As shown earlier, it is equation (25a), and thus equation (28a), which applies to modest rates of descent. Autorotation which requires zero, or negative, shaft power cannot be obtained until the descent rate is great enough to entail the use of equations (25b) and (28b). Thus, the theoretical minimum descent rate in full autorotation is  $V_G/w_h = -2$ . At this descent rate, equation (28b) indicates a power ratio of -1; that is, the rotor is extracting as much power from the air as it required for power input during hovering.

Figure 5 presents a comparison of theoretical (eq. (28)) and experimental data in terms of shaft power. In this presentation the experimental data of figure 4 have been converted to power ratio by means of equation (26). If a transfer similar to that proposed in the discussion of figure 4 is assumed, figure 5 shows that the theory indicates a lesser power than is actually required. A lower bound on power is obviously an upper bound on efficiency.

#### Power to Climb

For a conventional airplane, where the induced velocities are small compared with the large forward speed, the power to climb is merely equal to the rate of gain of potential energy. A different result is obtained for a rotor at low speed because the flight speed affects the mass flow through the rotor in a nonlinear manner. This effect may be demonstrated in the following analysis.

The power required to climb from hover is the difference between the shaft power while climbing and the shaft power while hovering; thus,

$$\frac{P_c}{P_h} = \frac{P_s - P_h}{P_h} = \frac{P_s}{P_h} - 1 \quad (29)$$

In climb, or when descending at moderate rates,  $P_s/P_h$  is given by equation (28a); thus,

$$\frac{P_c}{P_h} = \frac{1}{2} \frac{V_G}{w_h} + \sqrt{1 + \frac{1}{4} \left( \frac{V_G}{w_h} \right)^2} - 1 \quad (30)$$

Observe that in deriving equation (28), the glide slope was taken as  $90^\circ$ ; hence a climb velocity is represented by a negative value of  $V_G$ . Therefore, the nondimensional rate of gain of potential energy is

$$\frac{\dot{E}_P}{P_h} = \frac{-V_G L}{-w_h L} = \frac{V_G}{w_h} \quad (31)$$

Now divide equation (30) by equation (31) to obtain the ratio of the climb power to the rate of gain of potential energy

$$\frac{P_c}{\dot{E}_P} = \frac{\frac{1}{2} \frac{V_G}{w_h} + \sqrt{1 + \frac{1}{4} \left( \frac{V_G}{w_h} \right)^2} - 1}{\frac{V_G}{w_h}} \quad (32)$$

Equation (32) is indeterminate at  $V_G/w_h = 0$ ; however, it may be evaluated in the limit by the use of L'Hospital's rule

$$\lim_{\frac{V_G}{w_h} \rightarrow 0} \left[ \frac{P_c}{\dot{E}_P} \right] = \lim_{\frac{V_G}{w_h} \rightarrow 0} \left[ \frac{\frac{1}{2} \frac{V_G}{w_h} + \sqrt{1 + \frac{1}{4} \left( \frac{V_G}{w_h} \right)^2} - 1}{\frac{V_G}{w_h}} \right] = \frac{1}{2} \quad (33)$$

Equations (32) and (33) show that a rotor is exceptionally efficient in vertical climb. For small rates of climb the power required to climb is only one-half of the rate of gain of potential energy. This result is obtained because the climb rate increases the mass flow through the rotor and thereby decreases the power required to sustain the necessary vertical force.

Conversely, because of the reduction in mass flow in descent, the descending rotor is exceedingly inefficient. The required shaft power is reduced by only one-half of the rate of loss of potential energy.

Certain flight measurements (for example, fig. 5-8 of ref. 11) tend to support the foregoing analysis. On the other hand, figure 5 demonstrates that the actual situation can be even worse than predicted. The figure clearly indicates an essentially constant shaft power until the descent rate exceeds  $1.5|w_h|$ .

#### Control of Descent Rate

Altitude control by a pilot is largely dependent upon his control of power, either directly or indirectly, by the use of collective pitch. Thus, the experimental data of figure 5, which indicate an essentially neutral power stability ( $\partial P_s / \partial V_G$ ), present a basic problem in controlling moderate rates of vertical descent. The problem is compounded by the fact that the pilot's instinctive feel for the relationship between power and rate of descent is formed largely on the basis of his experience in cruising flight or in conventional aircraft where (see eqs. (27) and (29)) the power to climb is essentially equal to the rate of gain of potential energy (that is,  $P_c = E_p$  which is also shown in fig. 5). It is evident that the pilot does not attain such a relationship until he is approaching full autorotation.

#### Reversed Response to Power and Collective Pitch

At larger rates of descent there is a distinct possibility that the initial reaction to an increase in power or collective pitch is in the wrong direction. For example, consider a helicopter established in vertical descent with  $V_G > |1.5w_h|$ . Collective pitch is applied to check the descent rate. The thrust responds in fractions of a second, increasing the magnitude of  $w_h$  and  $P_h$ ; however, the descent rate cannot respond as rapidly since it requires a deceleration of the entire mass of the helicopter. The net effect is a reduction in the ratio  $|V_G/w_h|$ . As indicated in figure 5, this reduced ratio requires a greater ratio of  $P_s/P_h$  in addition to the increase in  $P_h$  itself. The required shaft power  $P_s$  may increase so rapidly that the engine response rate is overpowered. Thus, the rotor merely slows down, reducing the thrust, and the helicopter continues to settle for a while, perhaps even more rapidly than before the application of control. Since the thrust now decreases,  $w_h$  and  $P_h$  also decrease and reverse the foregoing sequence of events. The eventual result may be a response in the intended direction; however, there is likely to be a major loss of altitude before the final equilibrium state is reached.

Operationally, the importance of the altitude loss is emphasized by the fact that the foregoing sequence of events is most likely to be encountered when trying to land from a rapid descent. It becomes almost impossible to land without crashing. Vertical descents should be avoided whenever possible. If the task demands a vertical descent, such as the placement of an external sling load in a confined area, the vertical portion of the descent

should be from the minimum possible height above the ground and should be made at the minimum possible descent rate.

#### Multiengine Helicopters

As noted earlier, the experimental data of figure 5 indicate that the rate of descent does not depend upon the shaft power until very large descent rates are obtained. Thus, if one engine of a multiengine helicopter fails while hovering, the resulting descent rate in vertical flight is essentially the same rate that would be obtained with a total loss of power. The remaining engines provide no significant reduction in the vertical descent rate and thus no additional margin of safety. Indeed, the multiengine helicopter may be less safe since, if equal engine reliability is assumed, the probability that one engine of a group will fail is greater than the probability that a single engine will fail. Thus, in vertical flight, the "dead-man's region" (from which safe autorotative recovery is impossible) cannot be reduced by multiengine design unless sufficient engines are provided so that hovering flight is possible with one engine out.

It should be specifically noted that the preceding discussion is limited to vertical flight. If a forward speed exists at failure, or if it is possible to attain a large forward speed subsequent to failure, the remaining engines may be of some help. Power calculations for forward flight conditions are presented in the "Descent in Forward Flight" section of this paper.

#### Ideal Autototation

Ideal autorotation is defined as that descent rate for which the shaft power is zero. Thus, set  $P_s/P_h$  equal to zero in equation (26) and solve for  $V_G$  to obtain

$$V_G = -w_0 \quad (34)$$

For the case of vertical descent (where  $\gamma = 90^\circ$  and  $\theta = 0^\circ$ ), substitute equation (34) into equation (5) to obtain the resultant velocity through the rotor as

$$V_R = 0 \quad (35)$$

Therefore, in ideal autorotation, there is no flow through the rotor. It might appear from equation (1) that the vertical force also vanishes; however, this is not the correct result because as  $V_R$  approaches zero,  $w_0$  approaches infinity. (See eq. (7).) In order to obtain the vertical force, rewrite equation (1) as

$$F_Z = 2\rho\pi R^2 \left( \frac{-V_R}{w_0} \right) w_0^2 \quad (36)$$

Now substitute equation (8) into equation (36) to obtain

$$F_Z = 2\rho\pi R^2 w_h^2 \quad (37)$$

Thus, the vertical force remains constant and a function only of  $w_h$  even though there is no mass flow through the rotor. However, in the theory, ideal autorotation can only be achieved at an infinite rate of descent. This fact is illustrated by figure 4 which shows equation (34) and demonstrates that it is the common asymptote to equations (25a) and (25b).

#### Vertical-Drag Coefficient

Rotor performance in autorotation is occasionally presented in terms of an equivalent rotor vertical-drag coefficient (refs. 11 and 12). Such a presentation compares the performance of a rotor to that of a parachute. In this presentation, the effective drag is identical to the rotor vertical force; thus, the drag coefficient may be written as

$$C_{D,V} = \frac{F_Z}{\frac{1}{2}\rho V_G^2 \pi R^2} = \frac{F_Z / 2\rho\pi R^2}{V_G^2 / 4} \quad (38)$$

But, from equation (6), the numerator of the final form of equation (38) is merely  $w_h^2$ ; thus,

$$C_{D,V} = \frac{4}{\left( \frac{V_G}{w_h} \right)^2} \quad (39)$$

Equation (39) shows that the vertical-drag coefficient is merely an involuted manner of stating the minimum descent speed of the rotor in full autorotation. The theoretical minimum value of  $|V_G/w_h|$  in autorotation is 2.0; thus, equation (39) implies a maximum vertical-drag coefficient of 1.0.

As would be anticipated from the previous discussion of figure 5, experimental vertical-drag coefficients are obtained which are greater than the theoretical value. The flight measurements of reference 12 obtained vertical-drag coefficients ranging from 1.12 to 1.32, with an average value of 1.25. This average value would imply that  $V_G = -1.79w_h$  and, at this descent speed, the data of figure 5 indicate that  $P_s/P_h \approx -1/2$ .

The foregoing assessment of the shaft power in flight should be approximately correct. Even in hovering, the blade-profile power, which is omitted in momentum theory, tends to be about 25 to 30 percent of the induced power. Additional losses would be expected because of the inefficient operating conditions of some blade elements in autorotation. Still further power is required to overcome the losses associated with driving the tail rotor, gear boxes, and accessories. The source of power to overcome these losses can only be the rotor extracting power from the air.

## DESCENT IN FORWARD FLIGHT

### Shaft Power Required

The power required in forward flight was calculated on a digital computer by the direct solution of the momentum quartic (eq. (13)) followed by the evaluation of equation (22). The results are presented for a series of rotor inclinations at different glide slopes in figure 6 and for a series of glide slopes at different rotor inclinations in figure 7.

Observe that the presentations of figures 6 and 7 are for the rotor operating with constant vertical force and not constant thrust because of the definitions of the reference velocity  $w_h$  and the reference power  $P_h$  in terms of the vertical force rather than the thrust.

The nonlinear character of the required shaft power with changes in tip-path-plane inclination and glide slope is evident (figs. 6 and 7) particularly for speeds less than  $2|w_h|$ . These nonlinearities result from the complex interplay of  $\theta$  and  $\gamma$  in determining the resultant velocity at the rotor and, in consequence, the mass flow through the rotor. The multiple-valued solutions obtained at higher velocities along the glide slope are clear evidence of the existence of flow patterns equivalent to the vortex-ring state of the rotor in vertical flight. This evidence is confirmed by figure 8 which shows a time sequence of smoke-flow photographs (ref. 10) of a model rotor in inclined descent. The virulent nature of the flow changes with time are characteristic of the vortex-ring state. Again, observe that there is no semblance of the steady-state concept of a vortex ring. The steady-flow patterns (ref. 10) shown in figure 9 are evidence of the existence in forward flight of equivalents to the windmill-brake state (autorotation) and the normal working state (helicopter mode).

Experimental data to verify the theory in inclined flight are much sparser than in vertical descent. Figures 10 and 11 compare the theoretical results with the data bands of

reference 4. In the experiments of reference 4, considerably fewer conditions were tested in inclined descent than in vertical descent. Thus, the shape of these data bands may not be as definitive as in vertical flight; however, the indicated degree of agreement should be adequate to allow qualitative use of the theory.

### Power Settling

One important characteristic of descending flight is indicated by the nature of the power requirement at moderate speeds  $0 < |V_G/w_h| < 2$  in figure 7. As the glide slope steepens at constant speed, the power initially decreases; however, this trend does not continue indefinitely. After a certain glide slope is reached, further steepening of the glide slope requires more, rather than less, power.

The foregoing trends are shown more clearly in figure 12 which presents shaft power as a function of glide-slope angle. A reasonably fine increment in  $\gamma$  ( $5^\circ$ ) was used in preparing figure 12; however, when multiple values were obtained from equation (13), the smallest (most negative) power was chosen. In vertical flight, this procedure would yield a discontinuous jump such as that shown for the highly twisted ( $-12^\circ$ ) rectangular blades of figures 4 and 5. Thus, over a small range of  $V_G/w_h$  (say  $1.5 < |V_G/w_h| < 2$ ), figure 12 may represent a "worst-case" technique for a few conditions. In any event, the choice of this technique should not seriously affect the discussion to follow.

Figure 12 shows that the glide slope for minimum power is a function of the rotor inclination; it varies from about  $70^\circ$  when the rotor is tilted forward  $20^\circ$  to about  $35^\circ$  or  $40^\circ$  when the rotor is tilted rearward  $20^\circ$ . Such a trend might be expected from a consideration of the effect of  $\theta$  on the angle of attack measured with respect to the glide slope. It is even more evident in the sharp increase in power for  $V_G$  less than  $2.0|w_h|$  at a large  $\gamma$ . This peak in power represents an angle of attack of  $90^\circ$ ; that is, aerodynamically speaking the rotor is in "vertical descent." Figure 5 has already shown that the experimental trend in vertical descent indicates a constant shaft power in vertical descent for  $V_G$  less than  $1.5|w_h|$ . Thus, in practice, the powers near this "peak" point are greater than indicated by theory. A distinct minimum may exist even where not shown in the theory for very low speeds, and the slopes of the curves at large glide slopes may be considerably greater than indicated by the theory.

The required inclination depends on the speed and the parasite-drag coefficient since balanced flight requires a propulsive force equal to the drag. Vertical equilibrium is automatically satisfied in figure 12 since, as was noted earlier, the entire analysis is based on a constant vertical force. The primary concern herein is with steep approaches; the fuselage drag is small and equilibrium requires only a small nose-down inclination of the tip-path plane.

A pilot flying a steep approach generally flies with reference to the ground either visually or through the use of some avionics system. Although he can sense sidewinds as

a drift, his perception of a headwind or tailwind is poor. Even a light tailwind can produce a major difference between the glide slope with respect to the surrounding air mass and the geometric glide slope. If the flight is stabilized near one of the minimum power points, figure 12 shows many combinations of  $\gamma$ ,  $\theta$ , and  $V_G/w_h$  for which a tailwind-induced change of only  $10^\circ$  or  $15^\circ$  in  $\gamma$  increases the required shaft power by 50 to 100 percent of the installed power. In the presence of such a major increase in required power, the helicopter settles, thus increasing the glide slope and still further increasing the required power.

Operationally, the appearance of the phenomenon is rapid and usually unexpected. Pilots sometimes refer to it as "stepping into the sinkhole." The particular problem is that the pilot has no means of determining his aerodynamic flightpath. He may successfully negotiate a combination of geometric glide slope and speed so many times that he is confident of its safety; however, the next approach may encounter winds that produce disastrous consequences.

A similar sequence of events can be encountered even without a tailwind. If any disturbance increases the speed along the glide slope, the instinctive reaction of a pilot is to correct the airspeed by pulling back on the cyclic-pitch stick to increase the rotor inclination. If the original stabilized glide slope was near a minimum power condition, comparison of the various parts of figure 12 shows that such a rearward stick movement may result in a power requirement far in excess of that available in the helicopter.

The operational significance of this effect is that pilots should be specifically cautioned against any large or rapid rearward stick motions while in steep descents. Figure 12 indicates that there is no need for similar caution with regard to forward stick motions.

The normal reaction of a pilot to an excessive rate of sink is to increase collective pitch and power. The first effect of such control is an increase in vertical force, thereby increasing  $w_h$  and  $P_h$  and decreasing  $|V_G/w_h|$ . Figure 12 shows that this sequence initially requires a further increase in shaft power. Thus, the initial response to such control is likely to be an increased, rather than a decreased, rate of sink. The pilot's term for this phenomenon is "power settling"; the term is particularly apt and far more descriptive than "vortex-ring state."

#### Recovery From Power Settling

The optimum recovery from power settling cannot be obtained from considerations as simple as those presented herein. On the other hand, one obvious feature of a successful recovery, the effect of rotor inclination, is evident in figure 12. Figure 13 presents a direct comparison of shaft power for rotor inclinations of  $-10^\circ$  and  $10^\circ$ . For the steep approaches in which power settling is likely to be encountered, such a change from  $10^\circ$  to

$-10^\circ$  produces a major decrease in shaft power. Furthermore, the decrease in power is available only a few rotor revolutions after an abrupt forward movement of the cyclic stick. In addition, the forward rotor tilt increases the horizontal force  $F_X$  and the helicopter accelerates to a greater speed  $V_G$ , thus further reducing the required power. Conditions adequately safe for a major increase in collective pitch and power should be attained after a short time.

#### Avoidance of Power Settling

Any recovery from power settling is likely to result in a significant loss in altitude. Thus, the safest procedure is to fly so as to avoid power settling at all times. Many pilot's manuals are not very descriptive of the conditions to be avoided; however, certain obvious conclusions can be drawn from figure 12.

First, power settling is not likely to occur if the speed along the flightpath is reasonably high. A speed of 2 to 2 1/2 times  $|w_h|$  safely avoids power settling for any glide slope. On steep approaches, such speeds almost inevitably lead to negative shaft powers, that is, complete autorotation. Indeed, the power returned through the rotor can be so great at these speeds that there may be difficulty in preventing dangerous rotor overspeed conditions. Furthermore, if the glide slope is steep, such high speeds lead to excessive descent rates. (Observe that at  $\gamma = 45^\circ$ , the vertical and horizontal speeds of the helicopter are equal.)

Second, power settling is unlikely to occur if the glide slope is shallow. Limiting glide slopes to  $10^\circ$  or  $15^\circ$  avoids power settling at almost any forward speed.

### AUTOROTATION IN FORWARD FLIGHT

The preceding figures have illustrated many conditions for which the shaft power is less than or equal to zero. Such results should be anticipated in view of the known autorotative capability of rotorcraft. The following sections of this paper pursue this aspect of the momentum theory in an effort to delineate the conditions for which autorotative flight is possible.

#### Ideal Autorotation

Ideal autorotation is the condition of zero shaft power; thus, in equation (19), set  $P_s$  equal to zero, and solve for  $F_X/F_Z$ , to obtain

$$\frac{F_X}{F_Z} = \frac{-(w_0 + V_G \sin \gamma)}{u_0 + V_G \cos \gamma} \quad (40)$$

Inspection of figure 1 shows that the right-hand side of equation (40) is merely the cotangent of the wake skew angle  $\chi$ . Furthermore, from equation (10),  $F_X/F_Z$  is the tangent of the rotor inclination  $\theta$ ; thus  $\tan \theta = \cot \chi$ , or

$$\theta = 90^\circ - \chi \quad (41)$$

Equation (41) shows that for ideal autorotation  $\theta$  is the complement of  $\chi$ . Under these conditions figure 1 shows that the resultant velocity  $V_R$  lies exactly in the plane of the rotor. Therefore, the condition for ideal autorotation in forward flight is similar to that in vertical flight; namely, the component of resultant velocity through the rotor disk is zero. On the other hand, there is also a significant difference because, in forward flight,  $V_R$  itself is not necessarily zero.

#### Conditions for Ideal Autorotation

Now that the character of the flow at zero shaft power is defined, the conditions of speed  $V_G$ , inclination  $\theta$ , and glide slope  $\gamma$  which result in ideal autorotation ( $P_s = 0$ ) can be determined. Substitute equation (41) into equation (17) to obtain

$$\sin \theta = \left( \frac{w_0}{w_h} \right)^2 \left( 1 + \frac{V_G}{w_0} \sin \gamma \right) \quad (42)$$

Now solve equation (42) for  $w_0/w_h$  to yield

$$\frac{w_0}{w_h} = -\frac{1}{2} \frac{V_G}{w_h} \sin \gamma + \frac{1}{2} \sqrt{\left( \frac{V_G}{w_h} \right)^2 \sin^2 \gamma + 4 \sin \theta} \quad (43)$$

Next solve equation (22) for  $w_0/w_h$  to obtain, after some trigonometric simplification,

$$\frac{w_0}{w_h} = \frac{-V_G}{w_h} \cos \theta \sin (\theta + \gamma) \quad (44)$$

Observe that  $\theta + \gamma = \alpha$ , the rotor angle of attack with respect to the flightpath. Finally, equate equations (43) and (44), and solve for  $(V_G/w_h)^2$  to obtain

$$\left( \frac{V_G}{w_h} \right)^2 = \frac{2}{\cos \theta \sin 2(\theta + \gamma)} \quad (45)$$

Equation (45) relates  $\theta$ ,  $\gamma$ , and  $V_G$  for ideal autorotation.

### Minimum Speed for Autorotation

In order to obtain the minimum speed for which ideal autorotation is possible, differentiate equation (45) with respect to  $\gamma$ , set the differential equal to zero, and solve for  $\gamma$  to obtain

$$\gamma = 45^\circ - \theta \quad (46)$$

Now substitute equation (46) into equation (45) to yield

$$\left(\frac{V_G}{w_h}\right)_{\min}^2 = \frac{2}{\cos \theta} \quad (47)$$

The minimum of equation (47) obviously occurs when  $\theta = 0^\circ$ , so that

$$V_{G,\min} = -\sqrt{2} w_h \quad (48)$$

This minimum speed occurs with  $\gamma = 45^\circ$  (eq. (46)) and  $\chi = 90^\circ$  (eq. (41)). It is interesting to observe that the minimum speed occurs when the wake is horizontal. Furthermore, since the glide slope is  $45^\circ$ , the horizontal and vertical components of  $V_G$  at minimum speed are identical and simply equal to  $-w_h$ .

### Maximum Vertical-Force Coefficient

It is of some interest to consider the maximum possible vertical-force coefficient in ideal autorotation. This coefficient may be rewritten as

$$C_Z = \frac{F_Z}{\frac{\rho}{2} \left(\frac{V_G}{w_h}\right)^2 w_h^2 \pi R^2} \quad (49)$$

Substitute equation (6) into equation (49) and simplify the result to yield

$$C_Z = \frac{4}{\left(\frac{V_G}{w_h}\right)^2} \quad (50)$$

Equation (50) shows that the maximum vertical-force coefficient is obtained at the minimum value of  $V_G$ ; substitute equation (48) into equation (50) to obtain

$$C_{Z,\max} = 2 \quad (51)$$

It is obvious that there is nothing really remarkable about the performance of the autorotating rotor. Even under optimum ideal conditions, the low-speed performance is largely obtained by the relatively large swept area of the rotor disk and the absence of separation except locally on some blade elements.

#### Maximum Lift Coefficient

When steep glide slopes are permitted, the lift coefficient may be significantly different from the vertical-force coefficient. To obtain the lift coefficient, consider the vector diagram of figure 14, from which

$$C_L = C_Z (\cos \gamma - \tan \theta \sin \gamma) \quad (52)$$

Substitute equations (45) and (50) into equation (52) and simplify to yield

$$C_L = 4 \sin(\theta + \gamma) \cos^2(\theta + \gamma) \quad (53)$$

Equation (53) depends only on the sum of  $\theta$  and  $\gamma$ . Since  $\theta + \gamma = \alpha$ , the tip-path plane angle of attack, such a result should be anticipated. To obtain the maximum value of  $C_L$ , differentiate equation (53) with respect to  $(\theta + \gamma)$ , set the differential equal to zero, and solve for  $(\theta + \gamma)$  to yield

$$\left. \begin{aligned} \cos(\theta + \gamma) &= \cos \alpha = \sqrt{\frac{2}{3}} \\ \sin(\theta + \gamma) &= \sin \alpha = \sqrt{\frac{1}{3}} \\ \theta + \gamma &= \alpha \approx 35.264^\circ \end{aligned} \right\} \quad (54)$$

Substitution of equations (54) into equation (53) yields

$$C_{L,\max} = \frac{8}{9} \sqrt{3} \approx 1.5396 \quad (55)$$

The maximum lift coefficient of the autorotating rotor is even less impressive than its vertical-force coefficient (eq. (51)). The speed for  $C_{L,max}$  differs from that for  $C_{Z,max}$ . To determine this speed, first solve equations (54) for  $\cos \theta$  to yield

$$\cos \theta = \sqrt{\frac{2}{3}} \cos \gamma + \sqrt{\frac{1}{3}} \sin \gamma \quad (56)$$

Now substitute equations (54) and (56) into equation (45) to obtain

$$\left(\frac{V_G}{w_h}\right)^2 = \frac{3\sqrt{3}}{2 \cos \gamma + \sqrt{2} \sin \gamma} \quad (57)$$

The minimum speed at which the classic autogyros of the 1930's could operate is obtained by setting  $\gamma$  equal to zero in equation (57) to yield

$$V_{G,min} = -\sqrt[4]{\frac{27}{4}} w_h \approx -1.6119 w_h \quad (58)$$

Operation at such low speeds is not particularly efficient, as may be seen from equation (10) by noting that for  $\gamma = 0$ ,  $F_X = D$ ,  $F_Z = L$ , and  $\alpha = \theta$ , so that from equations (54),  $L/D = \sqrt{2}$  at  $V_{G,min}$ .

When descending flight is permitted, the descent angle for minimum speed is obtained by differentiating equation (57) with respect to  $\gamma$ , setting the differential equal to zero, and solving for  $\gamma$  to obtain

$$\gamma = \cos^{-1} \sqrt{\frac{2}{3}} \approx 35.264^\circ \quad (59)$$

the corresponding rotor inclination is  $\theta = 0^\circ$  (from eqs. (54)). The minimum speed (corresponding to  $C_{L,max}$ ) is then obtained by substituting equation (59) into equation (57) to yield

$$V_{G,min} = -\sqrt[4]{\frac{9}{2}} w_h \approx -1.4565 w_h \quad (60)$$

The limiting lift coefficients found for the autorotating rotor are modest compared to those obtained from many wings. This subject is covered more completely in the appendix where equivalent expressions are developed for wings.

### Performance in Autorotation

The performance of the autorotating rotor is most conveniently shown in terms of the nondimensional rate of sink  $\left( -\frac{V_G}{w_h} \sin \gamma \right)$  and nondimensional forward speed  $\left( -\frac{V_G}{w_h} \cos \gamma \right)$ . For ideal autorotation, where the shaft power is identically zero, the combinations of forward speed and sink rate which produce autorotation are obtained simply from equation (45). These combinations are shown in figure 15(a).

In a practical rotorcraft, the rotor must extract sufficient additional power from the air to operate the tail rotor and to account for gearbox and accessory losses as well as to overcome blade-profile losses and inefficiencies in producing the induced forces. Thus, in practice, the theoretical shaft power must have a substantial negative value. By assuming a reasonable value of  $P_s/P_h$  of -0.5, the autorotative performance has been obtained by interpolation from calculations based on equations (13) and (22). These results are presented in figure 15(b).

In figure 15 the theoretical values are omitted for the steepest glide slopes where multiple values are obtained from equation (13). As noted in the sections on vertical descent, the minimum autorotative descent rates in vertical flight are found experimentally to be of the order of  $-1.8 w_h$ . This approximation should be adequate over most of the extreme glide-slope range ( $75^\circ$  to  $90^\circ$ ).

The theoretical curves of figure 15 satisfy the required power ratios and maintain constant vertical force. In addition, it is necessary to satisfy horizontal equilibrium. This equilibrium is obtained through a suitable variation of tip-path-plane inclination which must be zero when the speed is zero and must decrease in a parabolic manner as the speed increases. If such a variation of  $\theta$  is assumed and traced out in figure 15, the descent rate is found to have a minimum at some forward speed on the order of

$$2 < \left| \frac{V_G}{w_h} \right| \cos \gamma < 3. \text{ Further increases of speed require an increased descent rate.}$$

### Comparison With Flight Measurements

Autorotative conditions.- The theoretical curves of figure 15(b) ( $P_s/P_h = -0.5$ ) are compared to flight measurements in figure 16. The flight data were obtained by a research pilot; however, the aircraft was not specifically instrumented for the tests. In particular, no direct power measurements were made. The autorotation curve was delineated (subjectively to some extent) by listening for the point at which the transmission gear teeth began to chatter. Further, the vertical and horizontal speeds were obtained from the

normal aircraft instruments which are not precise throughout much of the range of interest. The rotor inclination in flight was not measured; however, as observed earlier, the inclination must vary from  $0^\circ$  in vertical flight to some modest negative value in forward flight in order to maintain a balance of forces in the X-direction. Thus, figure 16 shows the theoretical calculations for several rotor inclinations.

Despite the crude nature of both the theory and the experiment, the results shown in figure 16 are surprisingly good. At the maximum forward speed for which measurements were made, it is necessary to assume only a modest  $6^\circ$  or  $7^\circ$  rotor inclination to achieve agreement.

Additional comments.- In practice, full autorotation occurs in or near the windmill-brake state and serious problems no longer occur. No analogous definition of the onset of severe flight problems is to be found in the relatively smooth theoretical curves at small descent angles or small descent rates. Nevertheless, some problems do exist, and these problems are indicated by the flight data.

Figure 16 shows a boundary along which the pilot could sense vibration or unsteadiness. These features were barely perceptible on the boundary; however, they became greater in magnitude with proximity to the shaded region within which the aircraft became uncontrollable in pitch and roll. The same guidelines presented in the section entitled "Avoidance of Power Settling" ( $\gamma < 10^\circ$  or  $15^\circ$ , or  $V_G > 2$  to  $2.5|w_h|$ ) avoid these problems.

The uncontrollable region in near-vertical descent is of interest because of the very mild descent rates at which this region is encountered. Analyses based on the isolated rotor (refs. 4 and 13) indicate that this problem should not be anticipated except at descent rates twice those of figure 16. However, the data of figure 16 are confirmed by much earlier flight experiments such as those of reference 14. The smoke-flow photographs of figure 3 indicate clearly that major flow fluctuations occur at the fuselage at lesser descent rates than required for similar fluctuations at the rotor itself. It seems reasonable to assume that the onset of the difficulty is caused by the effect of this violently unstable flow on the fuselage rather than on the rotor.

#### CONCLUDING REMARKS

A momentum theory has been developed for the specific purpose of treating rotors in descending flight. Available experimental results indicate that, when properly interpreted, the theory yields the ideal performance of the rotor. Calculations and data indicate that multiengine design will not significantly reduce the "deadman's region" from which safe vertical autorotative recovery is impossible unless the design is such that the helicopter can still hover after the failure of one engine.

Calculations based on the theory indicate the cause of power settling as well as means of avoiding it. In addition, the calculations demonstrate the need, and the reasons, for severe operational restrictions on the descent of rotary wing aircraft. These restrictions include:

1. Vertical descent should be avoided whenever possible.
2. If vertical descent is required, it should be attempted only from the minimum allowable height above the ground and at the minimum possible descent rate.
3. Steep descents at low speeds should be avoided. Even small winds imperceptible to the pilot may result in power settling.
4. Pilots should be particularly cautioned against large or rapid rearward stick movement in steep descents.
5. Descending flight should be limited to glide-slope angles of no more than  $10^{\circ}$  or  $15^{\circ}$  and speed along the flightpath should be kept high, preferably in excess of 2 to  $2\frac{1}{2}$  times the hovering induced velocity.

Autorotation in forward flight has been examined and the optimum performance in autorotation has been determined. Flight measurements of autorotative performance indicate good agreement with the rates of descent obtained from the theory.

An appendix derives equivalent momentum theory equations for a wing. It is demonstrated that the ideal performance of an autorotating rotor is identical to that of a wing of equal aspect ratio. In addition, expressions for the limiting maximum lift of a finite wing are developed and it is shown that any other values of maximum lift would require that power must be either supplied to, or removed from, the wing itself.

Langley Research Center  
National Aeronautics and Space Administration  
Hampton, Va. 23665  
June 30, 1975

## APPENDIX

### COMPARISON OF THE MAXIMUM PERFORMANCE OBTAINABLE FROM AUTOROTATING ROTORS AND FINITE WINGS

Since the maximum lift and vertical-force coefficients indicated for autorotating rotors in the main sections of this paper are of the same magnitude as those which would be expected from a finite wing, it is interesting to compare the two lifting systems on a common basis. In this appendix, relations equivalent to those of the main text are developed for the finite wing, thus permitting a direct comparison. Two differences must be accounted for.

The first difference is that the effective area for determining the affected mass flow is not the wing area; instead, following Prandtl (ref. 15), the effective, or momentum, area is taken as the area of a circle circumscribing the wing tips, thus

$$A_m = \frac{\pi}{4} b^2 \quad (A1)$$

The area  $A_m$  must replace the rotor area  $\pi R^2$  in all of the equations of the main text. Note, in particular, that  $w_h$  now has no physical meaning since a wing cannot hover; however, it is still useful as a convenient reference velocity. Thus, substituting  $A_m$  for  $\pi R^2$  in equation (6)

$$w_h = -\sqrt{\frac{F_Z}{2\rho A_m}} = -V_G \sqrt{\frac{C_Z}{\pi A}} \quad (A2)$$

The second difference is that there is no simple relationship between  $\theta$  and  $F_X/F_Z$  to correspond with that for a rotor (eq. (10)). Thus, the derivation must be carried out without recourse to equation (10).

In considering the simple unpowered wing, it will be observed that the "shaft power" must always be zero, for, indeed, there is no equivalent of a shaft with which either to provide power or to extract power directly from the wing. The losses of the wing must always be overcome by the application of power elsewhere in the system. Therefore, following in the manner of equation (40)

$$\frac{F_X}{F_Z} = \cot \chi \quad (A3)$$

## APPENDIX

The resultant velocity  $V_R$  is not required to lie in the plane of the wing; however, equation (A3) requires that the resultant force vector be normal to the wake at the wing and, specifically, not normal to the far wake. Any other inclination of the resultant force vector would require an inadmissible power input or output through the wing.

Now solve equation (17) to yield

$$\frac{w_0}{w_h} = -\frac{1}{2} \frac{V_G}{w_h} \sin \gamma + \frac{1}{2} \sqrt{\left(\frac{V_G}{w_h}\right)^2 \sin^2 \gamma + 4 \cos \chi} \quad (A4)$$

Next, set  $P_s/P_h$  to zero in equation (21) and solve for  $w_0/w_h$  to obtain

$$\frac{w_0}{w_h} = \frac{-V_G}{w_h} \sin \chi \cos (\chi - \gamma) \quad (A5)$$

Finally, equate equations (A4) and (A5), and solve for  $(V_G/w_h)^2$ , to yield

$$\left(\frac{V_G}{w_h}\right)^2 = \frac{2}{\sin \chi \sin (\chi - \gamma)} \quad (A6)$$

The glide slope for the minimum flight speed is obtained by differentiating equation (A6) with respect to  $\gamma$ , setting the differential equal to zero, and solving for  $\gamma$  to obtain

$$\gamma = \chi - 45^\circ \quad (A7)$$

Now substitute equation (A7) into equation (A6) to obtain the minimum speed as a function of the wake skew angle

$$\left(\frac{V_G}{w_h}\right)_{\min}^2 = \frac{2}{\sin \chi} \quad (A8)$$

The minimum of equation (A8) obviously occurs when the wake, as before, is horizontal ( $\chi = 90^\circ$ ), and also, from equation (A7), the optimum glide slope is once more  $45^\circ$ . The minimum speed for the wing is

$$V_{G,\min} = -\sqrt{2} w_h \quad (A9)$$

## APPENDIX

Thus, for a given wing, there is a minimum possible flight speed determined by  $w_h$ . If a lower speed is required, it can only be obtained by increasing the wing span to decrease  $w_h$ . Equations (A1), (A2), and (A9) show that the minimum speed is directly proportional to  $1/b$ . Because the resultant force is normal to the wake,  $F_X/F_Z = 0$  for the above condition; however,  $L/D$ , which is referenced to the flightpath, is 1.0.

For a wing, the vertical-force coefficient may be rewritten as

$$C_Z = \frac{F_Z}{\frac{\rho}{2} \left(\frac{V_G}{w_h}\right)^2 w_h^2 \left(\frac{S}{A_m}\right) A_m} \quad (A10)$$

Substitute equations (A1) and (A2) into equation (A10), and note that  $A = b^2/S$ , to yield

$$C_Z = \frac{\pi A}{\left(\frac{V_G}{w_h}\right)^2} \quad (A11)$$

Equation (A11) shows that the maximum vertical-force coefficient can be obtained at the minimum value of  $(V_G/w_h)^2$ ; thus, substitute equation (A9) into equation (A11) to yield

$$C_{Z,\max} = \frac{\pi}{2} A \quad (A12)$$

The lift coefficient is obtained by substituting equation (10) into equation (52); thus,

$$C_L = C_Z \left( \cos \gamma - \frac{F_X}{F_Z} \sin \gamma \right) \quad (A13)$$

Now, substitute equation (A3) into equation (A13) to obtain

$$C_L = C_Z \frac{\sin (\chi - \gamma)}{\sin \chi} \quad (A14)$$

## APPENDIX

Then, substitute equation (A11) into equation (A14) to yield

$$C_L = \pi A \sin^2 (\chi - \gamma) \cos (\chi - \gamma) \quad (A15)$$

Thus,  $C_L$  is a function of  $\chi - \gamma$  only. It will be observed that  $\chi - \gamma = \chi_G$ , the wake skew angle measured from a normal to the glide slope. The maximum lift coefficient is found, by differentiation, to occur at

$$\left. \begin{aligned} \sin \chi_G &= \sin (\chi - \gamma) = \sqrt{\frac{2}{3}} \\ \cos \chi_G &= \cos (\chi - \gamma) = \sqrt{\frac{1}{3}} \\ \chi_G &= \chi - \gamma \approx 54.736^\circ \end{aligned} \right\} \quad (A16)$$

Now substitute equations (A16) into equation (A15) to obtain

$$C_{L,\max} = \pi A \frac{2}{3} \sqrt{\frac{1}{3}} \approx 1.2092A \quad (A17)$$

The forward speed at which this maximum lift coefficient is obtained is found by solving equations (A16) for  $\sin \chi$  to obtain

$$\sin \chi = \sqrt{\frac{2}{3}} \cos \gamma - \sqrt{\frac{1}{3}} \sin \gamma \quad (A18)$$

and then substituting equations (A16) and (A18) into equation (A6) to yield

$$\left( \frac{v_G}{w_h} \right)^2 = \frac{3\sqrt{3}}{2 \cos \gamma + \sqrt{2} \sin \gamma} \quad (A19)$$

which is identical to equation (57); thus, as before, the minimum speed in level flight is

$$v_{G,\min} = - \sqrt[4]{\frac{27}{4}} w_h \approx -1.6119 w_h \quad (A20)$$

with  $L/D = \sqrt{2}$ , and the minimum speed in descending flight is

## APPENDIX

$$V_{G,\min} = -\sqrt[4]{\frac{9}{2}} w_h \approx 1.4565 w_h \quad (A21)$$

with  $\gamma = \cos^{-1} \sqrt{\frac{2}{3}} \approx 35.264^\circ$ .

If the aspect ratio of a rotor ( $4/\pi$ ) is substituted for  $A$  in the equations of this appendix, the maximum lifts and minimum speeds of the main text are reproduced exactly. Thus, the theoretical ideal performance of the autorotating rotor is identical to that of a wing of equal aspect ratio. Differences exist in actual practice since the angles of attack required to obtain the maximum performance undoubtedly completely stall the wing, whereas, on the rotor, stall is confined to certain local blade elements.

Equation (A17) is of particular interest since it indicates a maximum lift coefficient which depends only on aspect ratio. The identical result was obtained earlier in reference 16. Other investigators (for example, refs. 17 to 19) have obtained different results; however, those results were attained by assuming the force vector  $\bar{F}$  to be normal to the final wake which may be rolled up. Such assumptions do not meet the requirements of zero "shaft" power at the wing (eq. (A3)) and, as observed earlier, would require an impermissible power input or output directly through the wing.

Even with extreme attempts at boundary-layer control, the flow generally separates from a wing prior to the attainment of lift coefficients as great as those given by equation (A17). The most appropriate data are often assumed to be those of reference 20, where the lift coefficients were obtained by subtracting the direct thrust contributions from the data obtained during wind-tunnel tests of a series of jet-flapped wings (ref. 19). Figure 17 compares those data with equation (A17) on the assumption that  $C_L$  is the "circulation" lift coefficient. The theoretical result is shown to be a good approximation to the measured data.

Even the differences between theory and experiment in figure 17 may result from the fact that the tests predated the development of modern wall-interference theories (such as ref. 21) which are appropriate to such large wake deflections. The presence of a wall-induced upwash is equivalent to a glide-slope angle. Since the wind-tunnel forces are measured on a balance aligned with the tunnel, or apparent, flow direction, the test data, to the extent that they are uncorrected, are the equivalent of  $C_Z$  rather than  $C_L$ . A comparison of equation (A12) to equation (A17) shows clearly that  $C_{Z,\max}$  may be greater than  $C_{L,\max}$  in the presence of a glide slope.

## REFERENCES

1. Kimball, Kent A.; Harden, Donald F.; and Hofmann, Mark A.: Army Autorotational Accidents. Escape Problems and Manoeuvres in Combat Aircraft, W. L. Jones, ed., AGARD-CP-134, Feb. 1974, pp. A14-1-A14-10.
2. De Bothezat, George: The General Theory of Blade Screws. NACA Rep. 29, 1919.
3. Lock, C. N. H.; Bateman, H.; and Townend, H. C. H.: An Extension of the Vortex Theory of Airscrews With Applications to Airscrews of Small Pitch, Including Experimental Results. R. & M. No. 1014, British A.R.C., Sept. 1925.
4. Washizu, Kyuichiro; Azuma, Akira; Kōo, Jiro; and Oka, Tōichi: Experiments on a Model Helicopter Rotor Operating in the Vortex Ring State. J. Aircraft, vol. 3, no. 3, May-June 1966, pp. 225-230.
5. Castles, Walter, Jr.; and Gray, Robin B.: Empirical Relation Between Induced Velocity, Thrust, and Rate of Descent of a Helicopter Rotor as Determined by Wind-Tunnel Tests on Four Model Rotors. NACA TN 2474, 1951.
6. Heyson, Harry H.: Nomographic Solution of the Momentum Equation for VTOL-STOL Aircraft. NASA TN D-814, 1961. (Also available as "V-STOL Momentum Equation," Space/Aeronaut., vol. 38, no. 2, July 1962, pp. B-18-B-20.)
7. Glauert, H.: A General Theory of the Autogyro. R. & M. No. 1111, British A.R.C., 1926.
8. Wald, Quentin: A Method for Rapid Estimation of Helicopter Performance. J. Aero-naut. Sci., vol. 10, no. 4, Apr. 1943, pp. 131-135.
9. Heyson, Harry H.: A Note on the Mean Value of Induced Velocity for a Helicopter Rotor. NASA TN D-240, 1960.
10. Drees, J. Meijer; and Hendar, W. P.: Airflow Patterns in the Neighbourhood of Helicopter Rotors. Aircraft Eng., vol. XXIII, no. 266, Apr. 1951, pp. 107-111.
11. Gessow, Alfred; and Myers, Garry C., Jr.: Aerodynamics of the Helicopter. Macmillan Co., c.1952.
12. Gessow, Alfred: Flight Investigation of Effects of Rotor-Blade Twist on Helicopter Performance in the High-Speed and Vertical-Autorotative-Descent Conditions. NACA TN 1666, 1948.
13. Volkovitch, Julian: Analytical Prediction of Vortex-Ring Boundaries for Helicopters in Steep Descents. J. American Helicopter Soc., vol. 17, no. 3, July 1972, pp. 13-19.
14. Reeder, John P.; and Gustafson, F. B.: On the Flying Qualities of Helicopters. NACA TN 1799, 1949.

15. Prandtl, L.: Applications of Modern Hydrodynamics to Aeronautics. NACA Rep. 116, 1921.
16. McCormick, Barnes W.: The Limiting Circulatory Lift of a Wing of Finite Aspect Ratio. J. Aero/Space Sci., vol. 26, no. 4, Apr. 1959, pp. 247-248.
17. Helmbold, H. B.: Theory of the Highly Loaded Finite Span Wing. Eng. Rep. No. RR-35, Fairchild Aircraft (Hagerstown, Md.), Sept. 26, 1956. (See also Helmbold, Heinrich B.: Limitations of Circulation Lift. J. Aeronaut. Sci., vol. 24, no. 3, Mar. 1957, pp. 237-238.)
18. Cone, Clarence D., Jr.: A Theoretical Investigation of Vortex-Sheet Deformation Behind a Highly Loaded Wing and Its Effect on Lift. NASA TN D-657, 1961.
19. Hancock, G. J.: Comments on "Limiting Circulatory Lift of a Wing of Finite Aspect Ratio." J. Aero/Space Sci., vol. 27, no. 1, Jan. 1960, pp. 65-66.
20. Lowry, John G.; Riebe, John M.; and Campbell, John P.: The Jet-Augmented Flap. Preprint No. 715, S.M.F. Fund Paper, Inst. Aeronaut. Sci., Jan. 1957.
21. Heyson, Harry H.: Linearized Theory of Wind-Tunnel Jet-Boundary Corrections and Ground Effect for VTOL-STOL Aircraft. NASA TR R-124, 1962.

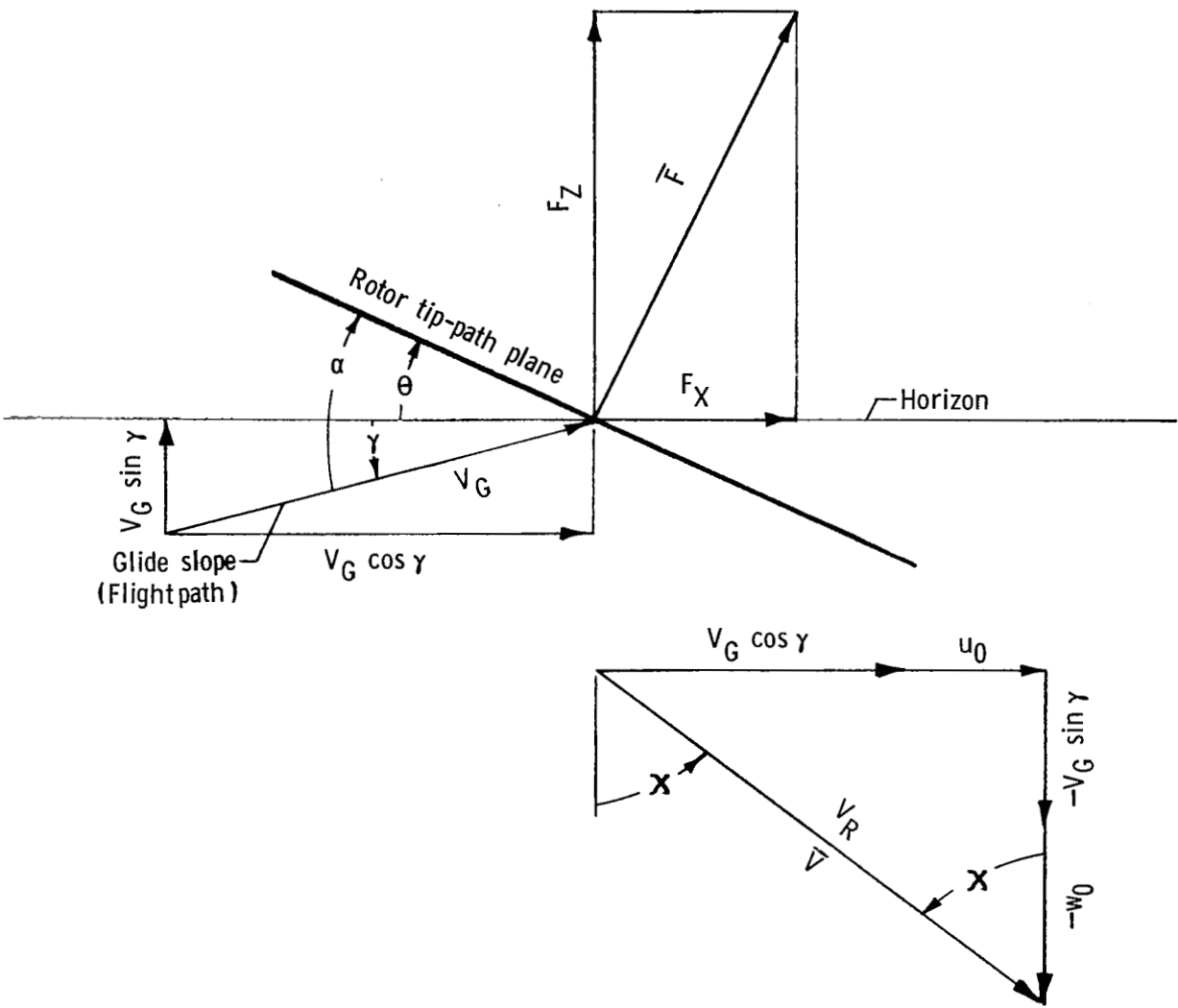
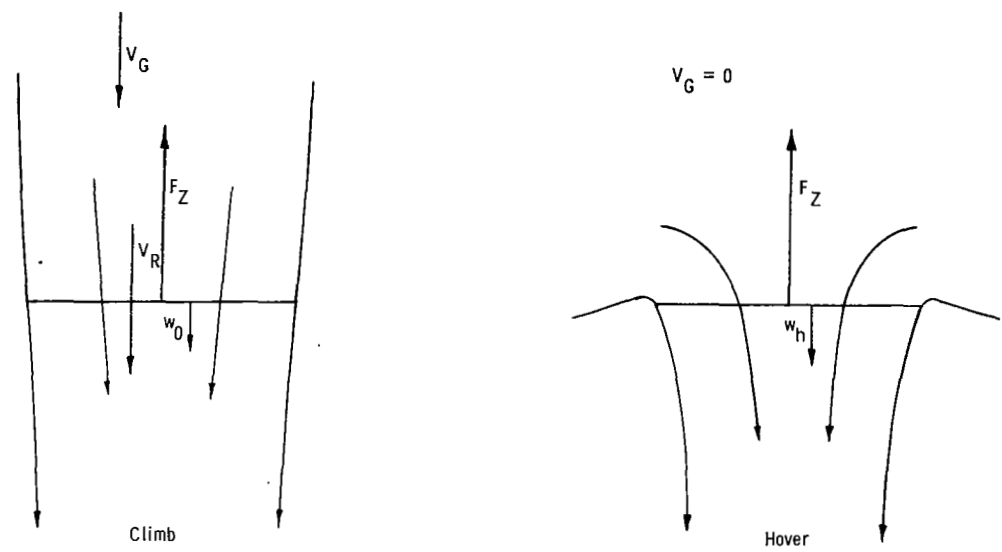
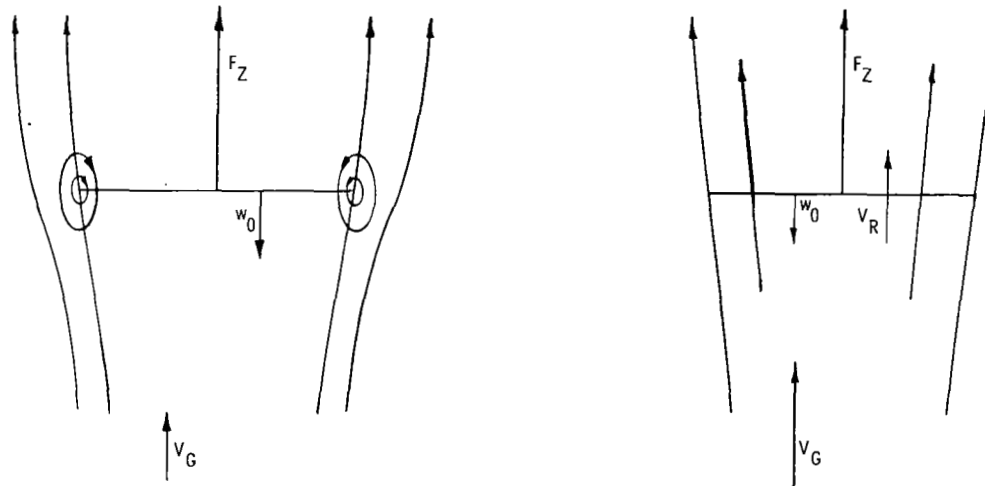


Figure 1.- Force and flow vectors at the rotor.



(a) Normal working state.



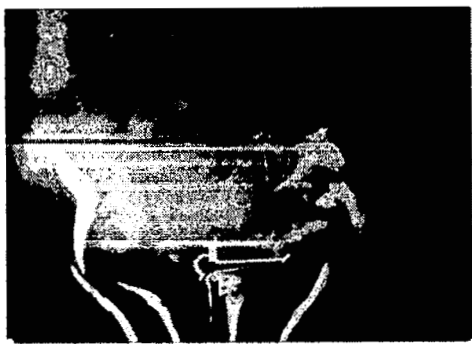
(b) Vortex-ring state.

(c) Windmill-brake state.

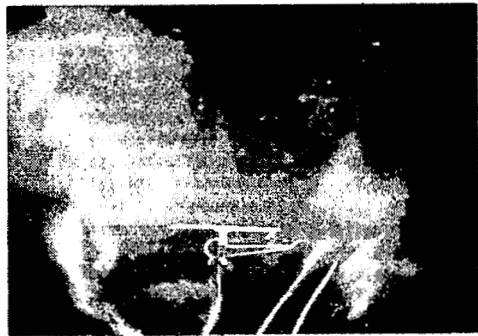
Figure 2.- Flow states of a rotor in vertical descent.



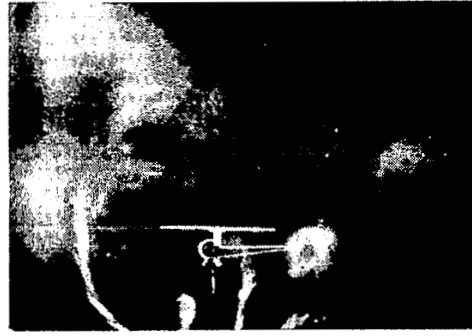
(a)



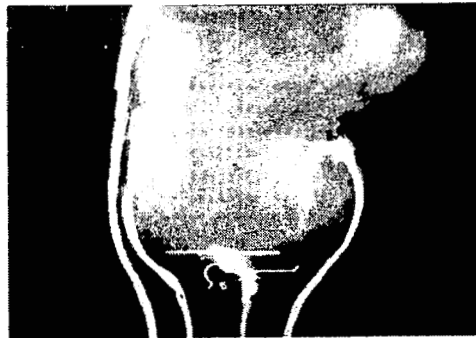
(b)



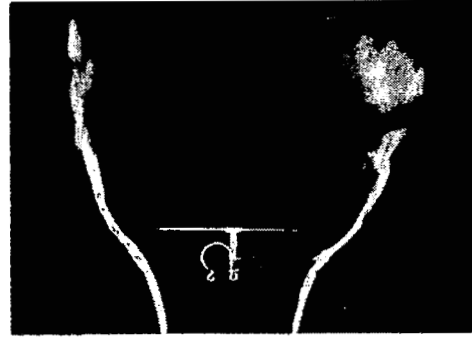
(c)



(d)



(e)



(f)

Figure 3.- Flow patterns in vertical descent with the descent rate increasing from (a) to (f). Hovering is shown in (a); the windmill-brake state in (f). (Photographs are from ref. 10.)

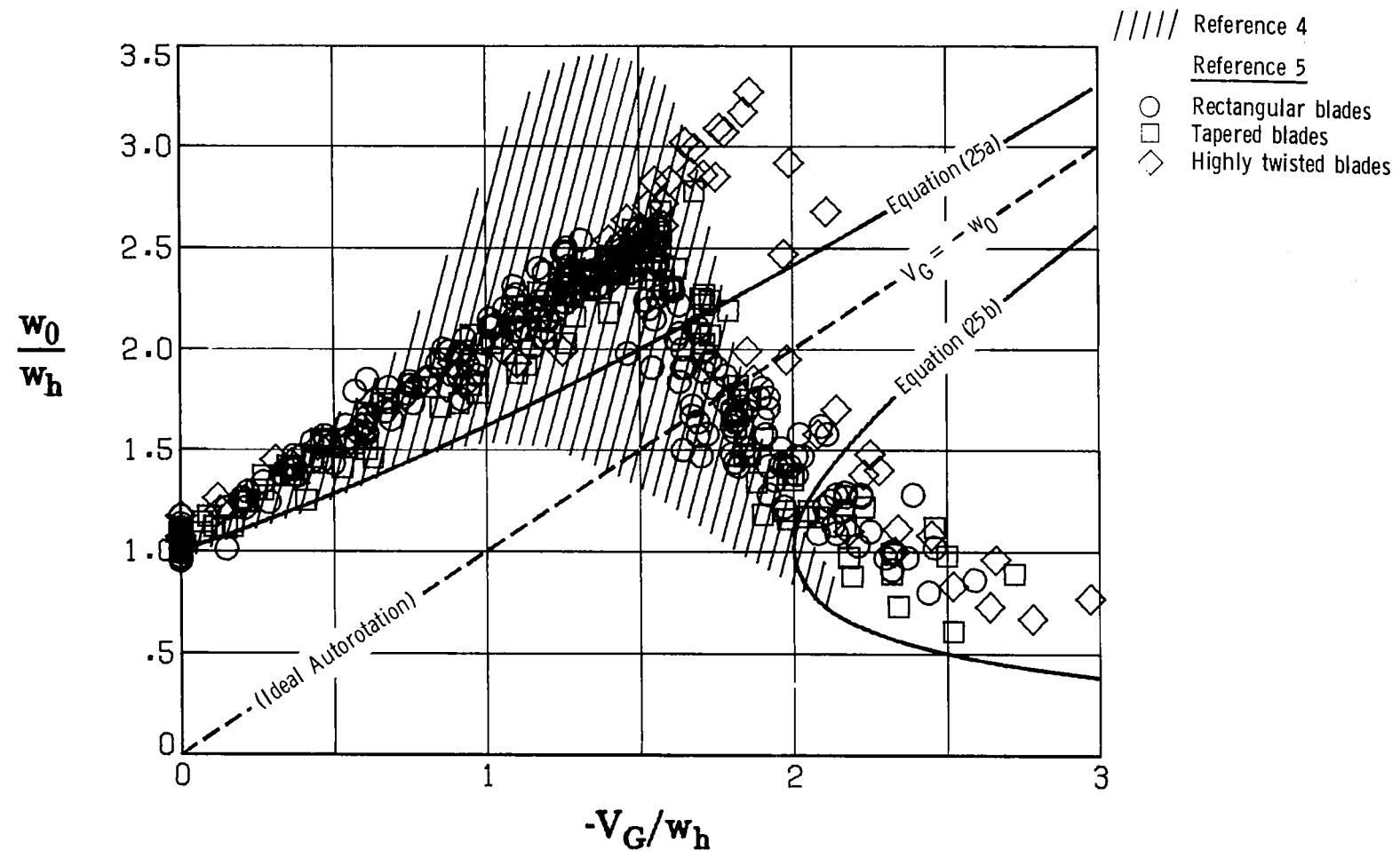


Figure 4.- Comparison of the theoretical induced-velocity ratio with the experimental data of references 4 and 5 ( $\gamma = 90^\circ$ ;  $\theta = 0^\circ$ ).

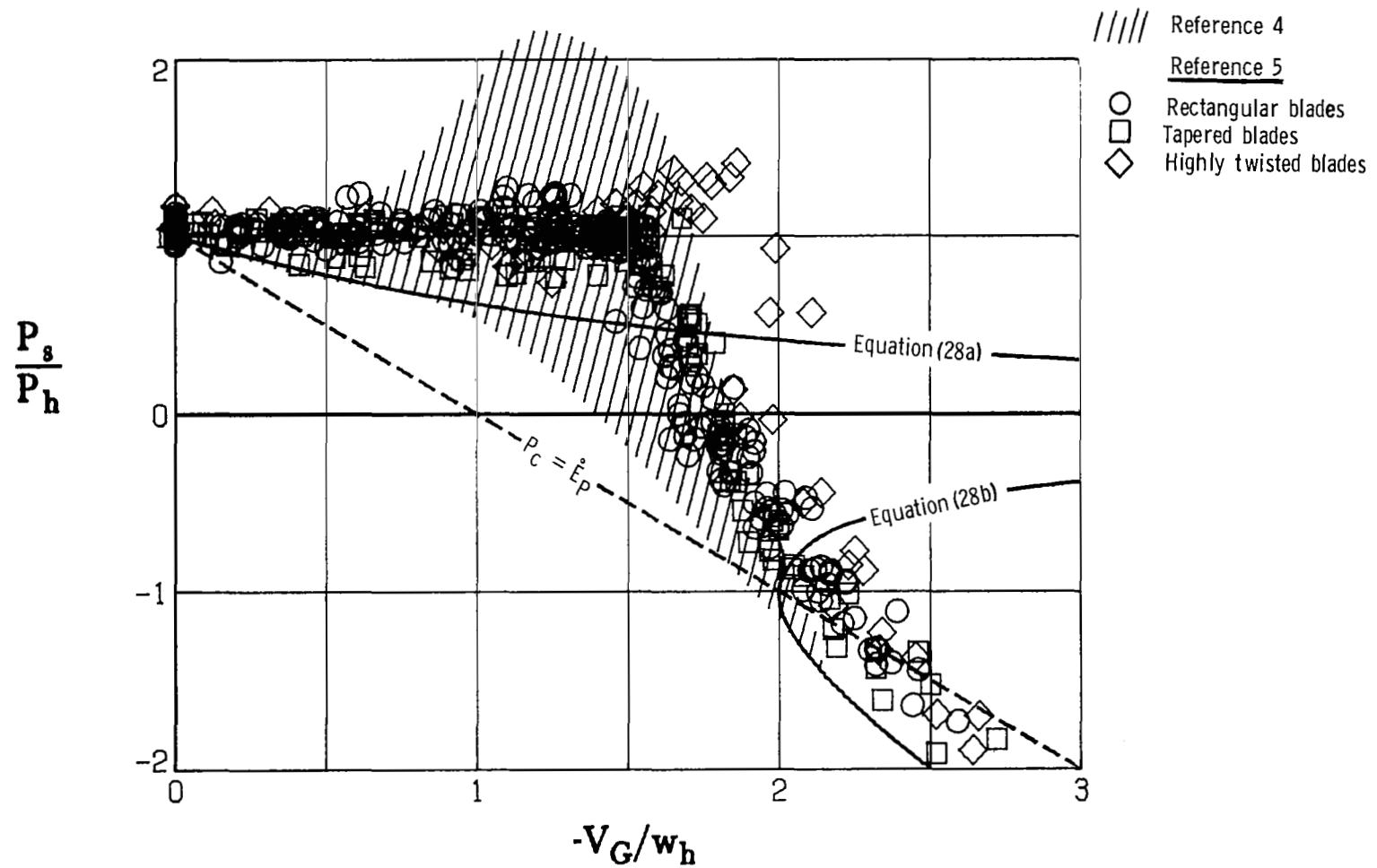


Figure 5.- Comparison of the theoretical shaft-power ratio with the experimental data of references 4 and 5 ( $\gamma = 90^\circ$ ;  $\theta = 0^\circ$ ).

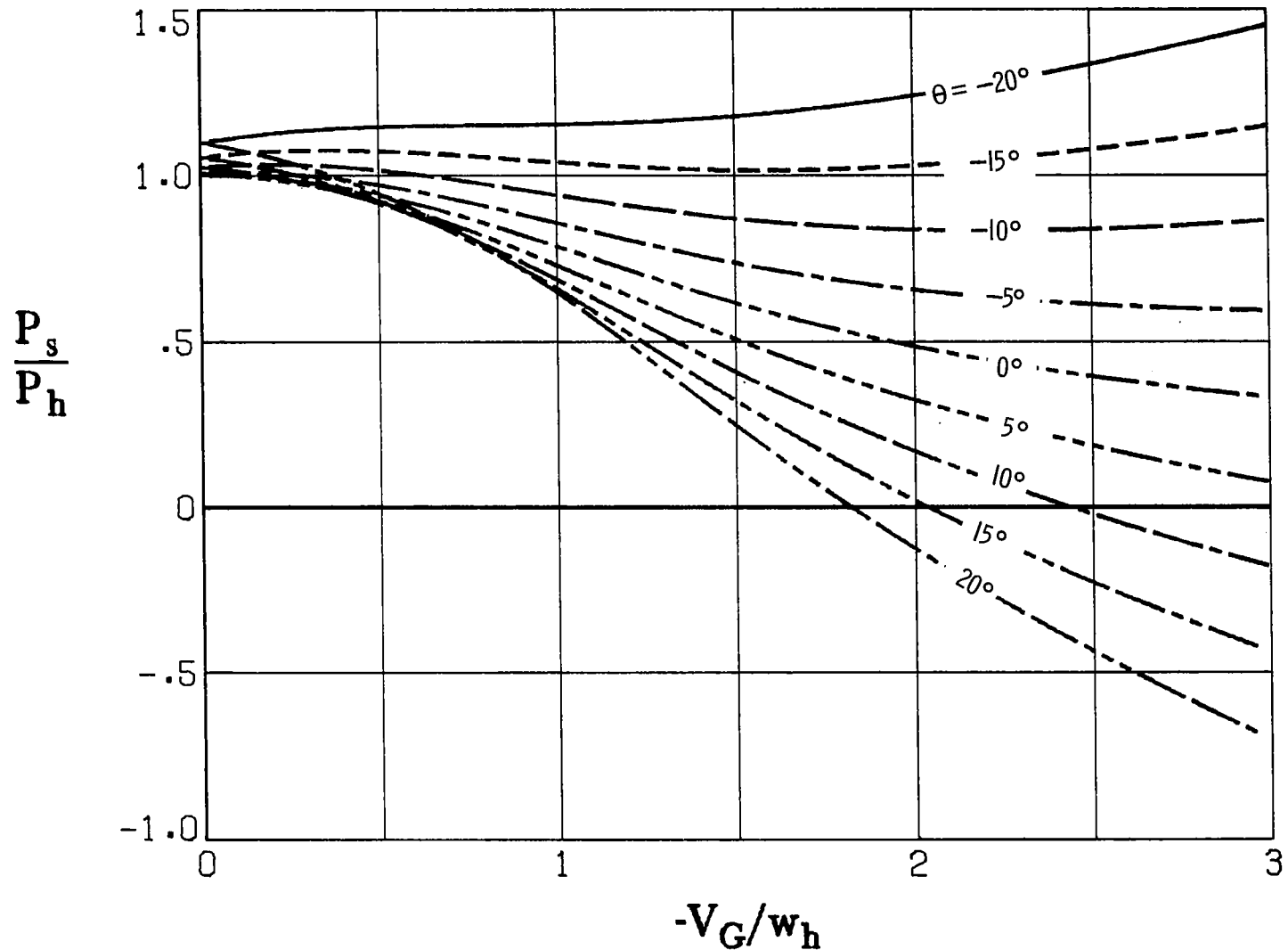
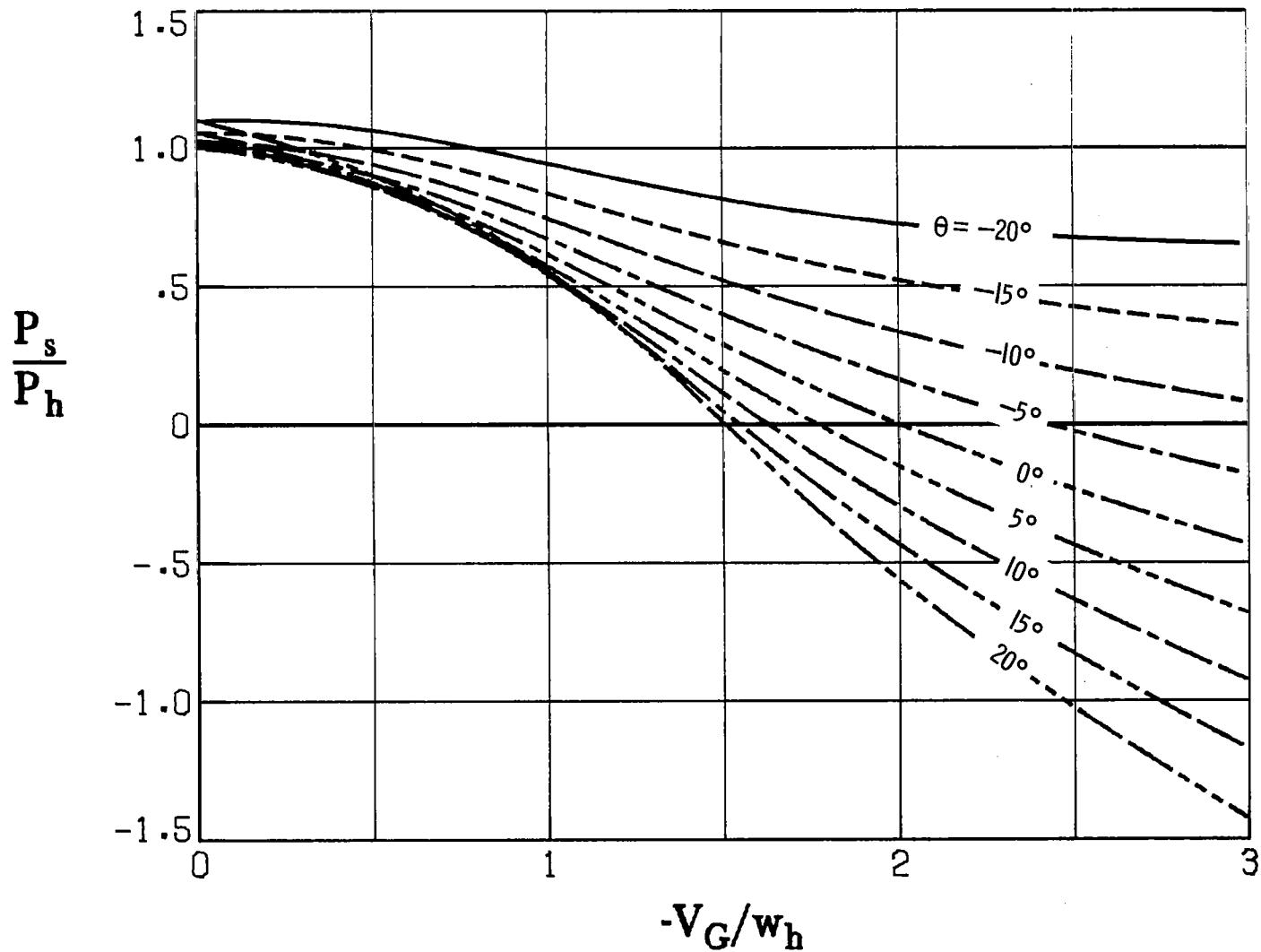
(a)  $\gamma = 0^\circ$ ; level flight.

Figure 6.- Shaft power as a function of glide-slope velocity at constant tip-path-plane inclination for different glide slopes.



(b)  $\gamma = 15^\circ$ .

Figure 6.- Continued.

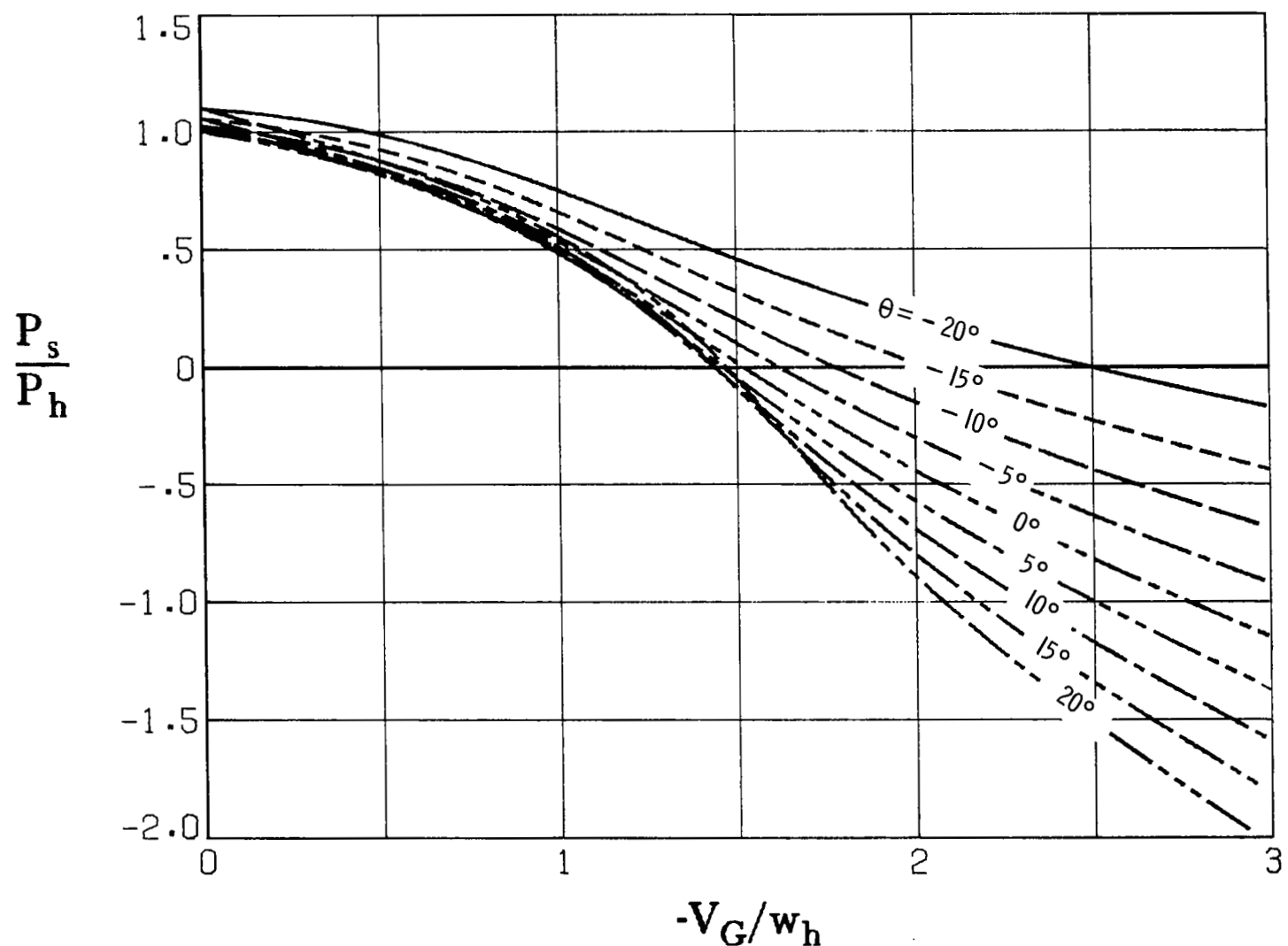
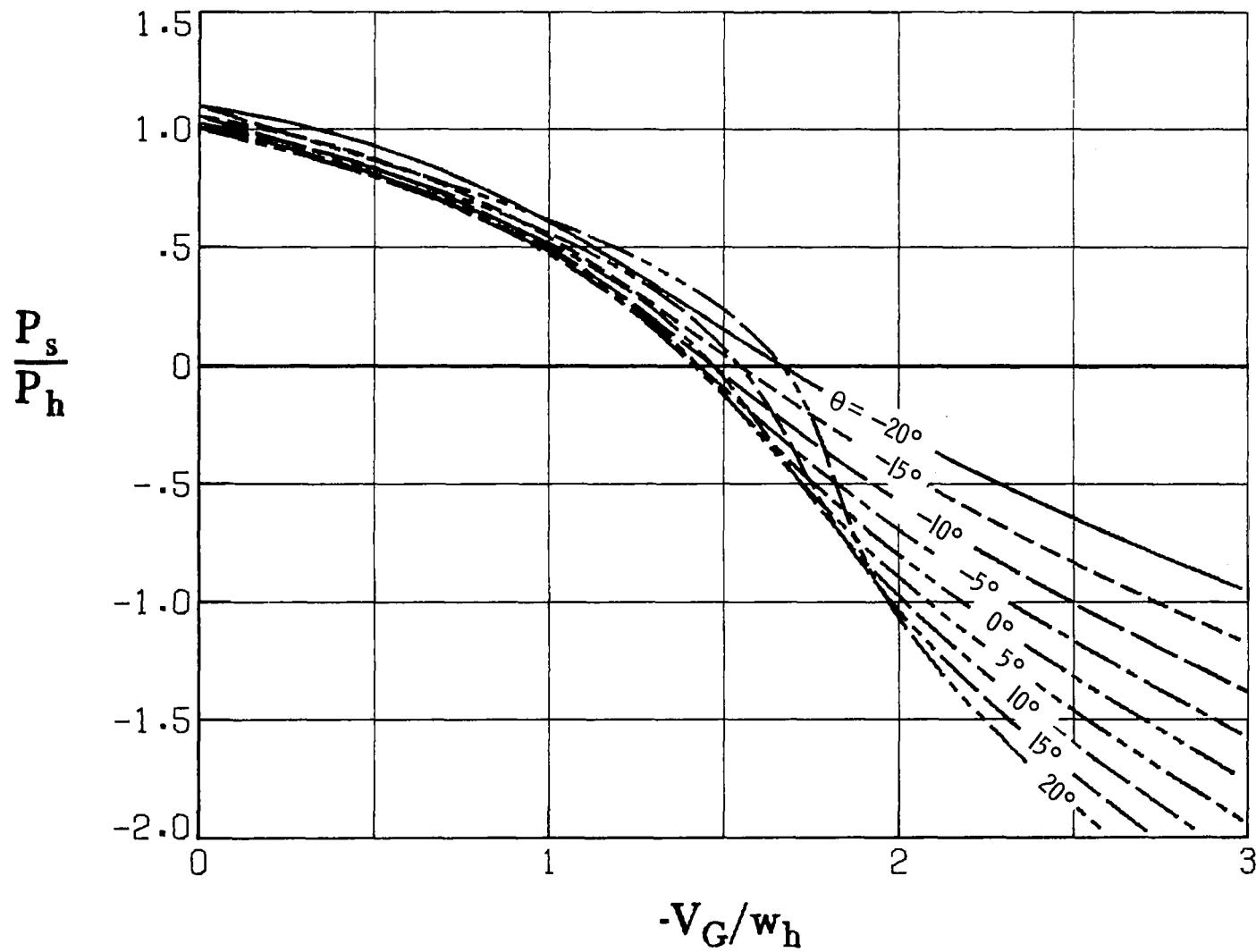
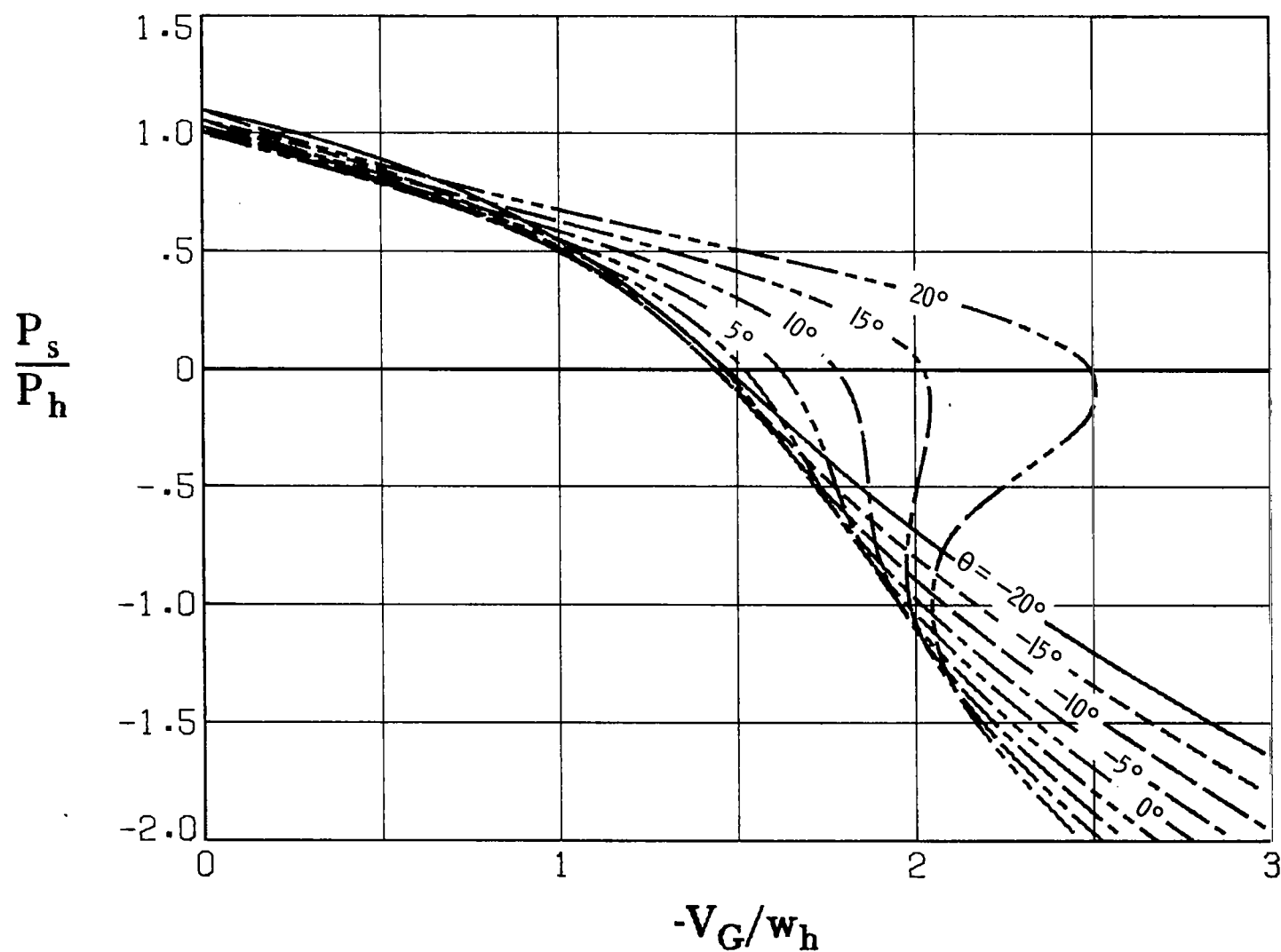
(c)  $\gamma = 30^\circ$ .

Figure 6.- Continued.



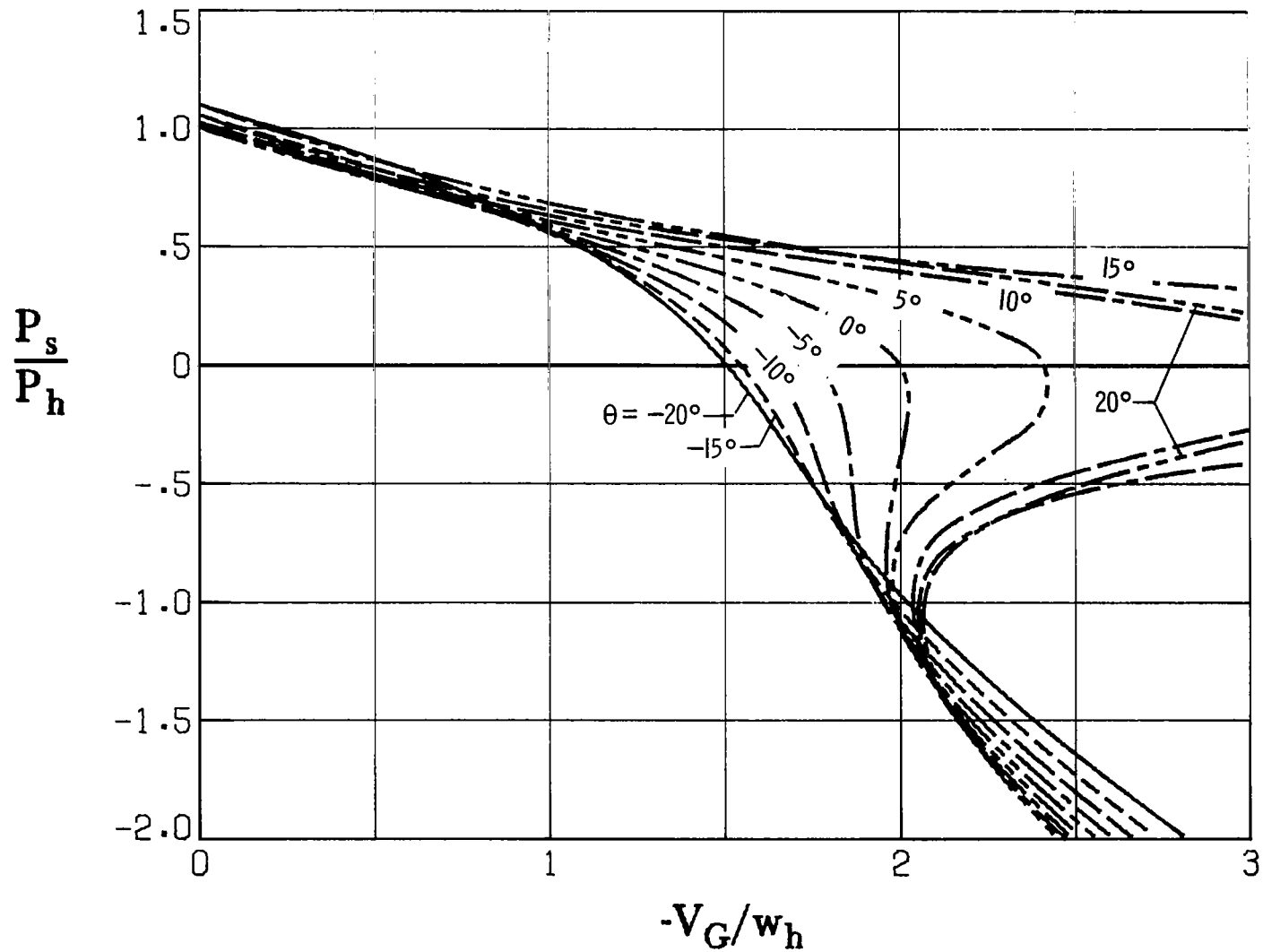
(d)  $\gamma = 45^\circ$ .

Figure 6.- Continued.



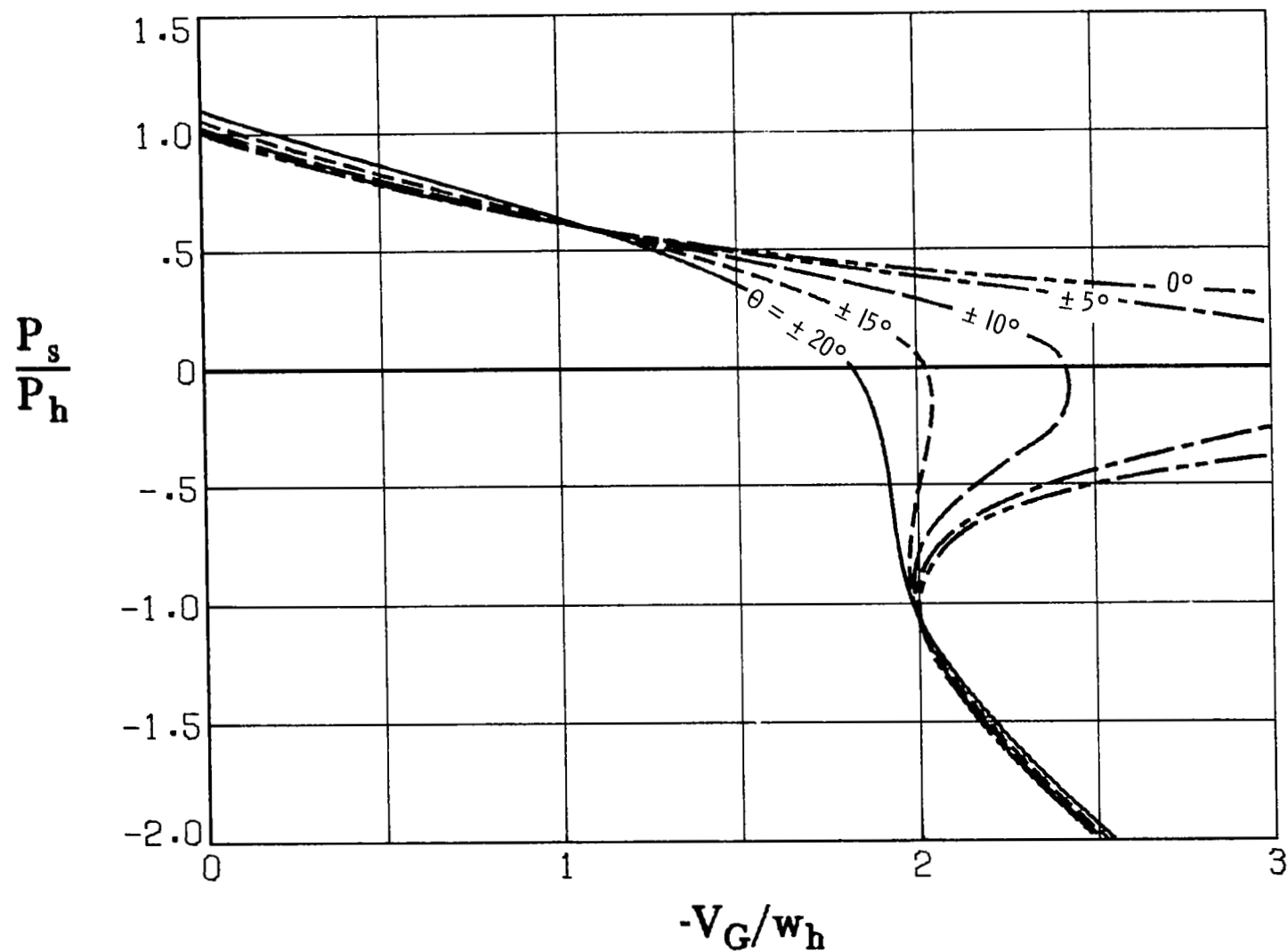
(e)  $\gamma = 60^\circ$ .

Figure 6.- Continued.



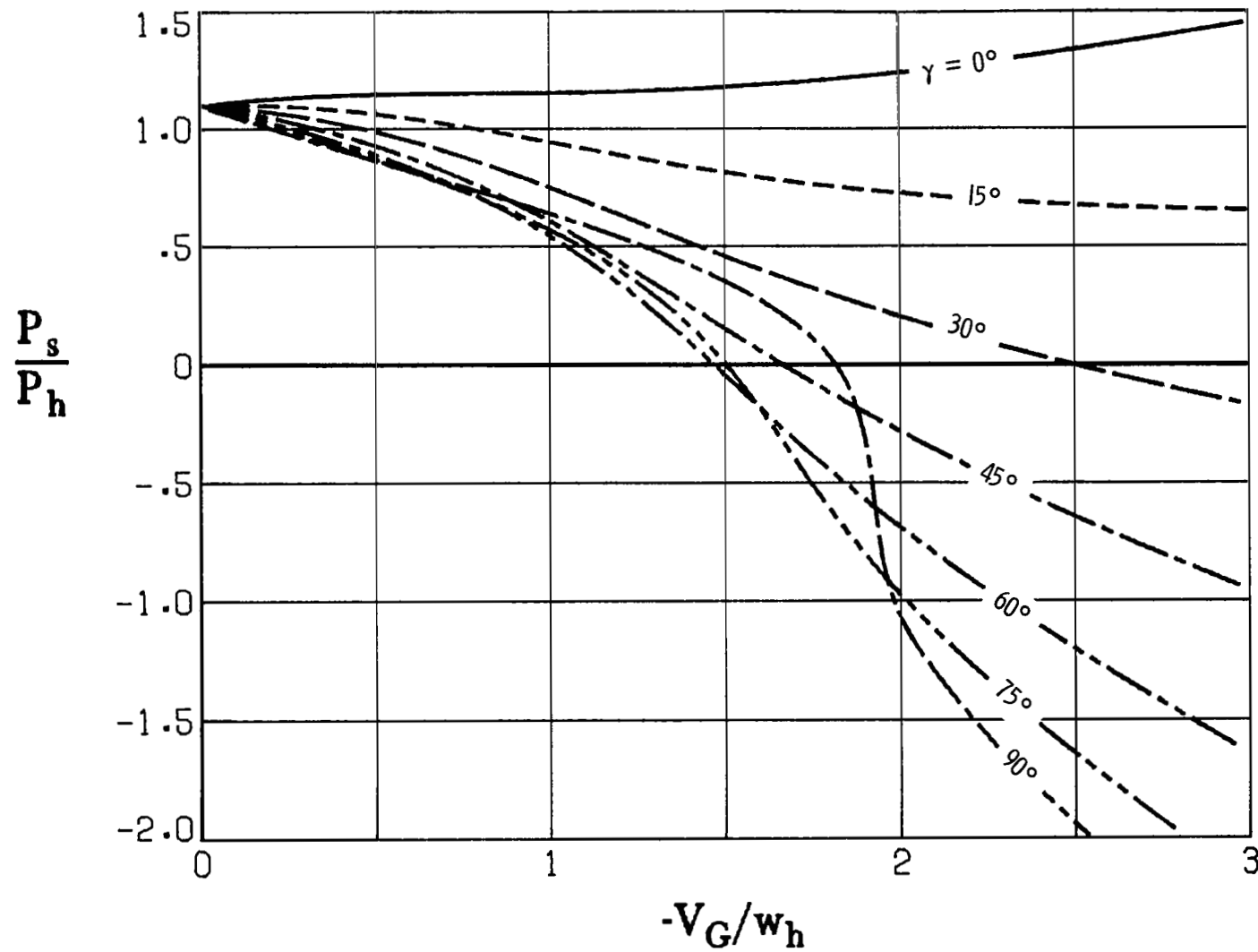
(f)  $\gamma = 75^\circ$ .

Figure 6.- Continued.



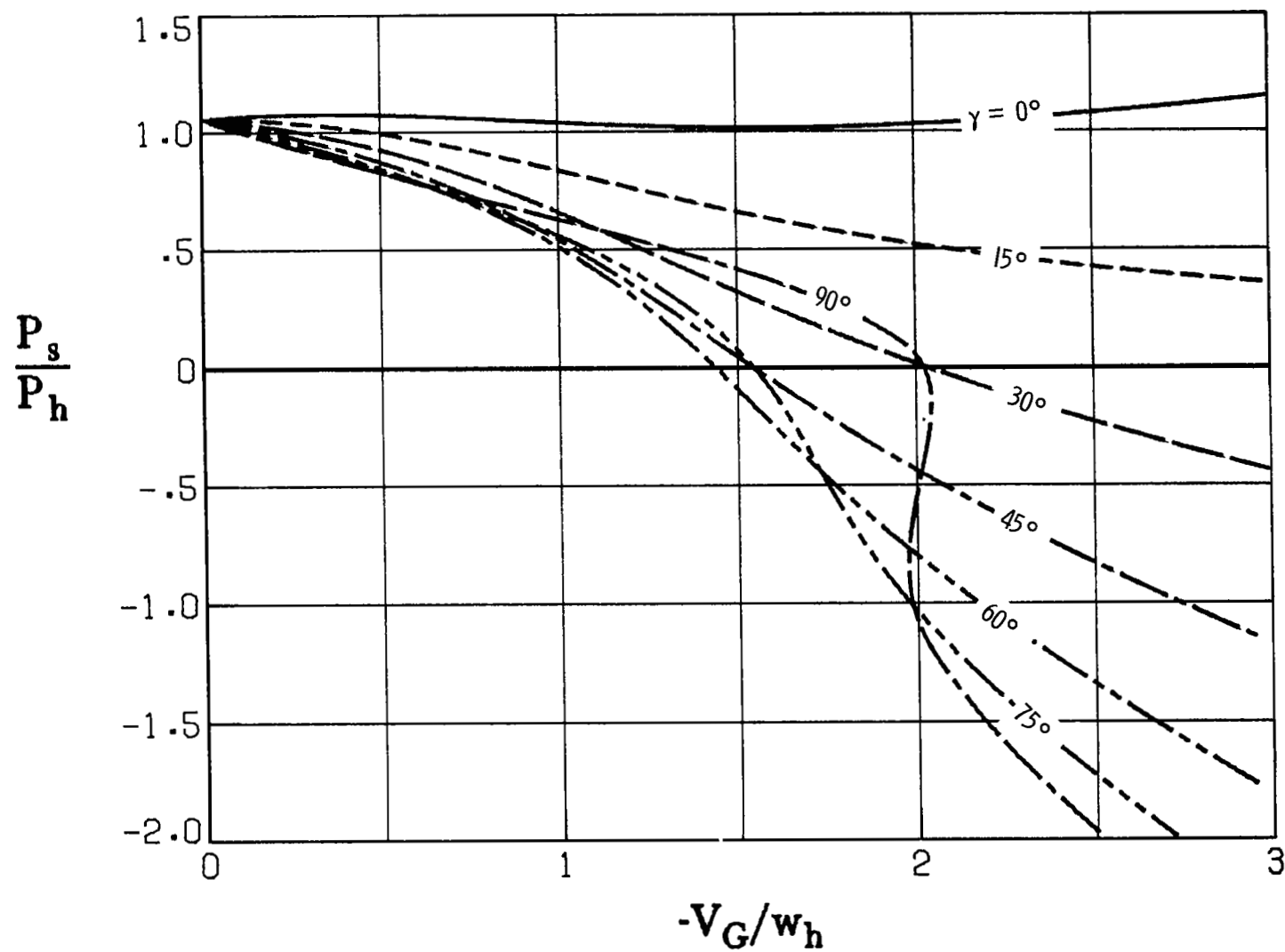
(g)  $\gamma = 90^\circ$ ; vertical flight.

Figure 6.- Concluded.



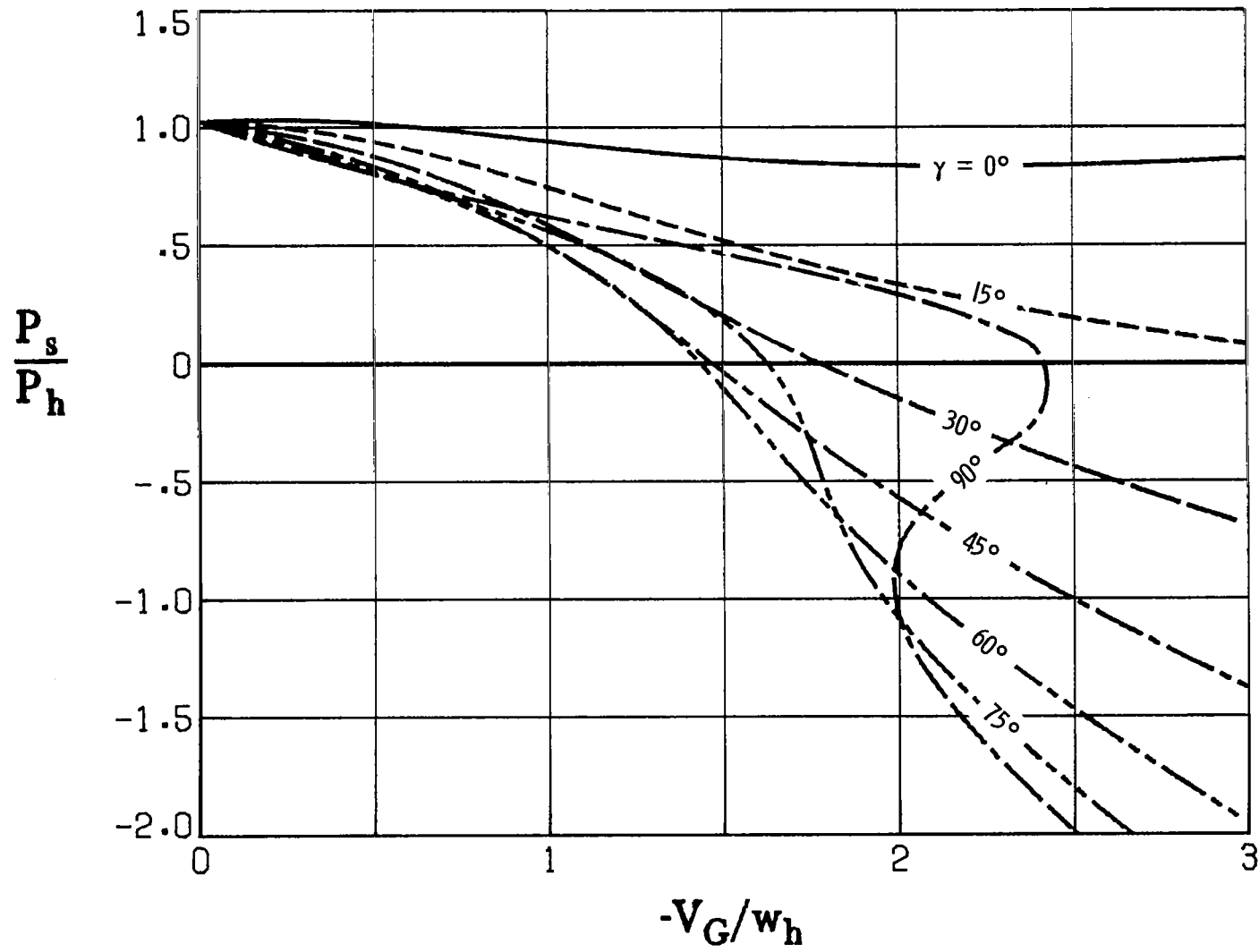
(a)  $\theta = -20^\circ$ .

Figure 7.- Shaft power as a function of glide-slope velocity on constant glide slopes  
for different tip-path-plane inclinations.



(b)  $\theta = -15^\circ$ .

Figure 7.- Continued.



(c)  $\theta = -10^\circ$

Figure 7.- Continued.

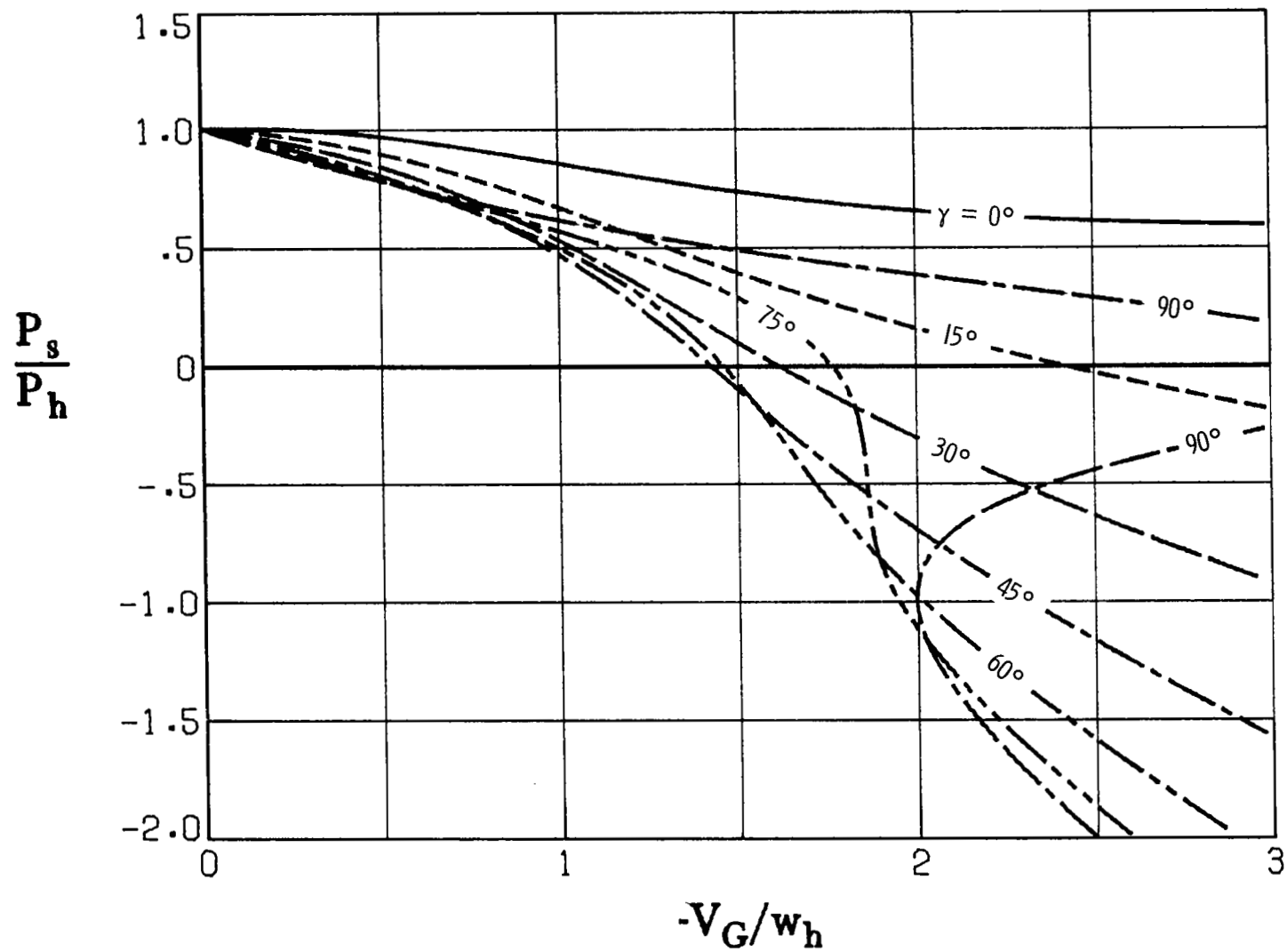
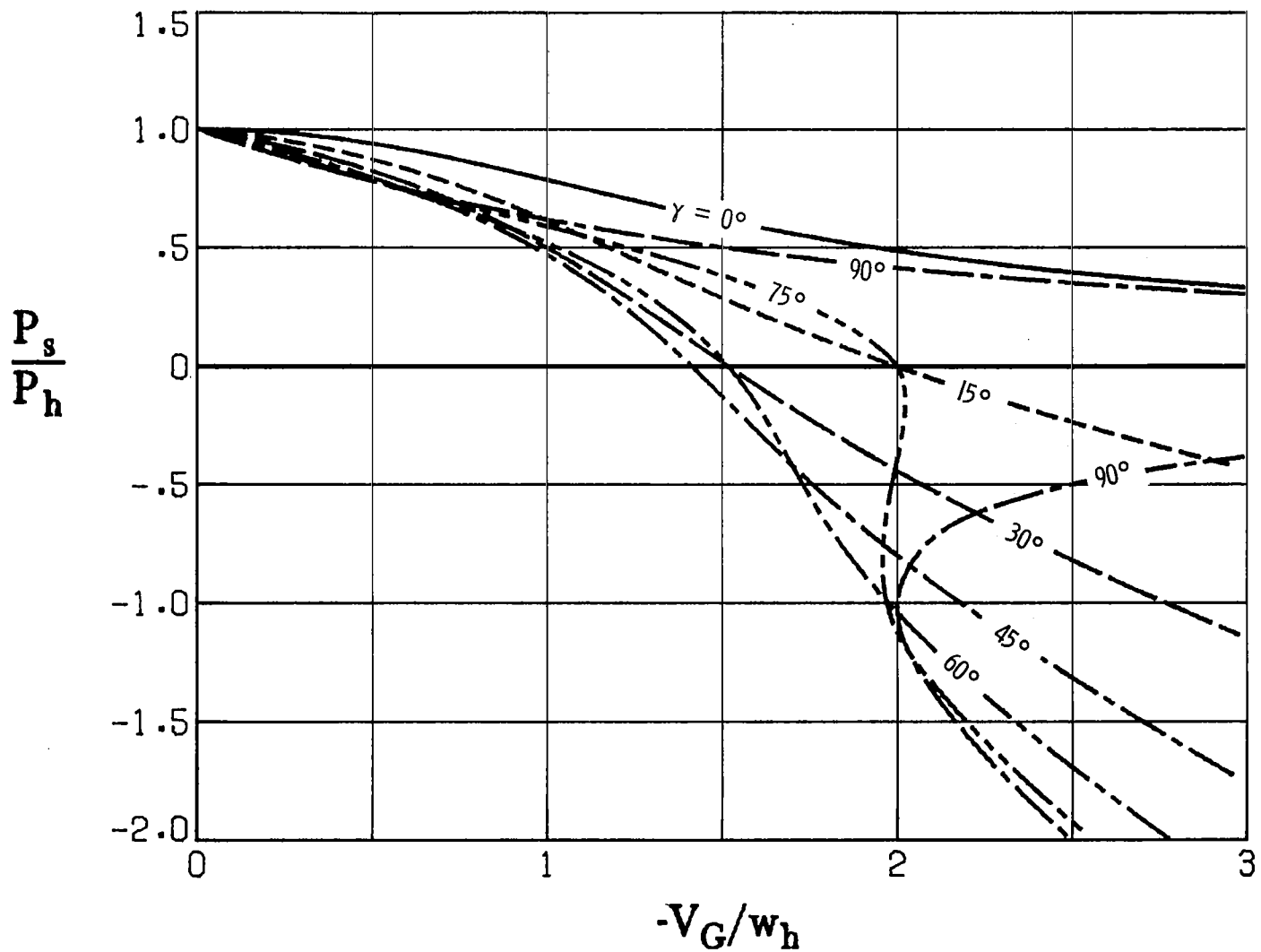
(d)  $\theta = -5^\circ$ .

Figure 7.- Continued.



(e)  $\theta = 0^\circ$ .

Figure 7.- Continued.

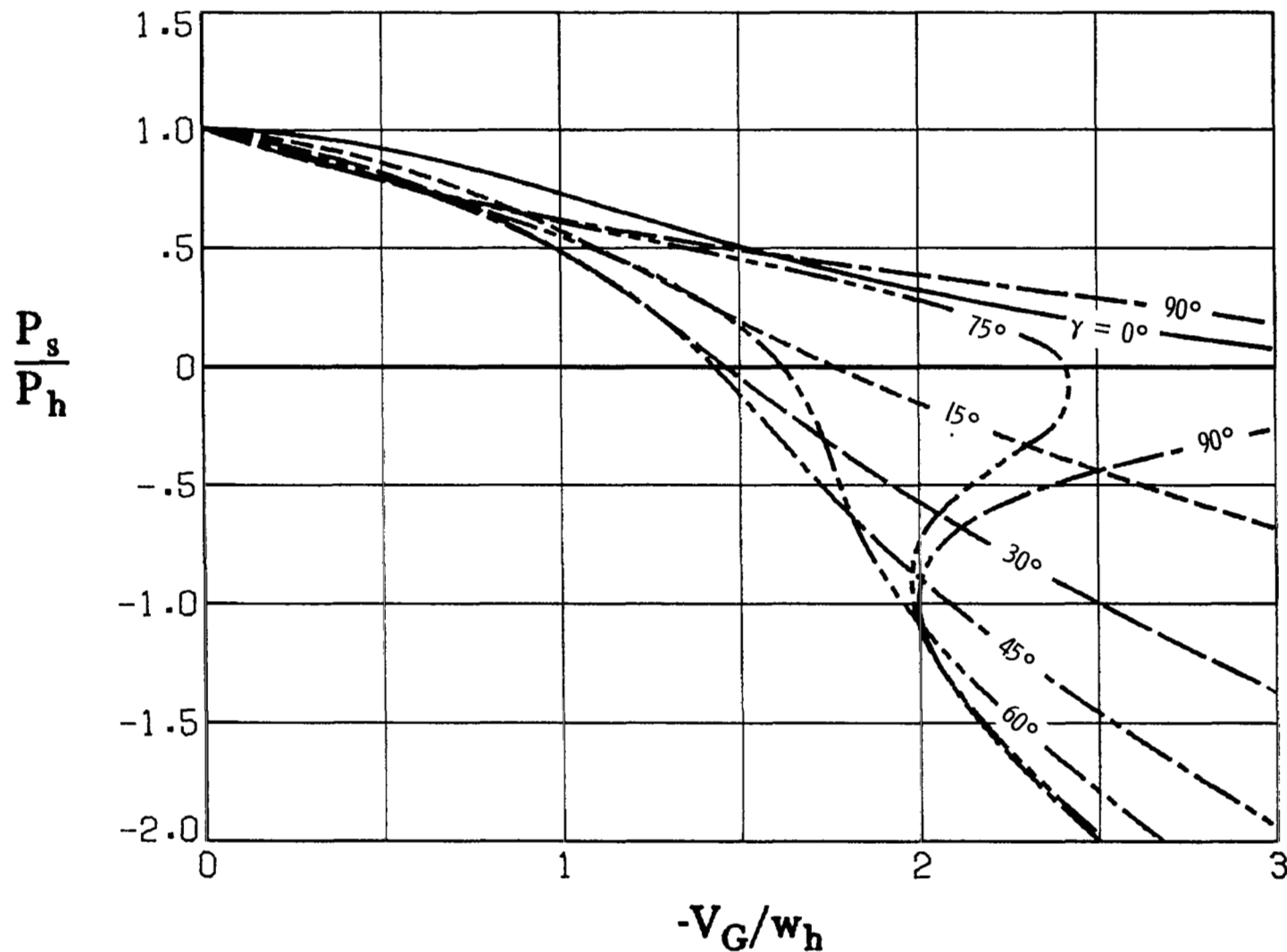
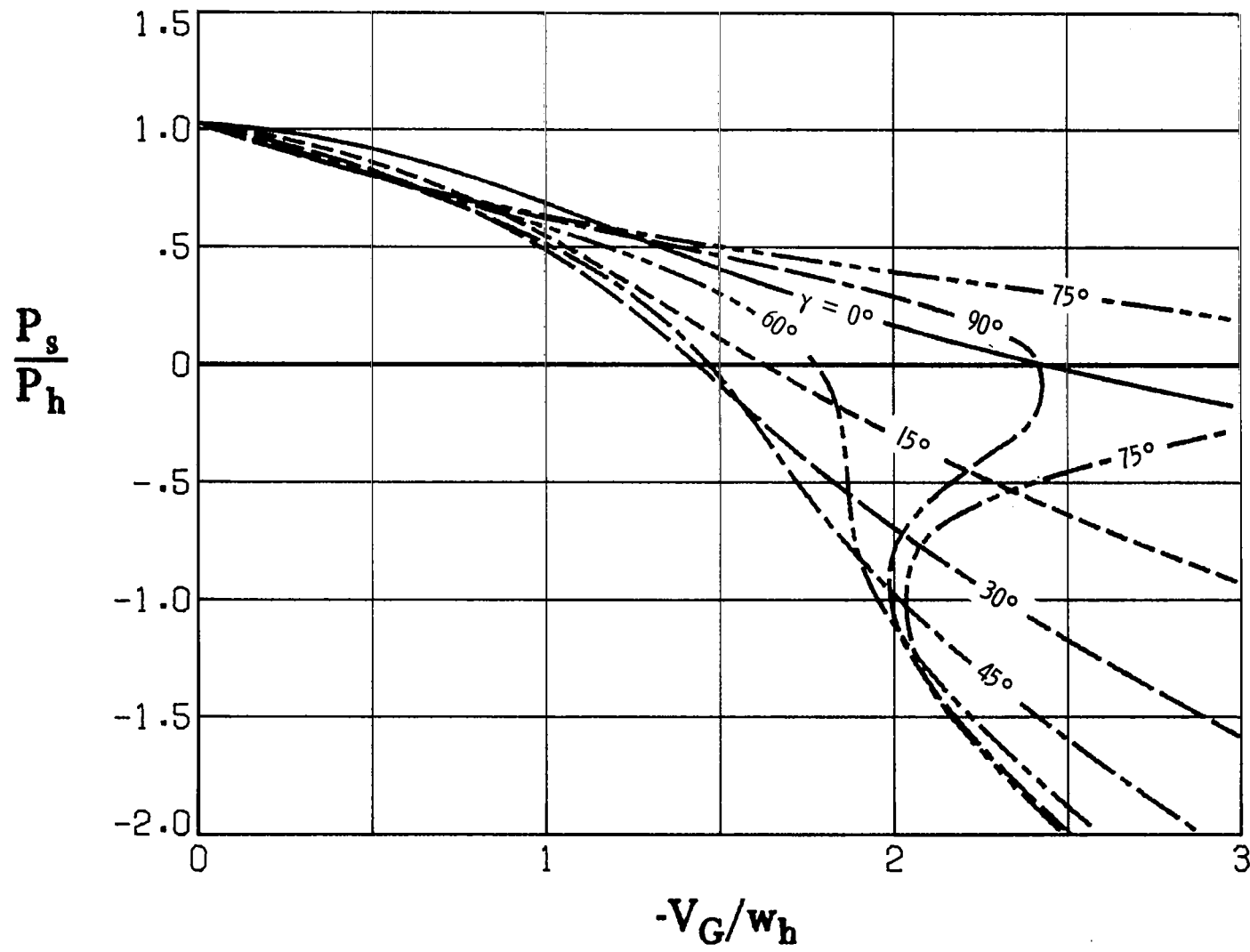
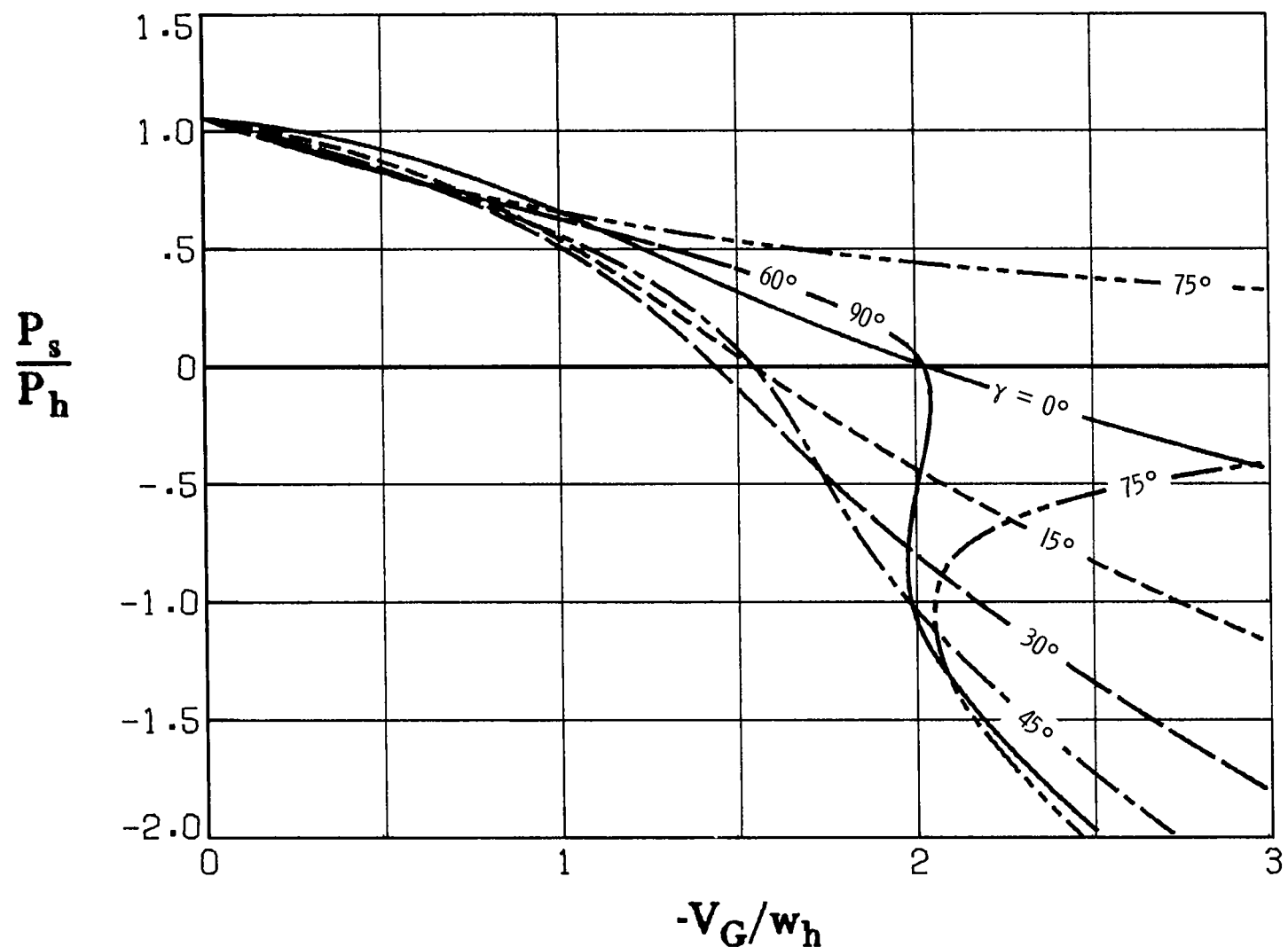
(f)  $\theta = 5^\circ$ .

Figure 7.- Continued.



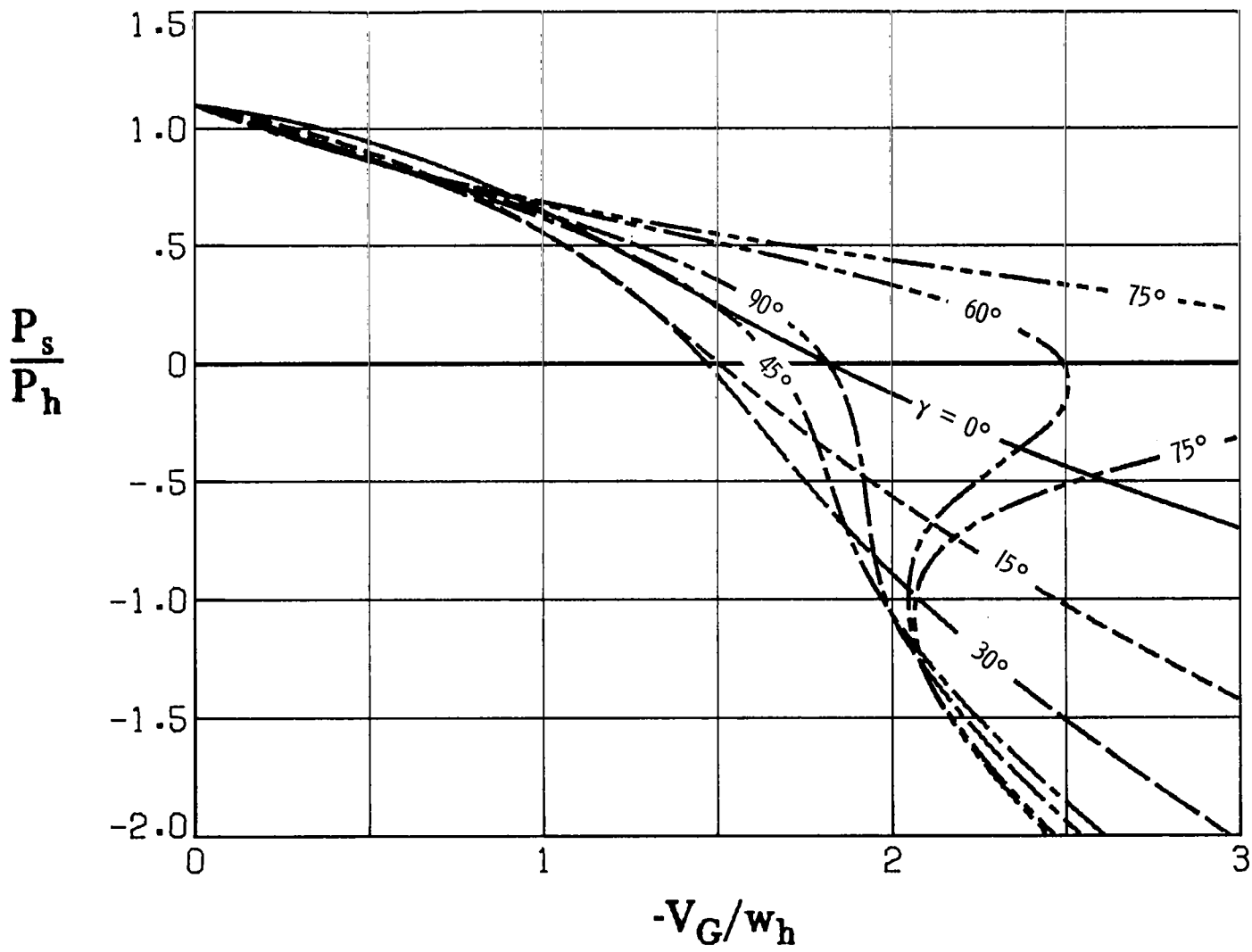
(g)  $\theta = 10^\circ$ .

Figure 7.- Continued.



(h)  $\theta = 15^\circ$ .

Figure 7.- Continued.

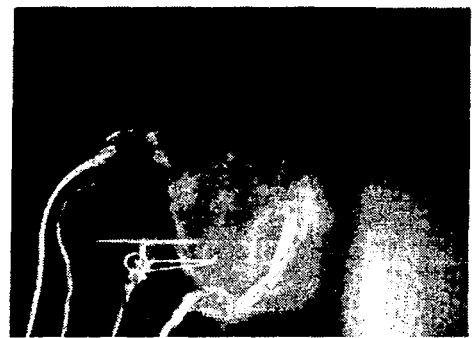


(i)  $\theta = 20^\circ$ .

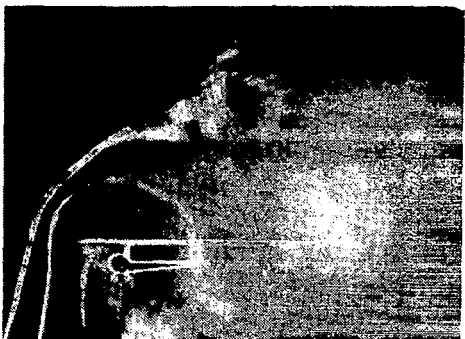
Figure 7.- Concluded.



(a)



(b)



(c)



(d)

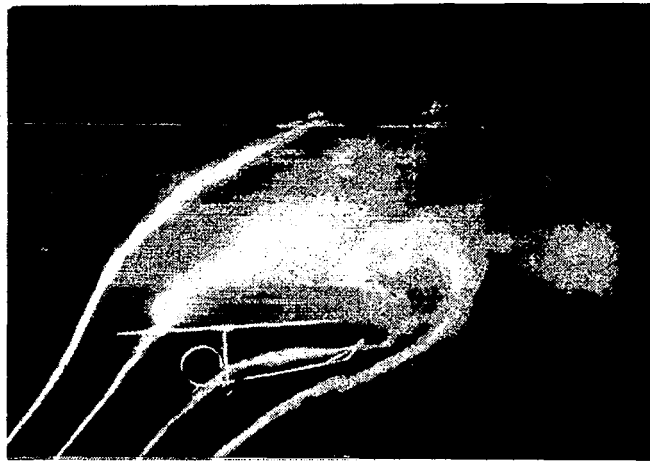


(e)

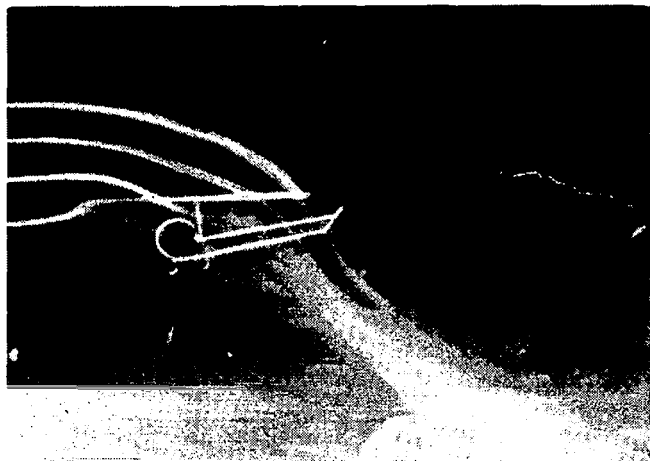


(f)

Figure 8.- Time sequence of flow patterns in steeply inclined descent.  
(Photographs are from ref. 10.)



(a) Autogyro mode (windmill-brake state).



(b) Helicopter mode (normal working state).

Figure 9.- Flow patterns in forward flight. (Photographs are from ref. 10.)

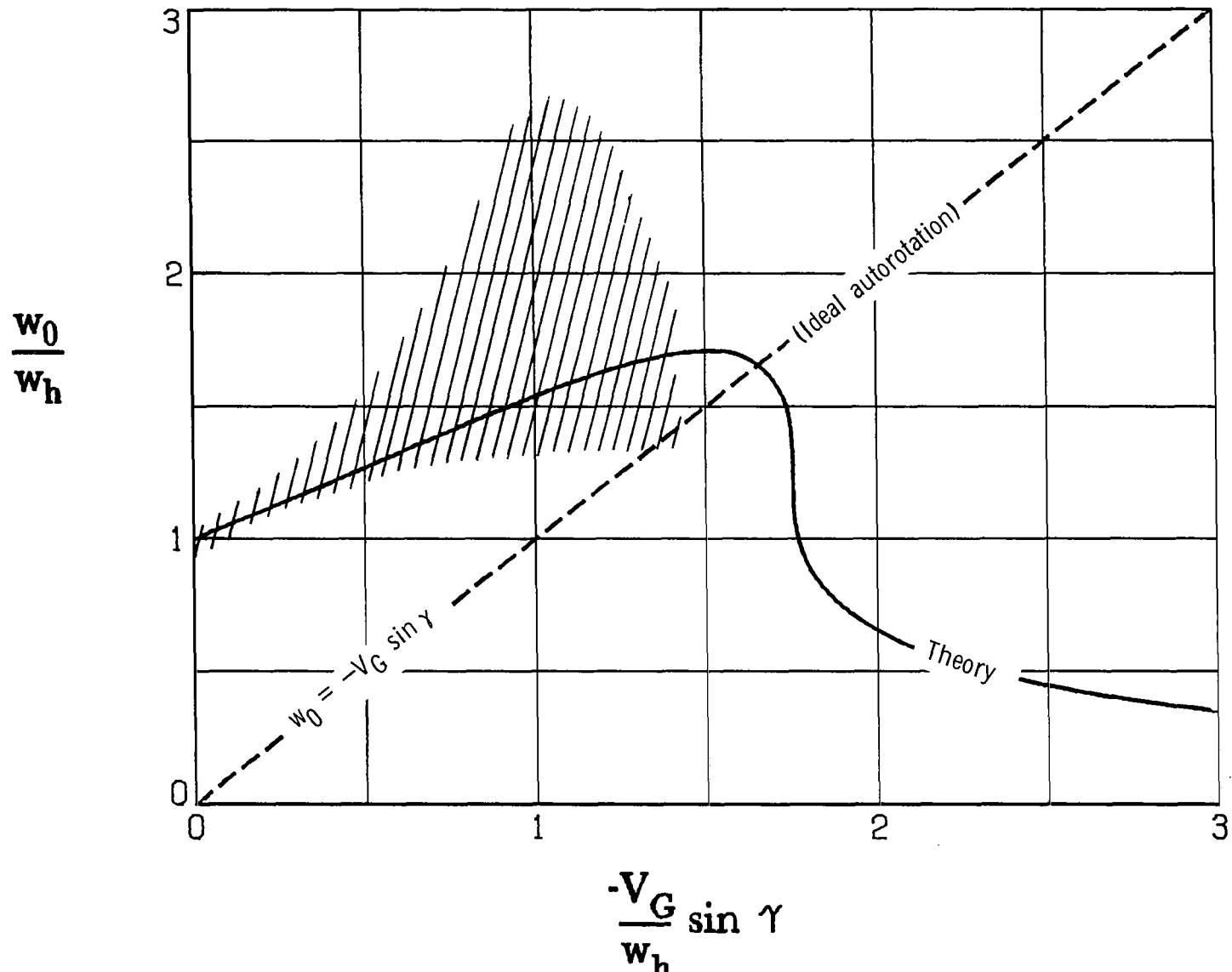
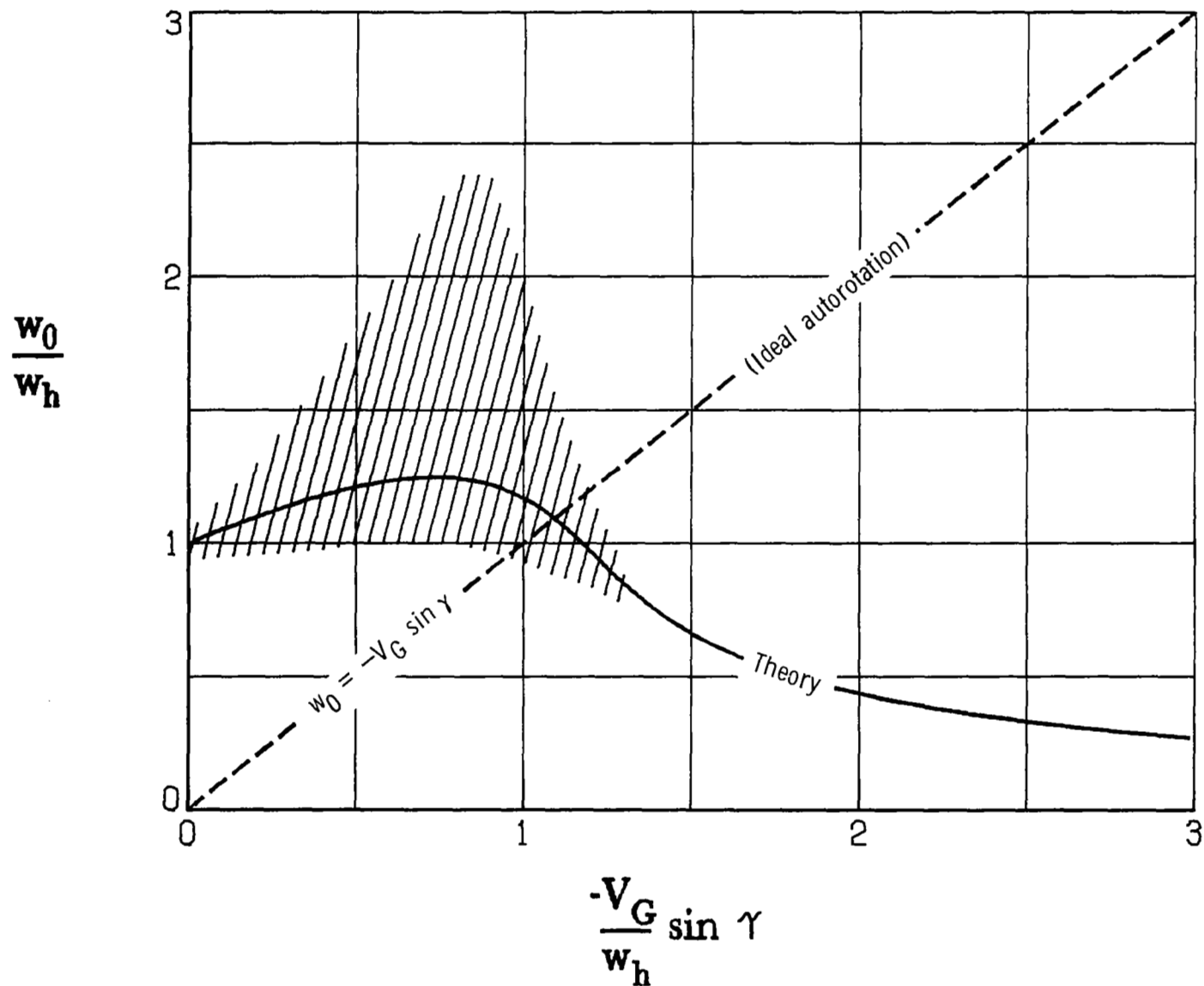
(a)  $\gamma = 70^\circ$ .

Figure 10.- Comparison of theoretical induced-velocity ratios with data band of reference 4  
 $(\theta = 0^\circ)$ .



(b)  $\gamma = 50^\circ$ .

Figure 10.- Continued.

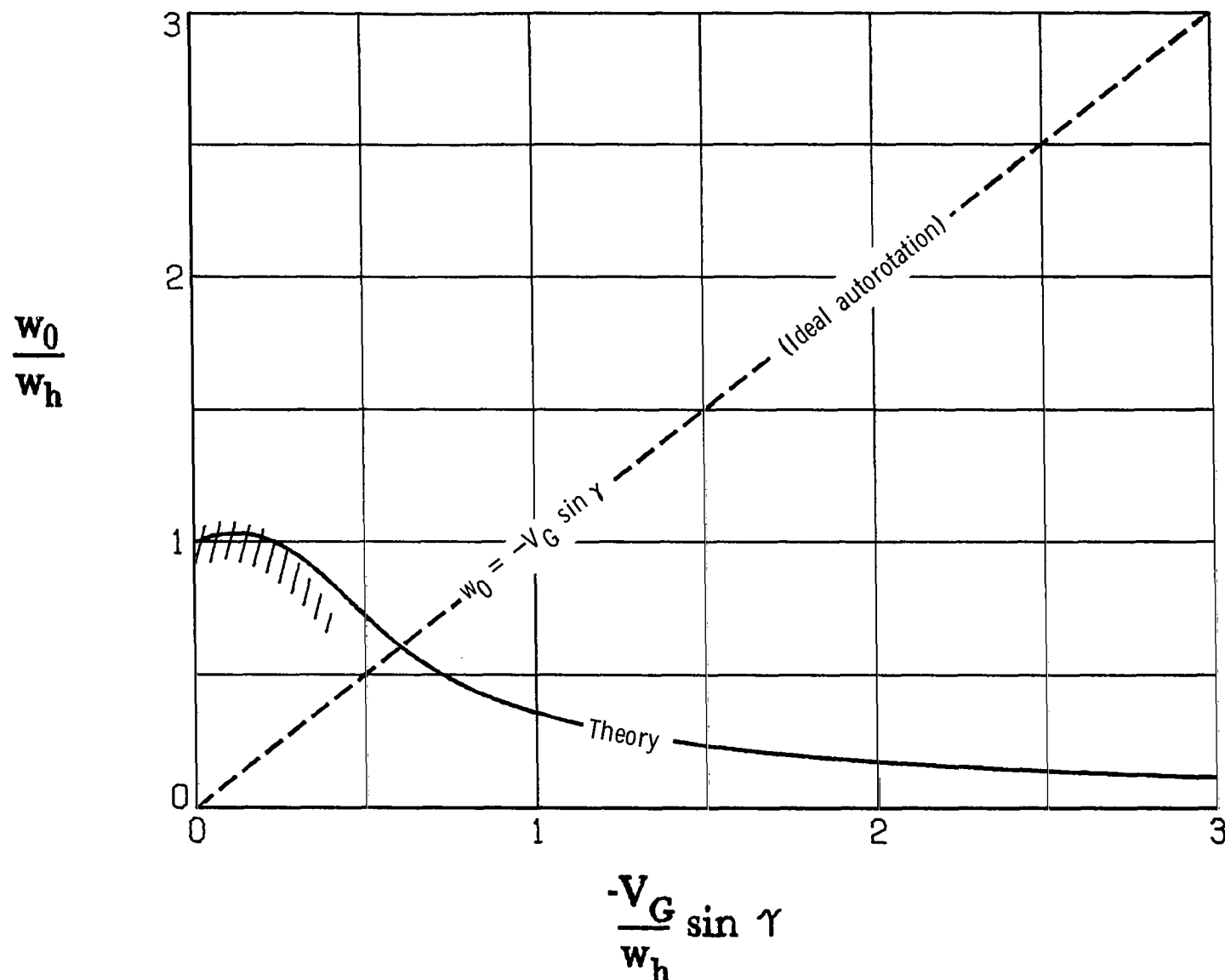
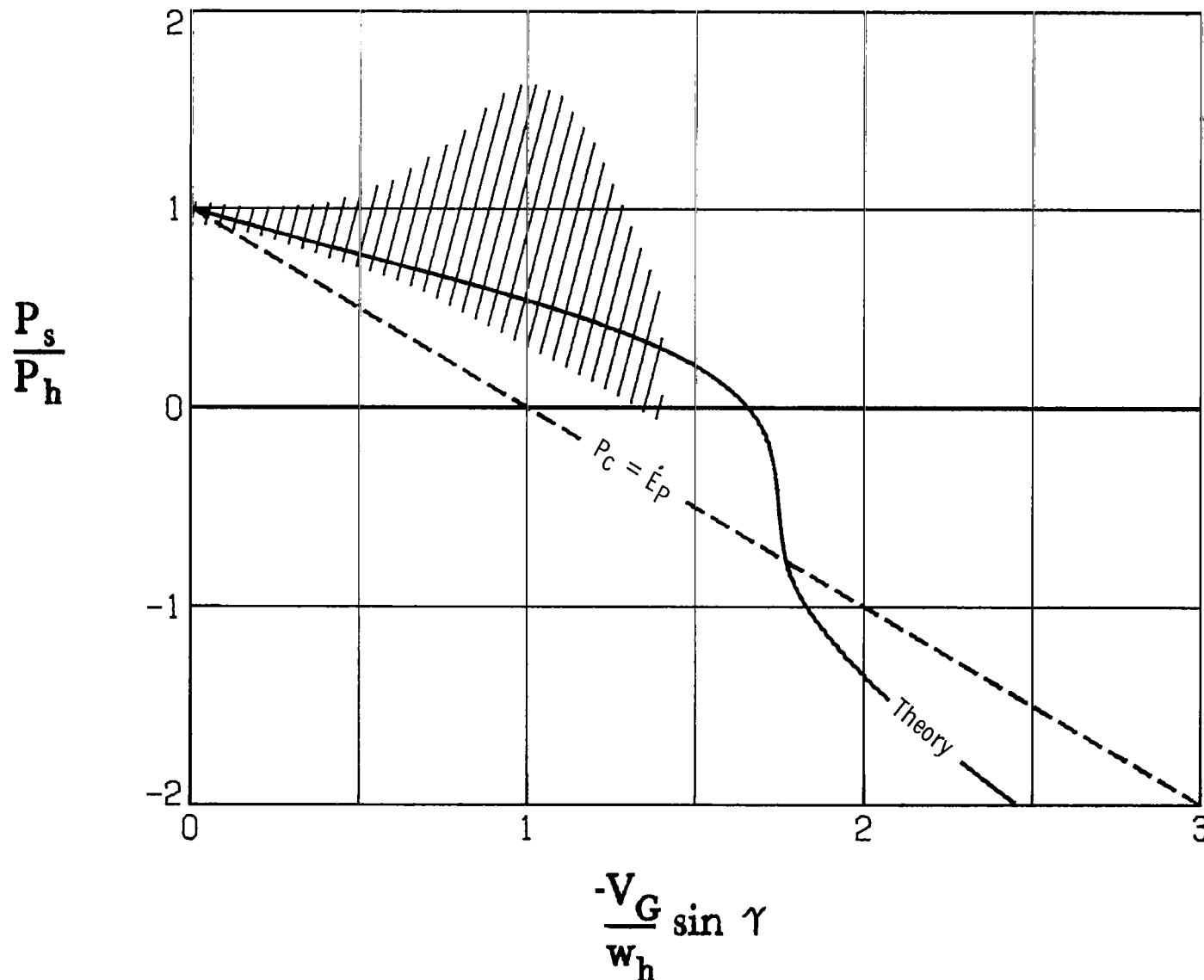
(c)  $\gamma = 20^\circ$ .

Figure 10.- Concluded.



(a)  $\gamma = 70^\circ$

Figure 11.- Comparison of theoretical power ratios with data band of reference 4 ( $\theta = 0^\circ$ ).

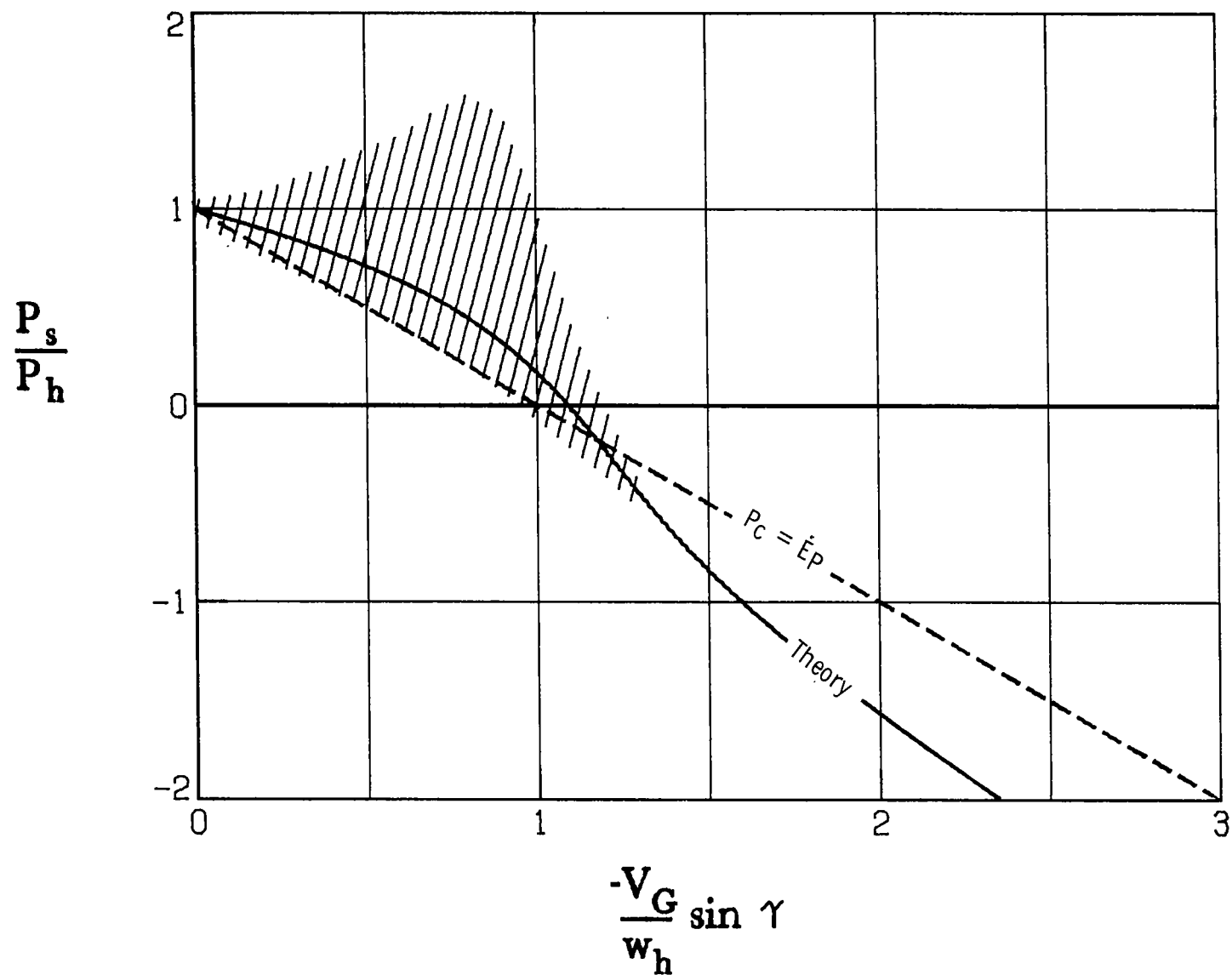
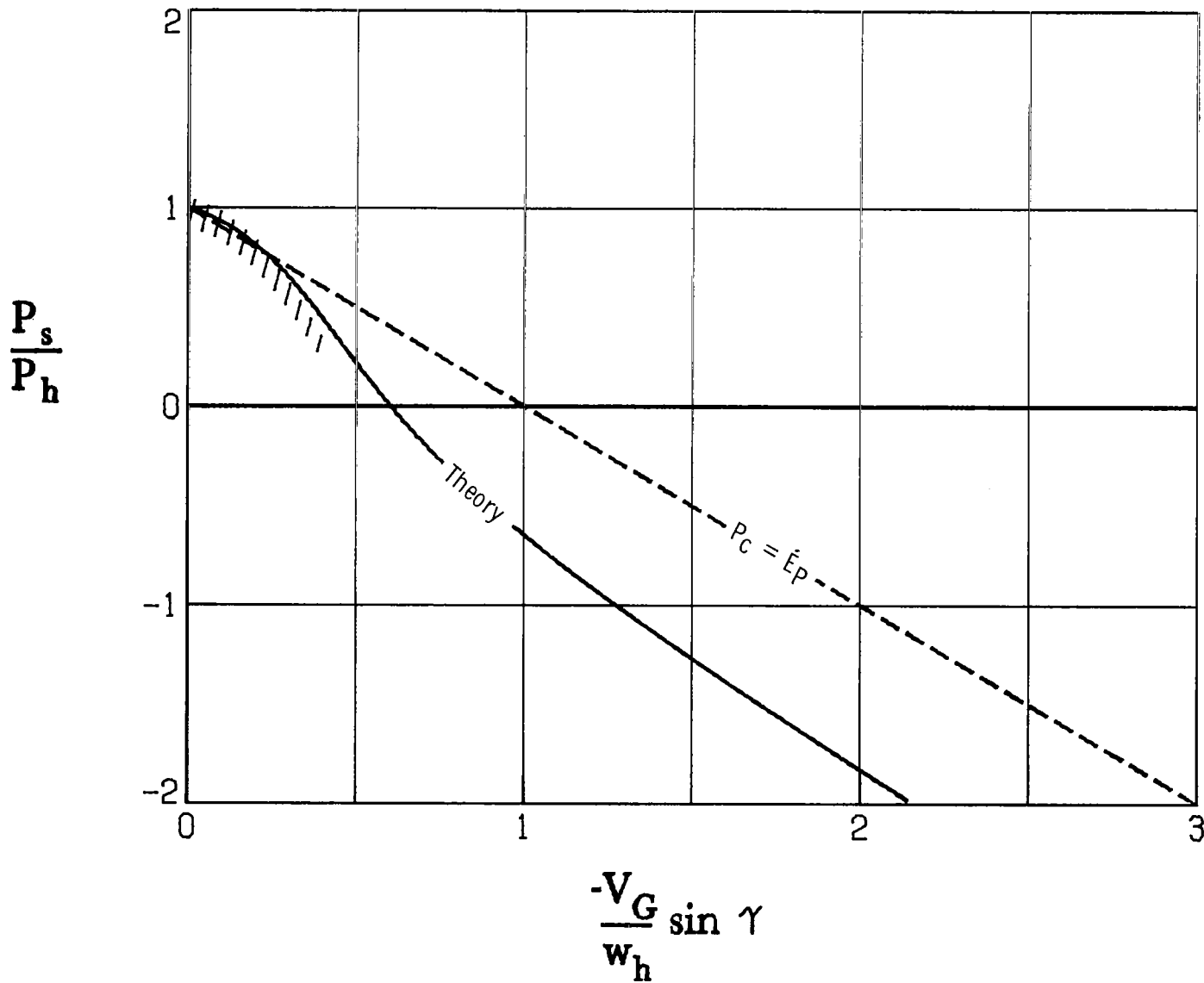
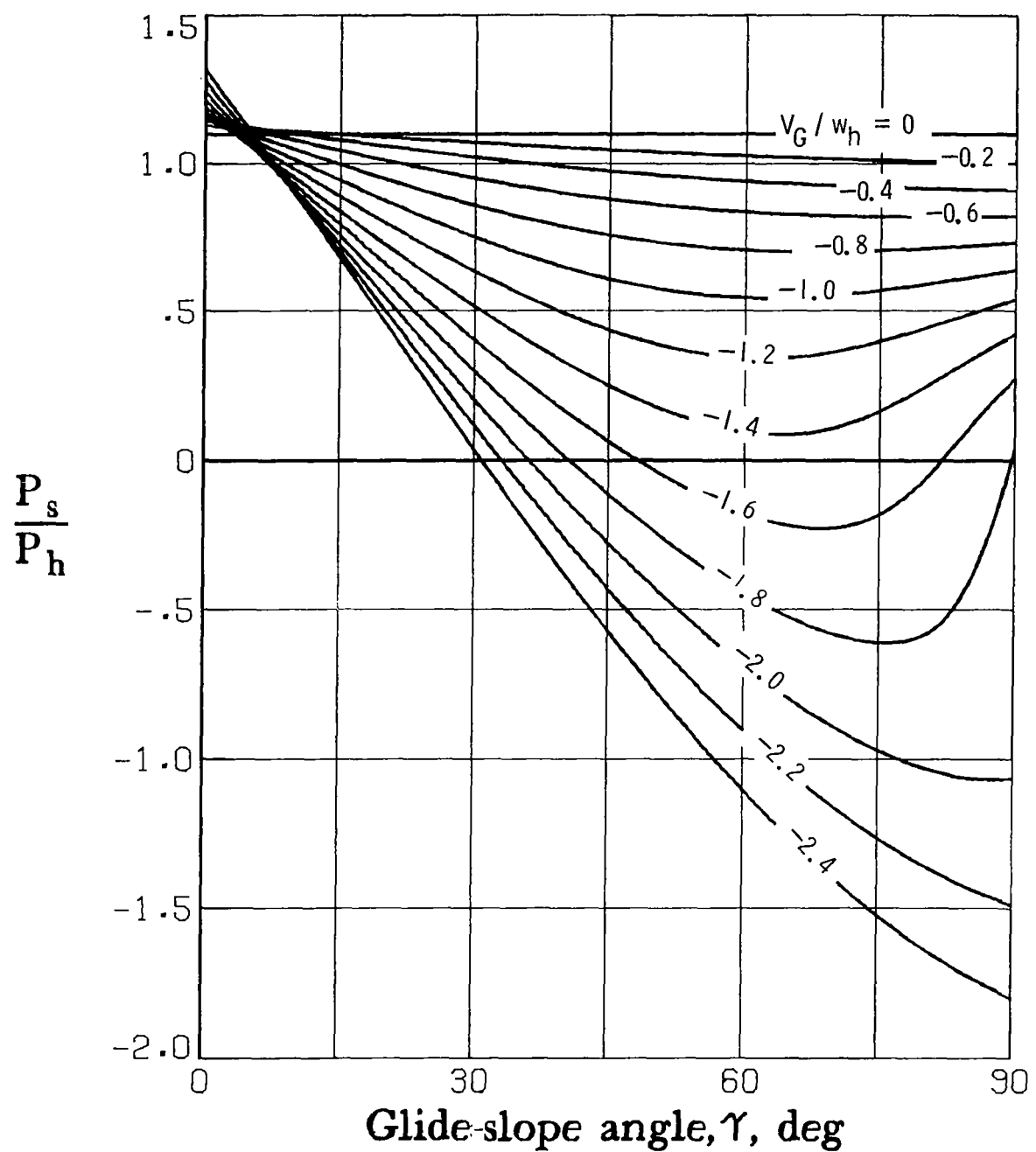
(b)  $\gamma = 50^\circ$ .

Figure 11.- Continued.



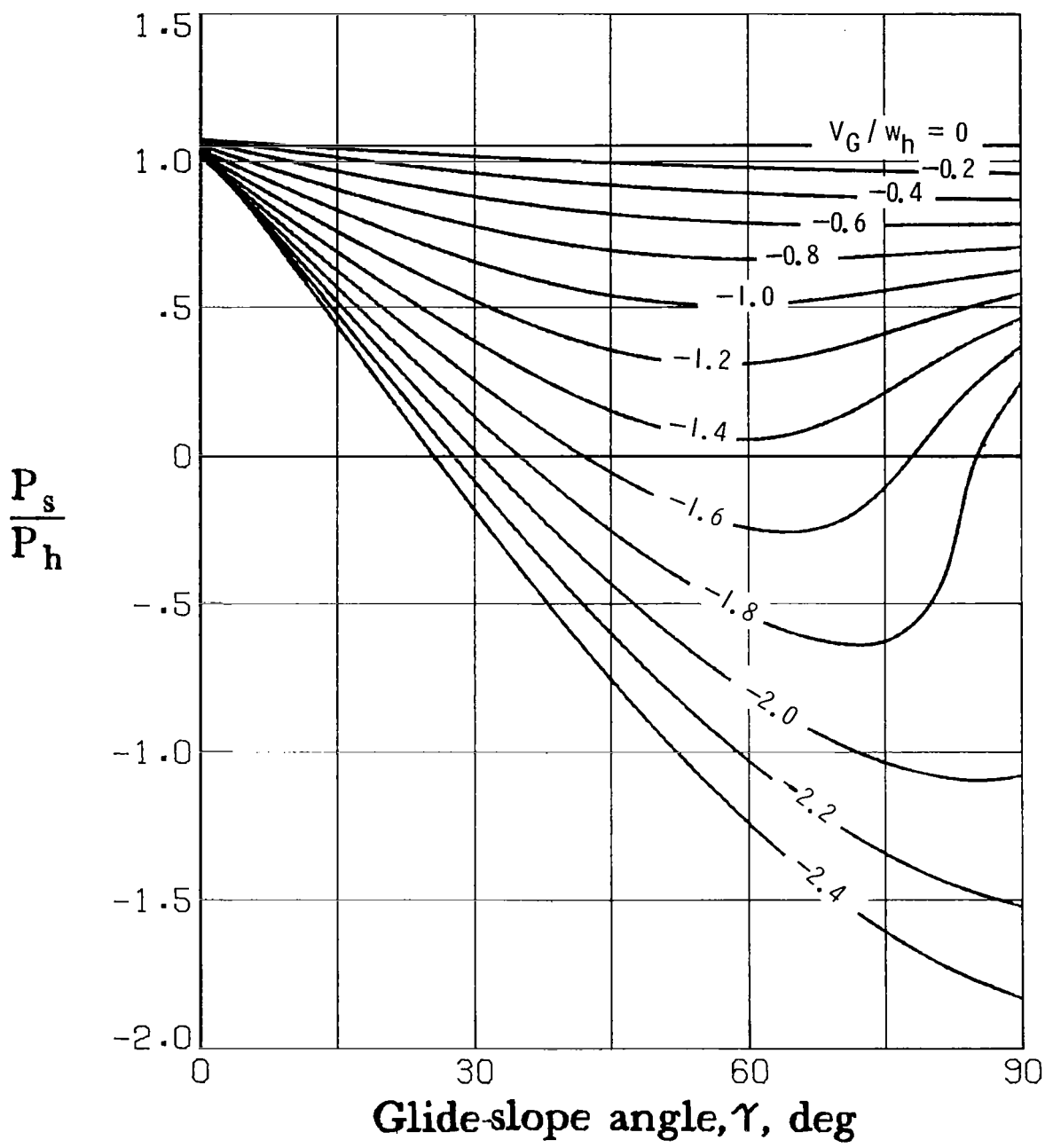
(c)  $\gamma = 20^\circ$ .

Figure 11.- Concluded.



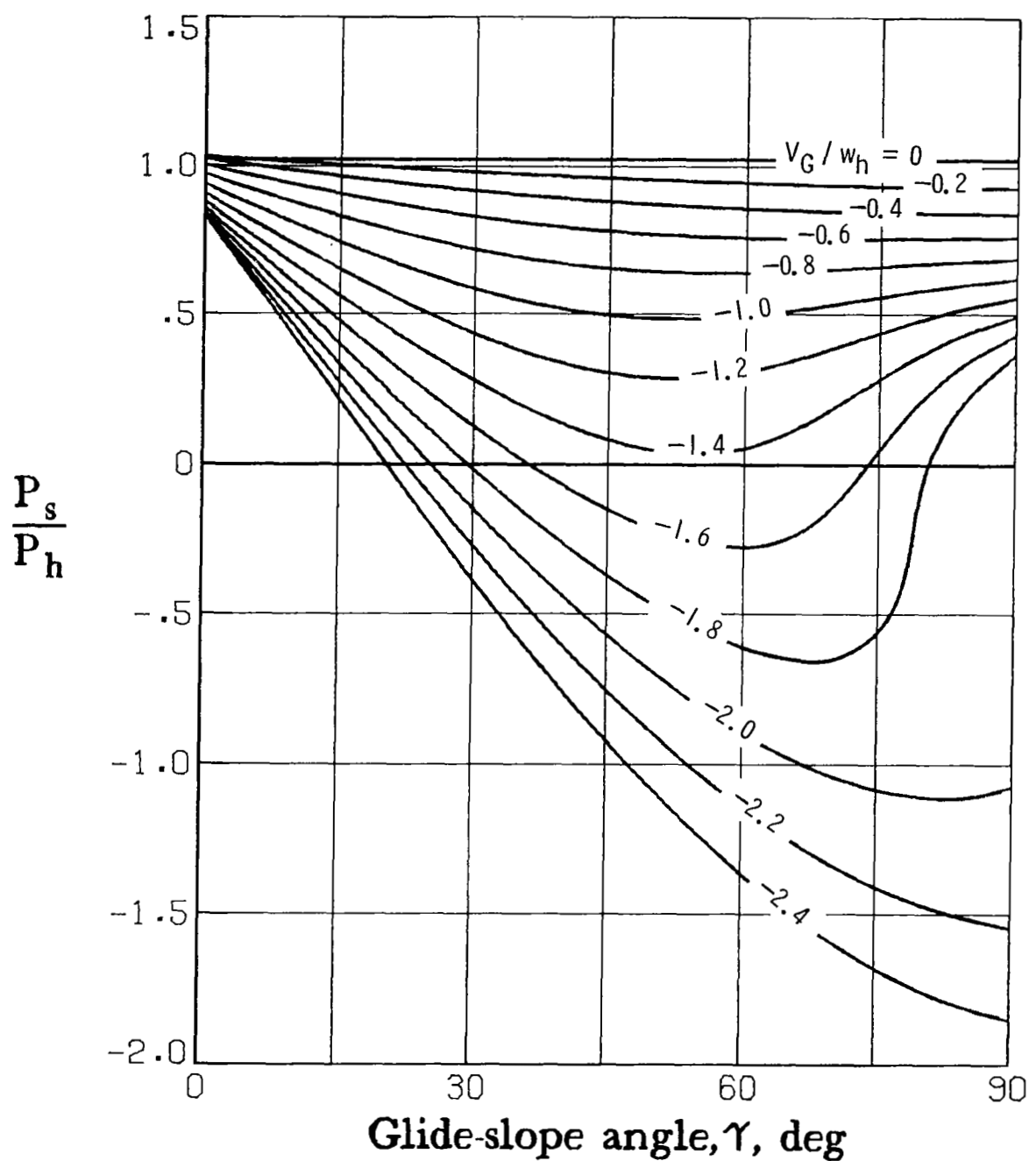
(a)  $\theta = -20^\circ$ .

Figure 12.- Required shaft power as a function of glide-slope angle  $\gamma$ .



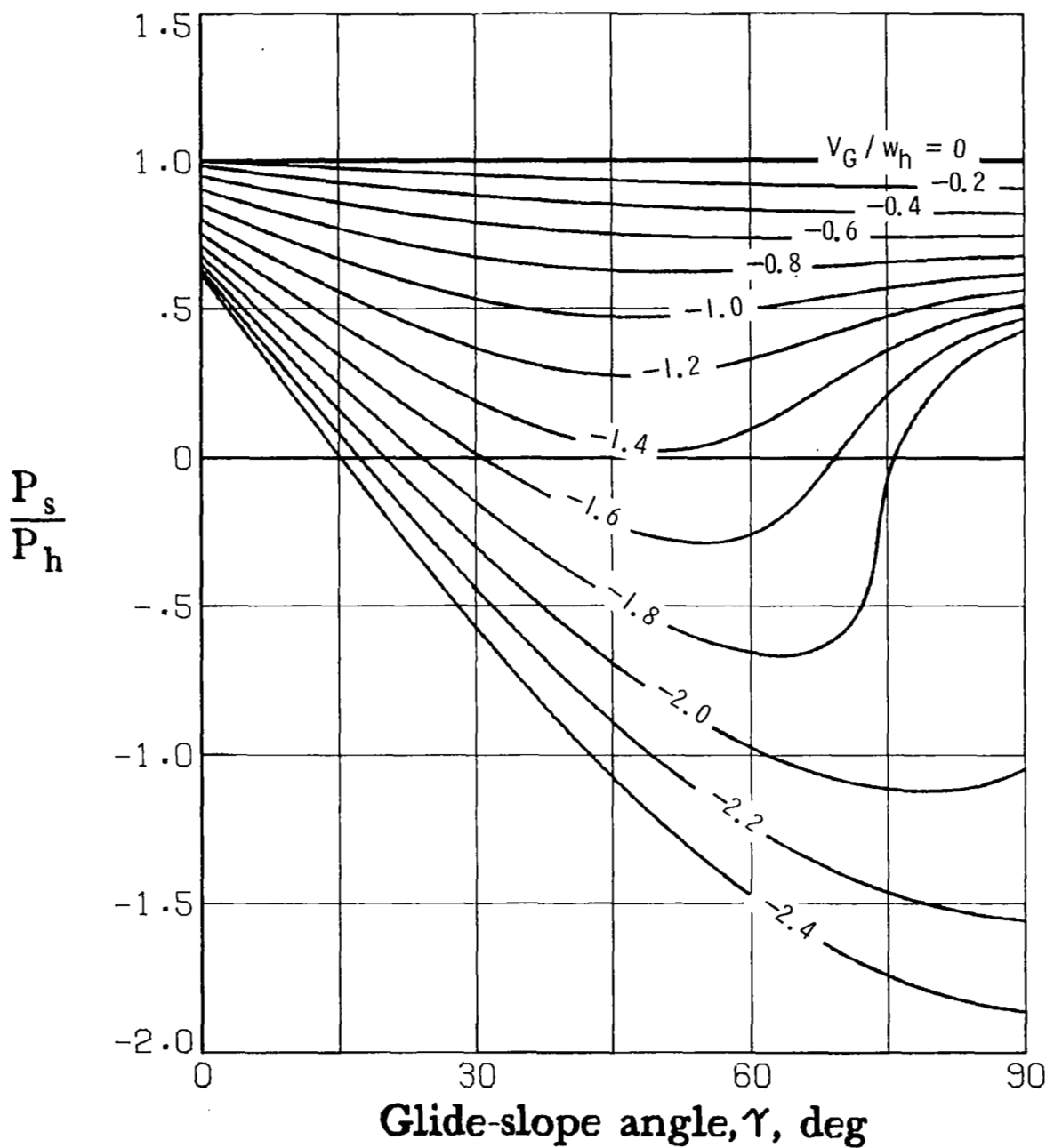
(b)  $\theta = -15^\circ$ .

Figure 12.- Continued.



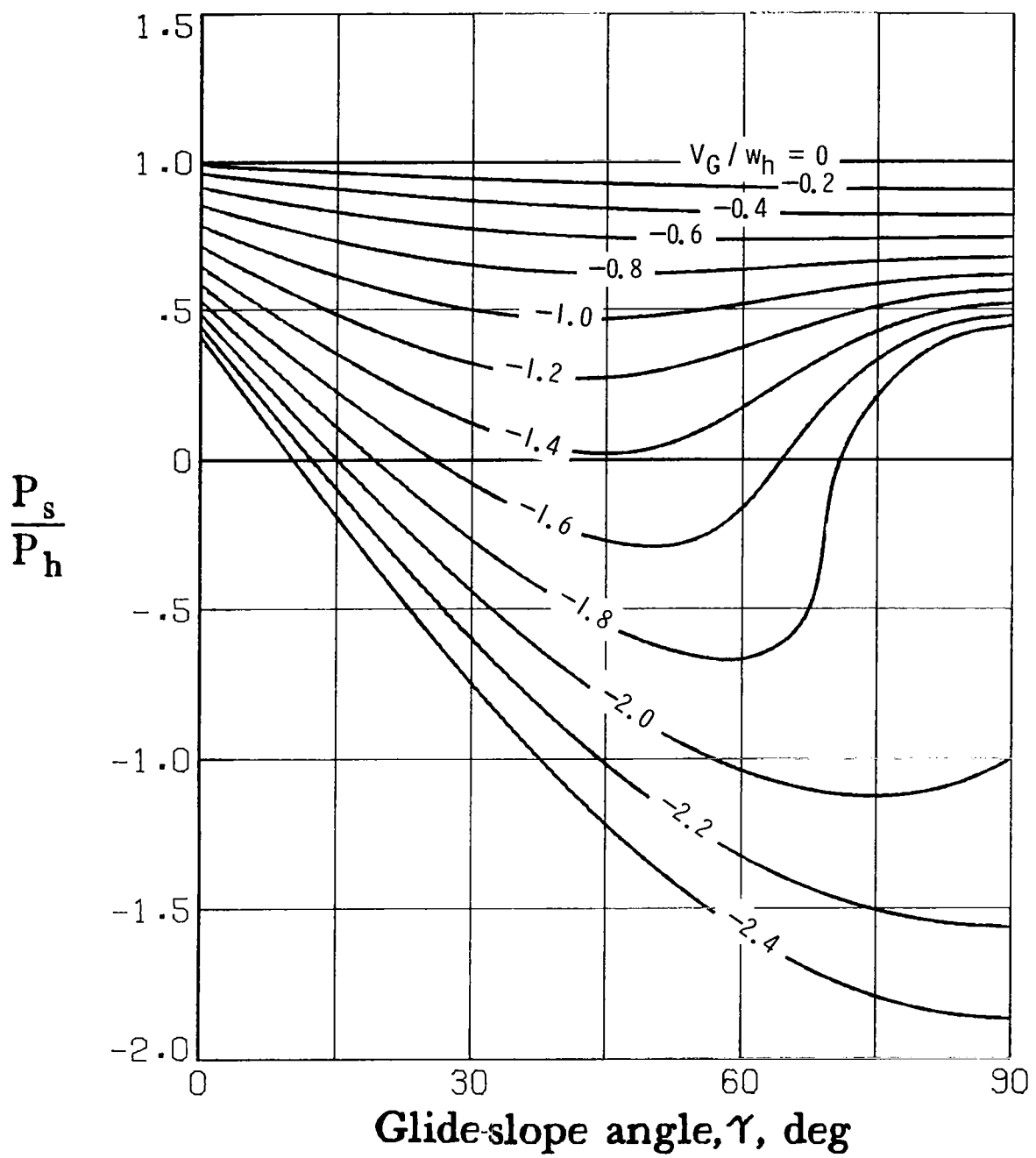
(c)  $\theta = -10^\circ$ .

Figure 12.- Continued.



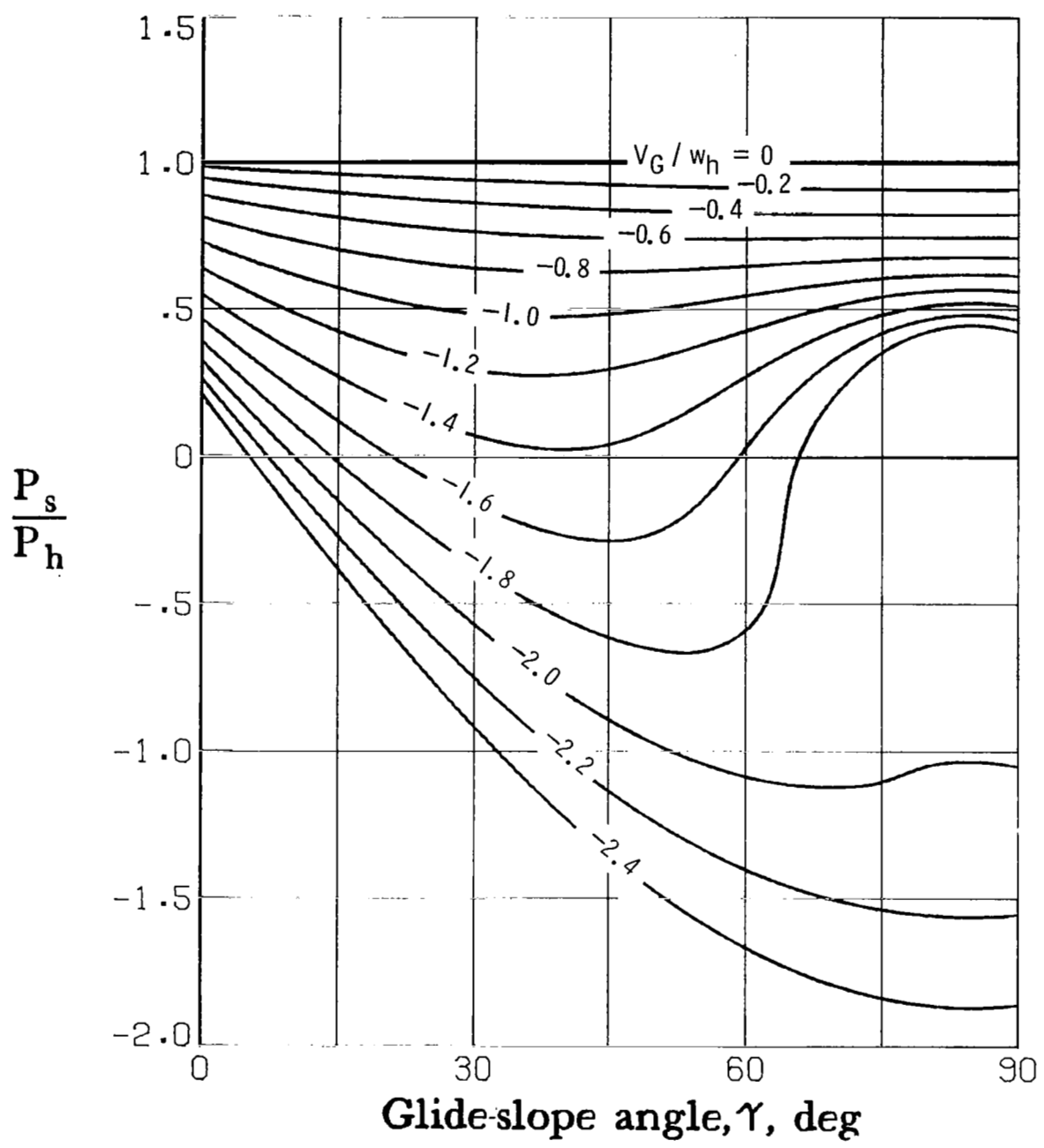
(d)  $\theta = -5^\circ$ .

Figure 12.- Continued.



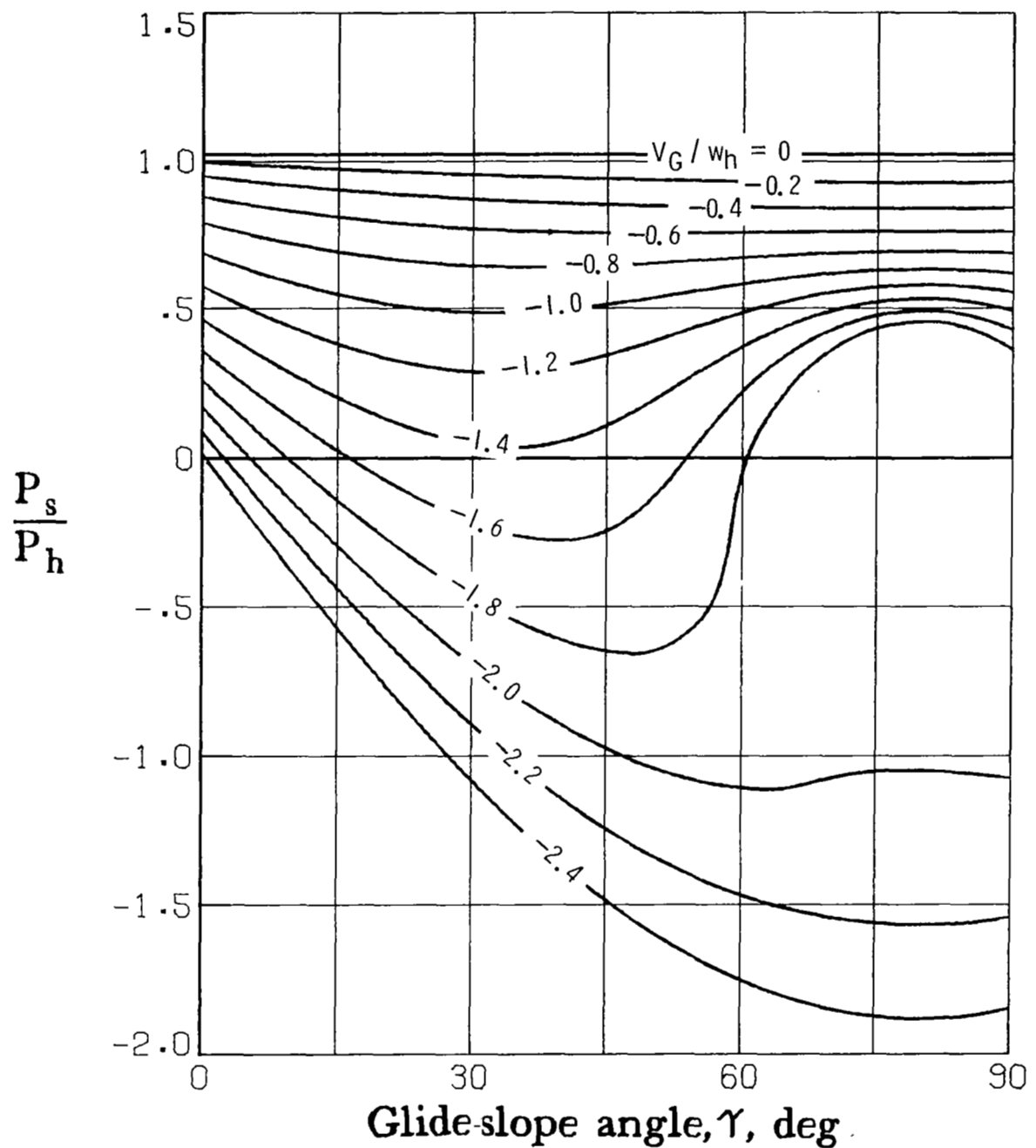
(e)  $\theta = 0^\circ$ .

Figure 12.- Continued.



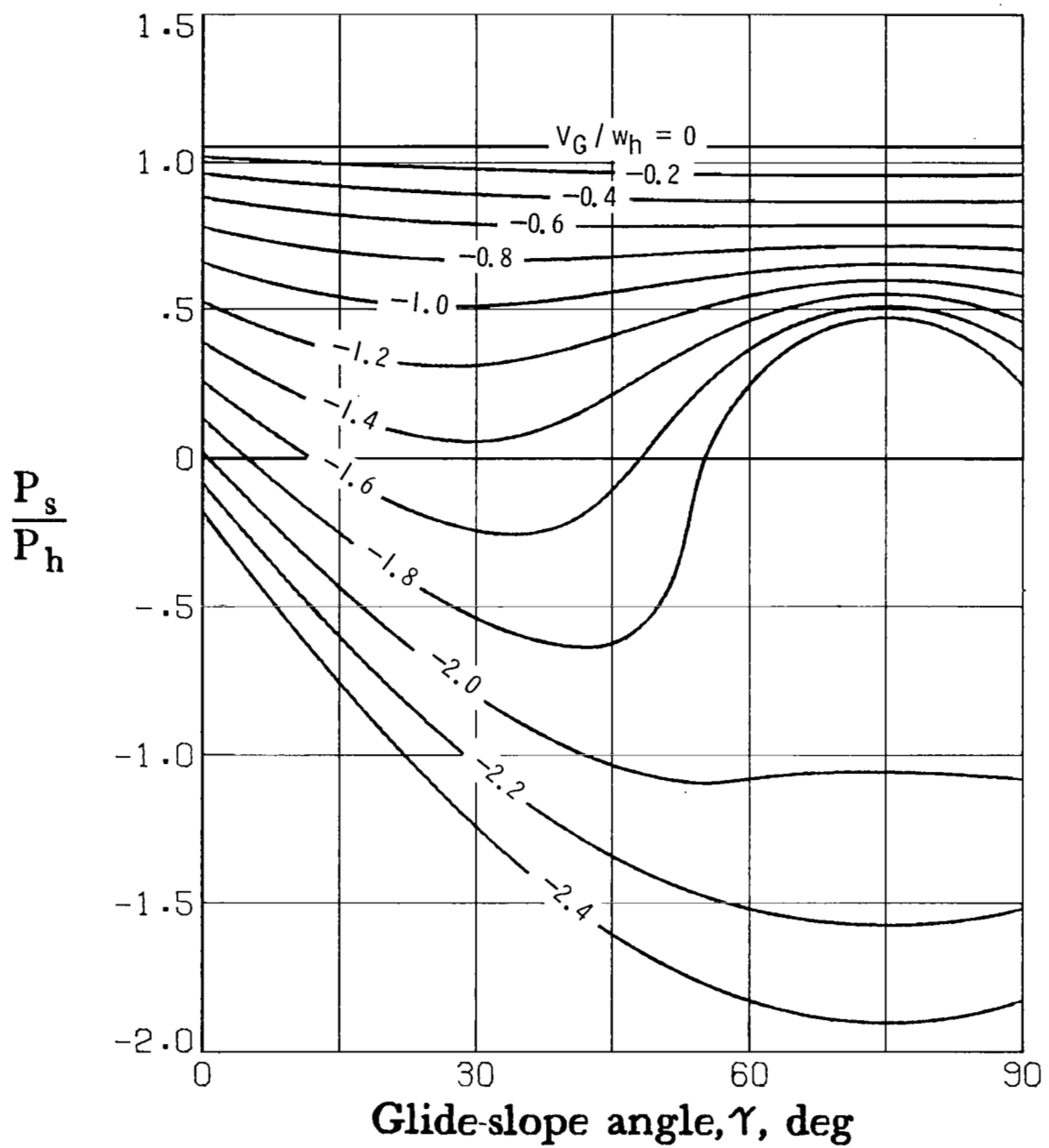
(f)  $\theta = 5^\circ$ .

Figure 12.- Continued.



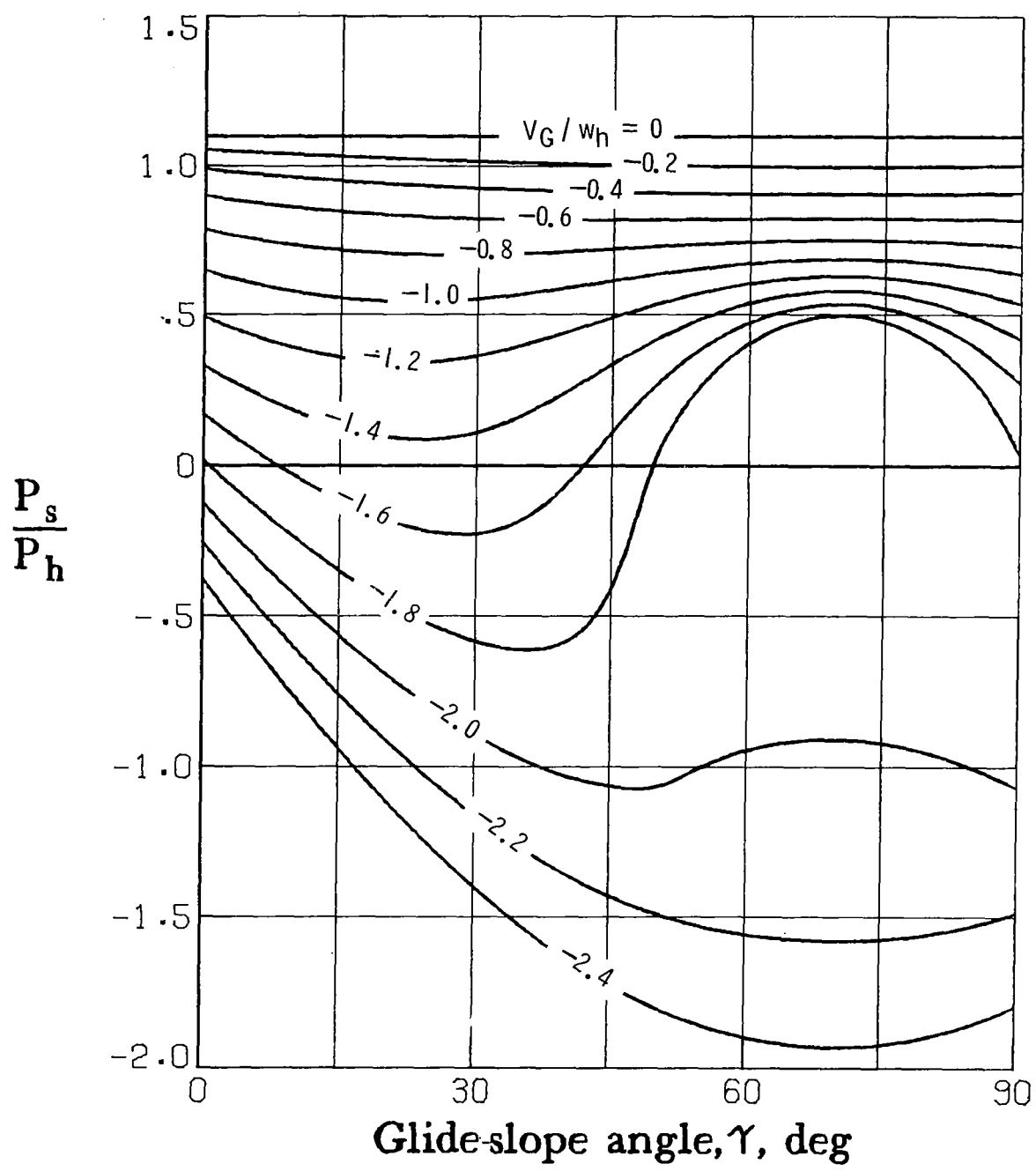
(g)  $\theta = 10^\circ$ .

Figure 12.- Continued.



(h)  $\theta = 15^\circ$ .

Figure 12.- Continued.



(i)  $\theta = 20^\circ$ .

Figure 12.- Concluded.

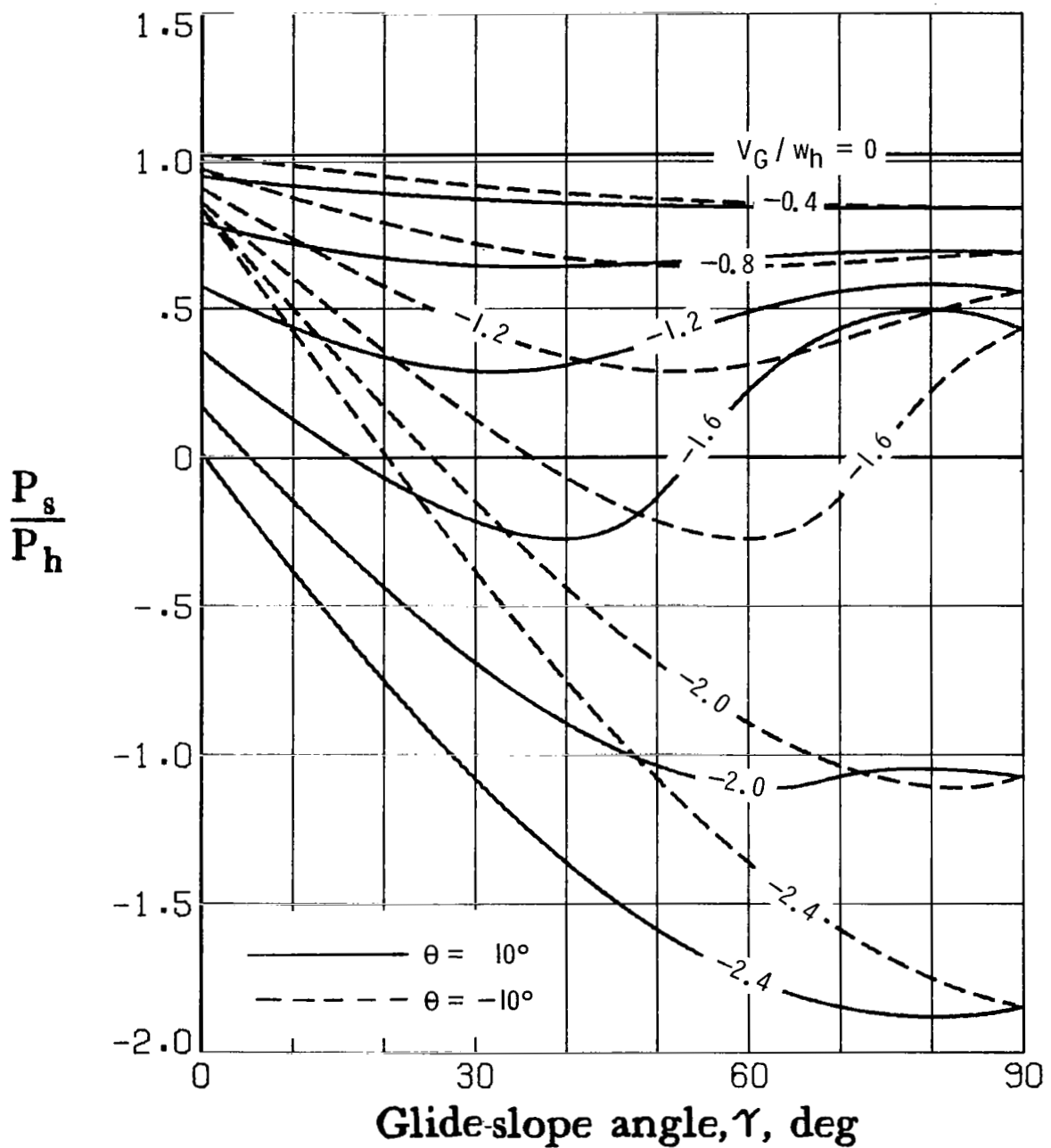


Figure 13.- Effect of change in tip-path-plane inclination on shaft power required for flight along glide slope.

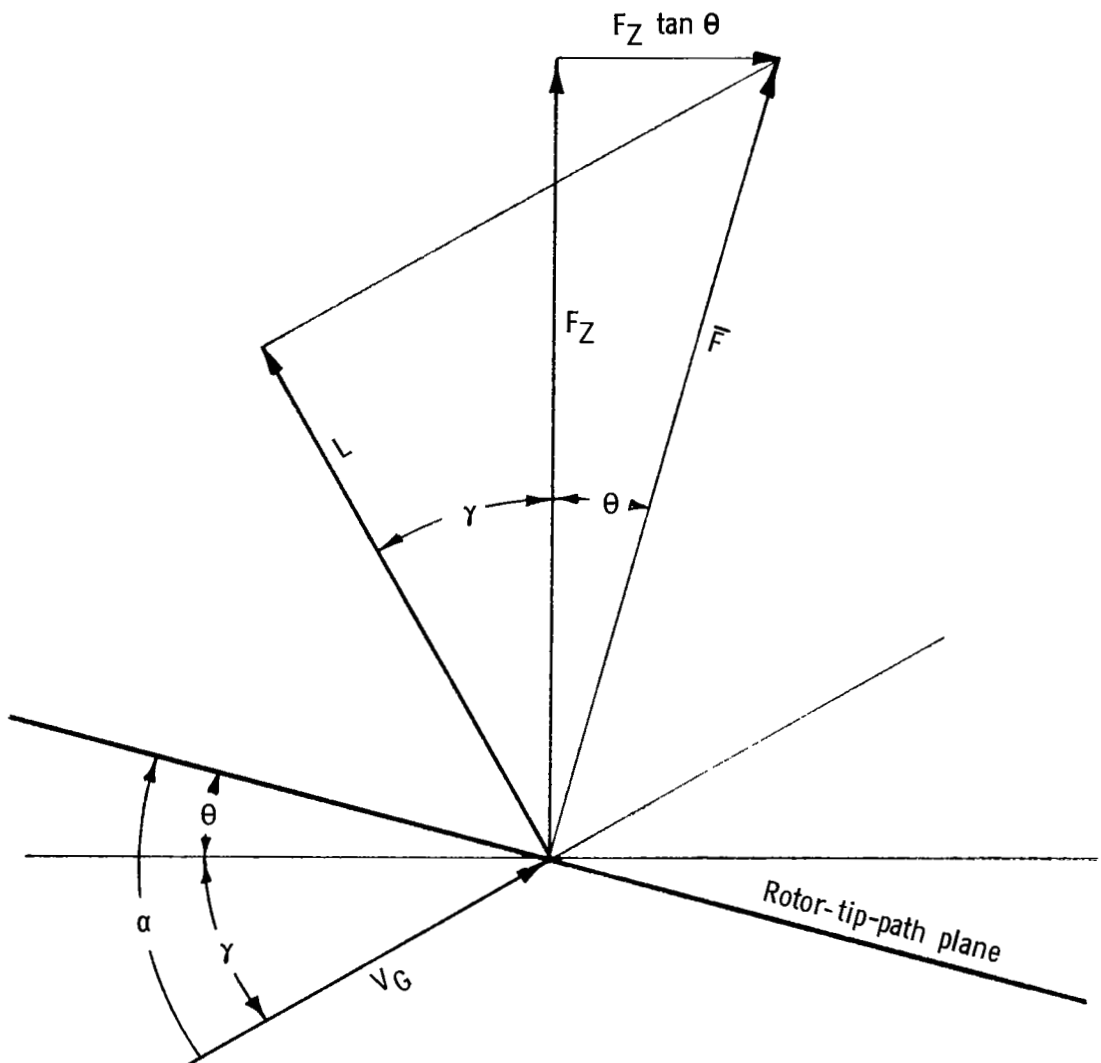


Figure 14.- Vector diagram for determining lift from vertical force.

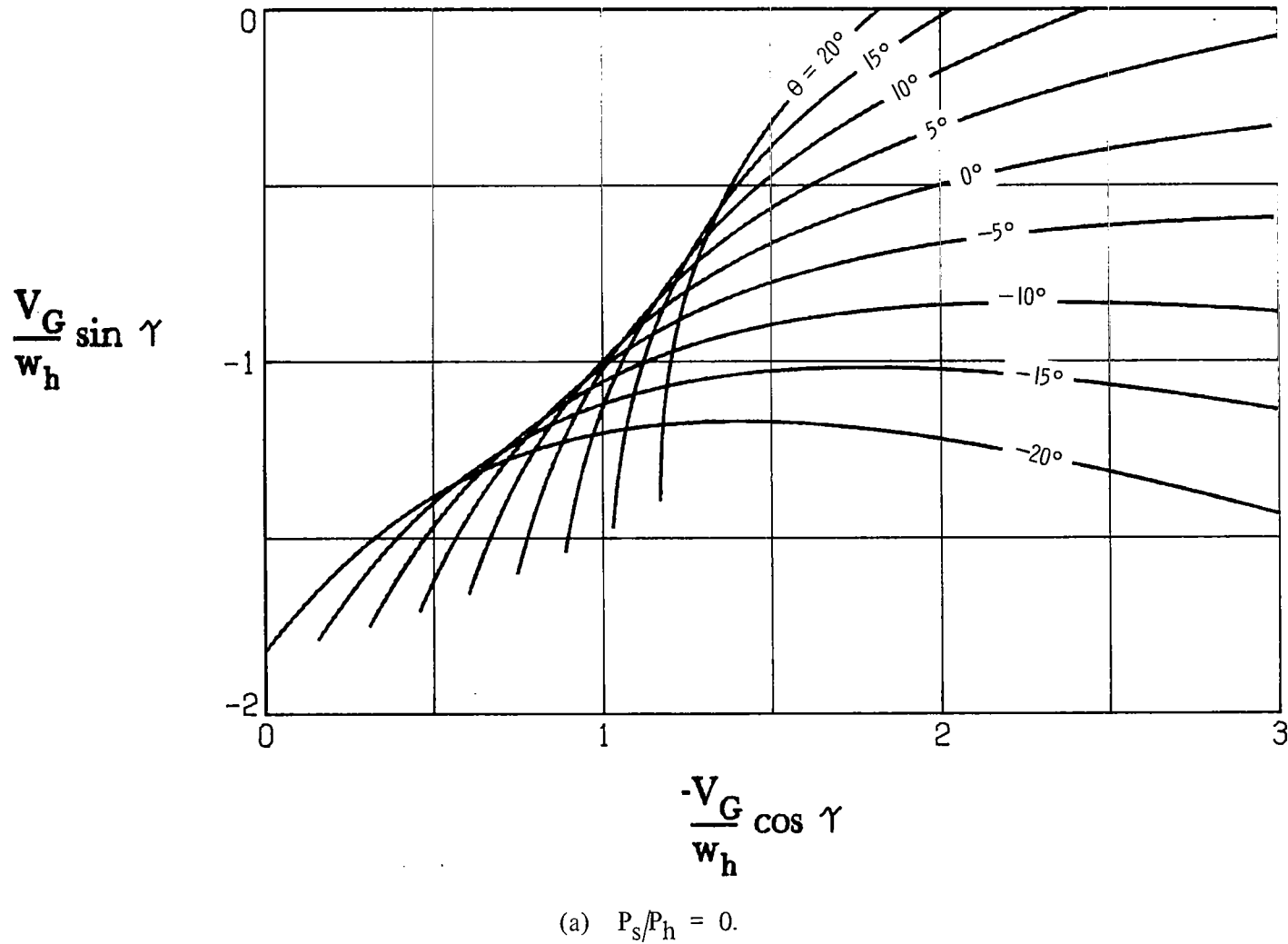
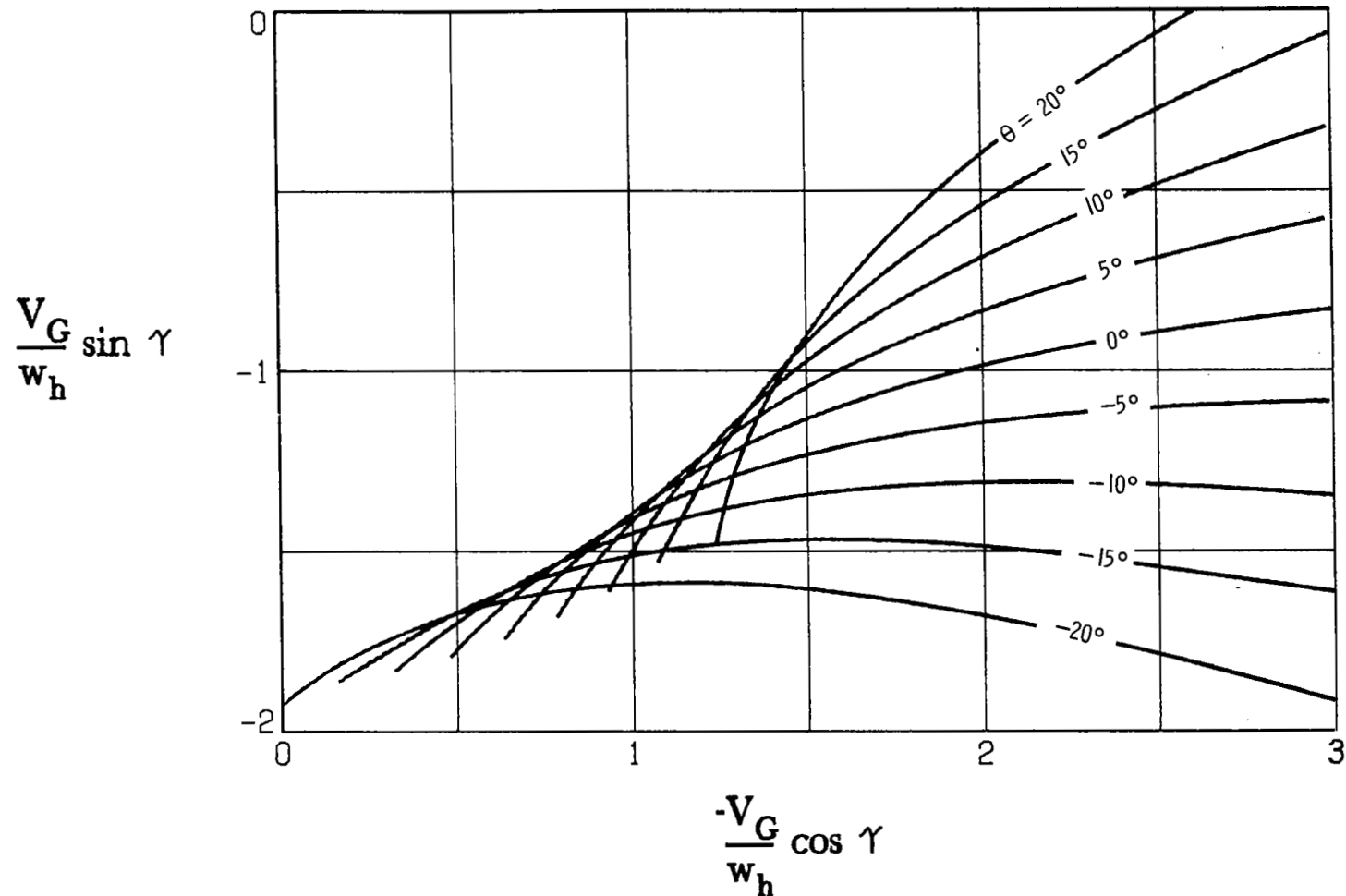


Figure 15.- Theoretical autorotative performance of a rotor in forward flight.



(b)  $P_s/P_h = -0.5$ .

Figure 15.- Concluded.

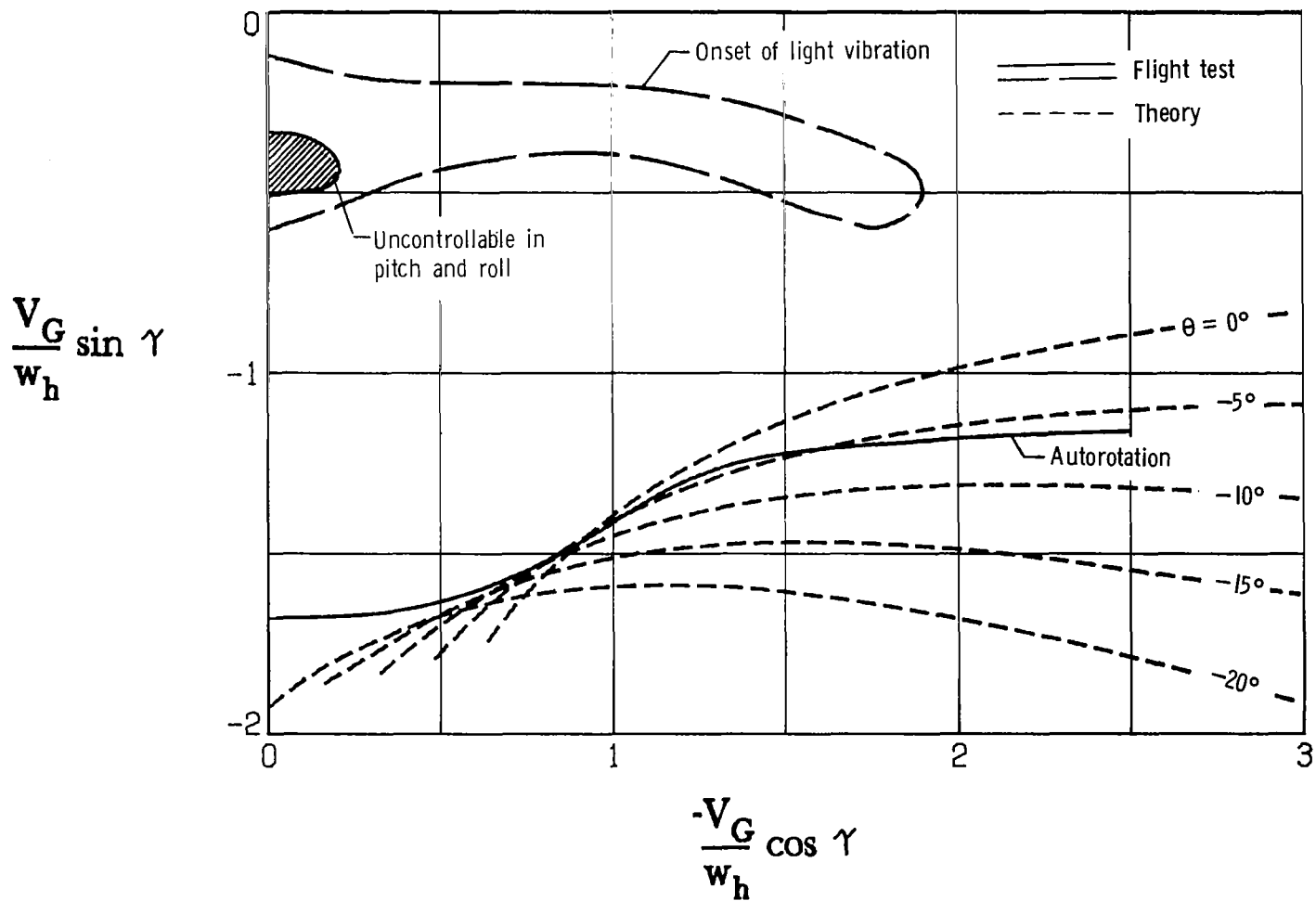


Figure 16.- Comparison of simple momentum theory with flight measurements of descent boundaries. The  $P_s/P_h$  is assumed to be -0.5 in theoretical calculations.

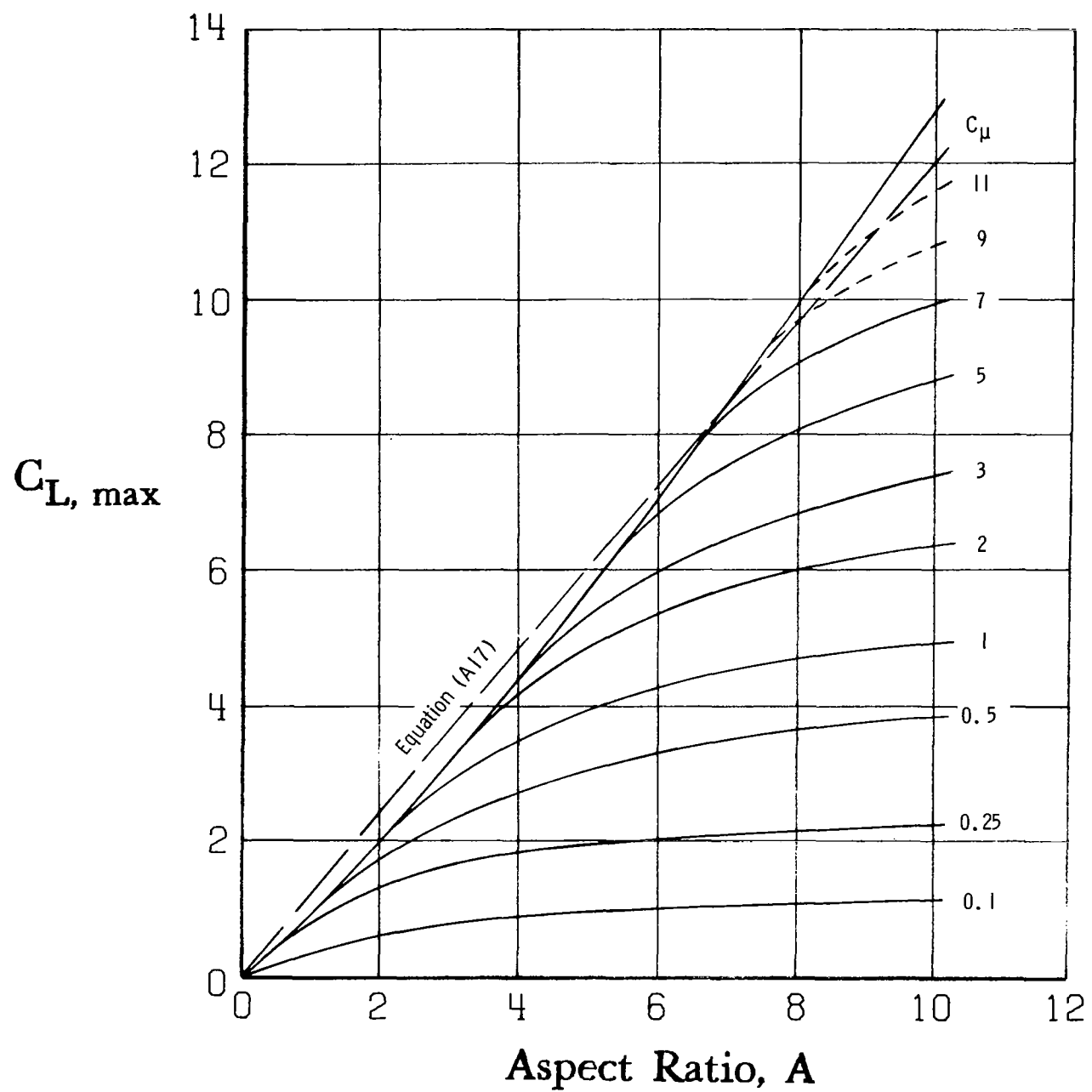


Figure 17.- Comparison of theoretical maximum lift coefficient to circulation-lift coefficient measured for jet-flap wings of reference 20. The wings were at  $0^\circ$  angle of attack with a jet deflection angle of  $85^\circ$ .